

THESIS FOR THE DEGREE OF DOCTOR OF PHILOSOPHY

Bottom-up Fabrication of Functional DNA Nanostructures

ERIK LUNDBERG



DEPARTMENT OF CHEMICAL AND BIOLOGICAL ENGINEERING
CHALMERS UNIVERSITY OF TECHNOLOGY

GÖTEBORG, SWEDEN 2012

Bottom-up Fabrication of Functional DNA Nanostructures

ERIK LUNDBERG

ISBN: 978-91-7385-647-8

© ERIK LUNDBERG, 2012

Doktorsavhandlingar vid Chalmers tekniska högskola

Ny serie nr: 3328

ISSN: 0346-718X

Department of Chemical and Biological Engineering

Chalmers University of Technology

SE-412 96 Göteborg

Sweden

Tel: +46 (0)31 772 10 00

Cover art: The largest DNA nanostructure constructed in this thesis, consisting of 17 synthetic three-way oligonucleotides. Each side is a 10 nucleotide long DNA duplex (3.4 nm) and the color-coding indicates unique sequences.

Back cover photo: © Jonas Hannestad

Chalmers Reproservice
Göteborg, Sweden 2012

Bottom-up Fabrication of Functional DNA Nanostructures

ERIK LUNDBERG

Department of Chemical and Biological Engineering
Chalmers University of Technology

Abstract

This thesis demonstrates bottom-up fabrication of a fully addressable non-repetitive network on the nanometer scale, assembled by synthetic DNA molecules. Each side constitutes a unique sequence of 10 bases, *i.e.* 3.4 nm in length, and can be considered the smallest practical unit of DNA in a nanotechnological context. Working with units of this length scale ensures a system fit for non-mundane molecular nanotechnology. The thesis features a progressive growth of the nanostructure, from the formation of the single-ringed hexagonal unit-cell to an asymmetric four-ring network of 17 nodes. Each structure is formed in a one-step self-assembly reaction.

Alongside construction of the DNA-based nanostructural template, the thesis also illustrates three different aspects of functionalization. Firstly, a fixation strategy infusing stability in the delicate network by chemical ligation. The click chemistry based strategy will pave the way for modular build-up of larger nanostructures. Results show that multiple site-specific click reactions can perform simultaneously and independently of each other on a hybridized DNA template. Fixated modules are resistant to denaturing agent and can be freeze-dried. The second important aspect is incorporation of these DNA nanoconstructs onto lipid bilayers, for development of soft-surface nanotechnology. This creates controllable new interfaces in an aspiration towards membrane-integrated applications, *e.g.* mimicking a photosynthetic reaction centre. This thesis features two different molecular anchors: a multi-functional porphyrin moiety and a more universal lipid anchor. Both anchors are shown to align a DNA nanostructure with the membrane surface, a conformational arrangement that also depends on position of anchoring points. The last theme of this thesis is triplex recognition as a method for site-specific functionalization of preformed DNA nanostructures. The specific function of energy transfer is demonstrated in a simple photonic device, which can be switched ON and OFF by slight adjustment of pH.

This DNA-based nanoscopic system is envisioned as a platform for high-precision control over molecular processes towards nanotechnological applications. It is part of an ambition in molecular nanoscience to fabricate systems from the bottom-up, based on principles of self-assembly and with functional complexity on levels not achievable by a conventional top-down perspective to nanoscience. The great leap of molecular nanoscience stems from inspiration of biological systems. New advancement in technological progress is possible by harvesting benefits of Darwinian evolution.

Keywords:

dna, nanotechnology, self-assembly, lipid membrane, click chemistry, triplex recognition, cross-linking, fixation, spectroscopy, linear dichroism, gel electrophoresis, fret

List of Publications

Paper I

Addressable High-Information-Density DNA Nanostructures

John Tumpane, Peter Sandin, Ravindra Kumar, Vicki E.C. Powers, Erik P. Lundberg, Nittaya Gale, Piero Baglioni, Jean-Marie Lehn, Bo Albinsson, Per Lincoln, L. Marcus Wilhelmsson, Tom Brown, Bengt Nordén
Chemical Physics Letters 2007, 440, 125-129.

Paper II

Triplex Addressability as a Basis for Functional DNA Nanostructures

John Tumpane, Ravindra Kumar, Erik P. Lundberg, Peter Sandin, Nittaya Gale, Iris S. Nandhakumar, Bo Albinsson, Per Lincoln, L. Marcus Wilhelmsson, Tom Brown and Bengt Nordén
Nano Letters 2007, 7 (12), 3832-3839.

Paper III

Nanofabrication Yields. Hybridization and Click-Fixation of Polycyclic DNA Nanoassemblies

Erik P. Lundberg*, Calin Plesa, L. Marcus Wilhelmsson, Per Lincoln, Tom Brown, and Bengt Nordén
ACS Nano 2011, 5, (9), 7565-7575.

Paper IV

A New Fixation Strategy for Addressable Nano-Network Building Blocks

Erik P. Lundberg, Afaf H. El-Sagheer, Petr Kocalka, L. Marcus Wilhelmsson, Tom Brown and Bengt Nordén
Chemical Communications 2010, 46, (21), 3714-3716.

Paper V

Soft-Surface DNA Nanotechnology: DNA Constructs Anchored and Aligned to Lipid Membrane

Karl Börjesson, Erik P. Lundberg, Jakob G. Woller, Bengt Nordén, and Bo Albinsson
Angewandte Chemie International Edition 2011, 50, (36), 8312-8315.

Paper VI

Controlling and Monitoring Orientation of DNA Nanoconstructs on Lipid Surfaces

Erik P. Lundberg*, Amir Saeid Mohammadi, L. Marcus Wilhelmsson and Bengt Nordén
Submitted to Langmuir

* Corresponding author

Contribution Report

Paper I

Designed and performed electrophoresis experiments, data analysis and interpretation, and contributed to the discussion.

Paper II

Designed and performed electrophoresis experiments and interpretation of results. Contributed to the writing of the paper.

Paper III

Designed and supervised all experiments. Performed interpretation and analysis of the results. Wrote the paper.

Paper IV

Designed the system. Planned and performed all experiments. Performed interpretation and analysis of the results and wrote the paper.

Paper V

Designed the nanostructure. Planned and performed melting and DLS experiments. Contributed to interpretation of the results as well as to the writing of the paper.

Paper VI

Designed the system. Planned and supervised all experiments. Performed interpretation and analysis of the results and wrote the paper.

Contents

1. SIZE MATTERS	1
2. FUNDAMENTAL MATTERS	5
2.1 DNA	5
2.1.1 DNA STRUCTURE	5
2.1.2 TRIPLEX DNA	7
2.2 DNA NANOTECHNOLOGY	10
2.2.1 DNA CRYSTALLINE ARRAYS	10
2.2.2 DNA SOLITAIRES	13
2.2.3 DNA ORIGAMI	15
2.2.4 DNA NANO-MACHINES & MECHANICAL DEVICES	18
2.3 CLICK CHEMISTRY	22
2.4 PHOTOPHYSICS	25
2.4.1 EXCITED STATE PROCESSES	27
2.4.2 FÖRSTER RESONANCE ENERGY TRANSFER	28
2.5 LIPID MEMBRANES	30
2.6 SELF-ASSEMBLY	32
3 METHODOLOGY - THE DAILY MATTERS	35
3.1 SPECTROSCOPY	35
3.1.1 ABSORPTION	35
3.1.2 FLUORESCENCE	36
3.1.3 LINEAR DICHROISM	37
3.2 DYNAMIC LIGHT SCATTERING	42
3.3 GEL ELECTROPHORESIS	44
4. CONSTRUCTION OF AN ADDRESSABLE DNA NANONETWORK	47
4.1 INTRODUCTION – AMNA	47
4.2 PART I – ASSEMBLY OF POLYCYCLIC DNA NANOSTRUCTURES	53
4.3 PART II – CLICK FIXATION STRATEGY FOR MODULAR BUILD-UP	61
4.4 PART III – SOFT-SURFACE NANOTECHNOLOGY	67
4.5 PART IV – TRIPLEX RECOGNITION FOR SITE-SPECIFIC FUNCTIONALIZATION	75
5. CONCLUDING REMARKS - DOES THIS REALLY MATTER?	83
6. ACKNOWLEDGEMENTS - PEOPLE THAT MATTERED	87
7. BIBLIOGRAPHY	89

1. Size Matters

“There’s plenty of room at the bottom.”

Richard Feynman

The expansion of the technological evolution during the past century is unprecedented in the history of mankind. Development of new applications has had a vast impact on human society, perhaps most evident in computers and the information technology they brought on. Miniaturization is at the heart of this evolution, where the ever-expanding capacity of devices is tightly linked with their gradually diminishing size. Moore’s law, made famous by the co-founder of Intel, Gordon E. Moore¹, governs the exponential development of computer power.¹ This development has started to reach the limit of what is possible to achieve in terms of scaling down electrical devices with conventional microtechnology. New strategies working on even smaller length scale are thus a prerequisite for Moore’s law to stay applicable to the technological progress. The scientific frontier that pushes the boundaries of this endeavor is labeled nanoscience¹¹.

The fundamental principle of nanoscience is to create, control and understand systems on a length scale measured in nanometers (10^{-9} m). In doing so, scientists hope to develop new applications called for by the technological evolution. By mastering fabrication and manipulation of matter with nanometer precision many processes of today could potentially be carried out in systems of minute size. Guided by the principle of “doing more with less”, nanotechnological research also brings promise from an environmental perspective, generating a much desired frugality of natural resources. The aspiration of fulfilling these hopes and desires has spawned an interdisciplinary field of research exploiting the knowledge from all areas of science. Development of advanced analytical tools providing novel levels of characterization, such as atomic force microscopy (AFM) or super-resolution microscopy defying the diffraction limit of light (STED, STORM, PALM *etc.*), have nourished the expansion of the nanoscopic research field. It is important to remember that the technological evolution itself pushes the scientific frontier forward, enabling ever exceeding possibilities to study molecular processes in greater detail, which in turn paves the way for new technologies manifesting a progressive symbiotic spiral.

A difference in scientific perspective can be observed when comparing two alternative approaches of nanoscience. The more established strategy is that of material physics, adopting a top-down perspective on fabrication on the nanometer

¹ PhD from Caltech in Physical Chemistry 1954

¹¹ Etymology: Greek, ‘nano-’ meaning ‘dwarf’

scale, using various lithographic techniques. The precision of etching has increased, reaching higher levels of resolution by continued technical advancements. However, certain applications may require levels of complexity that cannot be achieved from a top-down approach. A shift in perspective is essential. The bottom-up approach to nanoscience of molecular science focuses on understanding intermolecular interactions and how this can be used for controlled construction through self-assembly processes. By allowing building blocks to come together in predetermined patterns, larger nanostructures can be created from the bottom-up. A major advantage of a bottom-up perspective is the possibility of incorporating functional complexity only achievable using chemical tools, having intrinsic sub-nanometer precision. The major challenge on the other hand is to build supramolecular structures sufficiently large for nanotechnological applications.

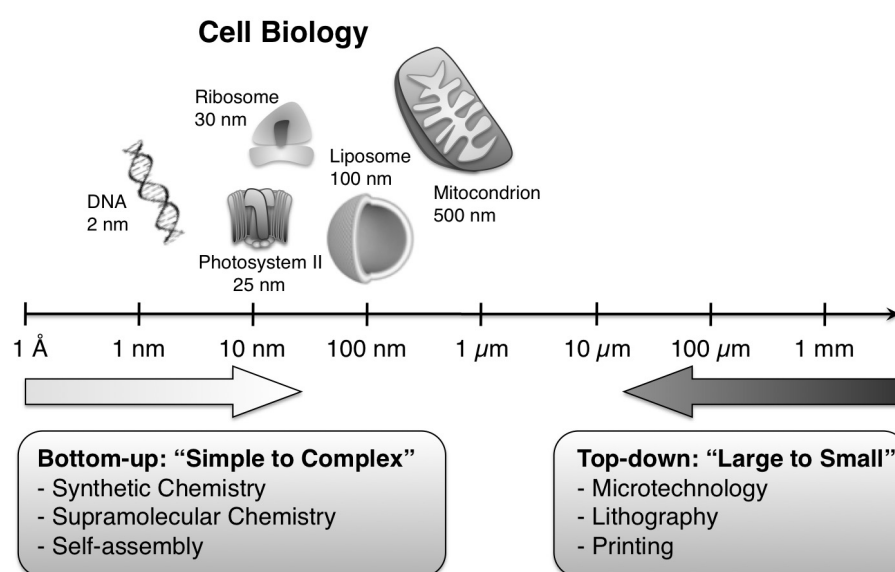


Figure 1.1. Diametric strategies in nanoscience: "bottom-up" and "top-down". The former emerged from supramolecular chemistry and is based on principles of self-assembly. The latter is founded in material physics, driven by miniaturization. The gap between these two approaches coincides with size of many molecular systems in cell biology, of which DNA is of special interest in this thesis (width ~ 2 nm). Interestingly, the enormous aspect ratio of the DNA molecule enables it to potentially span this entire length-scale (length of a human chromosomal DNA approx. 200 000 kb, ~ 0.7 mm). Figure inspired by Niemeyer (2001).²

With inspiration found in biological systems the structural challenge of nanoscience with a bottom-up approach may be addressed. Nature constructs functional materials built on principles of self-assembly with entirely new properties of the assembly disparate from the single entities. Furthermore, biological self-assembly is often hierarchical, rendering functioning systems of even higher complexity. Cellular processes are largely dependent on the intermolecular interactions of macromolecules on the nanoscopic scale. Eons of Darwinian evolution have yielded systems with diverse function of astonishing complexity. For instance, the photosynthetic reaction centre in chloroplasts that intertwines water

splitting and carbon fixation in an elaborate scheme of energy- and electron transfer pathways; or the sophisticated machinery, referred to as the central dogma of molecular biology, transforming genetic information encoded in DNA into enzymes with specific functions. The efficiency of these molecular machines motivates scientific efforts to harvest benefits of the evolutionary progress in technological advancement. A bio-inspired perspective on bottom-up nanoscience, combining self-assembly of macromolecules with functional complexity of supramolecular chemistry, could result in systems impossible to achieve with a traditional top-down strategy.

The self-assembly of DNA molecules is especially interesting in this context, governed by the precise recognition pattern of the Watson-Crick base pairs discovered in 1953.^{3, 4} The sequence of bases makes two complementary strands come together in a predictable manner, forming a double helix of DNA, and thereby creating an excellent system for programmable self-assembly within the framework of nanoscience. Together with the mere 3.4 Å separation between one base and the next in the helical stack, these properties have made DNA ideal for a bottom-up approach, demonstrated by the pioneer work of Ned Seeman⁵ in extensive pseudo-crystalline arrays and later by the controlled scaffold folding of DNA origami developed by Paul Rothemund⁶.

The work in this thesis concerns the creation of a structural platform that enables control over molecular processes on the nanometer scale. An advanced self-assembled system, based on synthetic nucleic acids, has been constructed combining the bio-inspired approach with the molecular bottom-up strategy. This strategy enables an addressable non-repetitive two-dimensional network, such that functional moieties may be added to it and positioned in space at high precision using specific recognizing sequences. Due to the possibility of versatile incorporation of functionalities, one can imagine many applications in molecular electronics (electron transfer), information technology (energy transfer) and chemical engineering (assembly lines of catalysts). This is attainable due to the possibility of unrestricted sequence design, ensuring the network to be non-periodic and by keeping the size of the building blocks to the smallest practical units of DNA. Having a non-repetitive structure is a prerequisite for introducing the concept of addressability in the system. Addressability is a key element for non-mundane functionalization of the structure, enabling precise positioning of desired functions throughout the network. This is part of a framework entitled AMNA (Addressable Molecular Node Assembly).⁷

The results and conclusions of this endeavor, on which this thesis is based, have rendered six scientific papers, concerning different aspects of the project. Construction of the addressable nanonetwork by self-assembly of novel three-way branched oligonucleotides stands as the main trajectory of the thesis, being the fundament of the project. Fabrication and subsequent characterization of the addressable DNA nanonetwork, is presented in the first three papers. The first generation of this nanogrid, a single hexagonal unit-cell, is presented in Paper I. The following two papers show evolution of the assembly into the largest structure yet

formed, a four-ring network of 17 nodes (Paper III). Development of fixation strategies infusing stability in the delicate system is an important subject. The fixation strategy demonstrated in Paper IV is based on click chemistry through site-specific cross-linking of a hexagonal unit cell using the copper(I)-catalyzed cycloaddition (CuAAC). This could potentially lead to alternative assembly approaches based on modular fabrication. Papers V and VI present progress in soft-surface nanotechnology by demonstrating two different strategies to integrate DNA nanostructures with lipid membranes. Exploring molecular anchors for controllable incorporation into lipid bilayer could pave the way for dynamic surface-based applications, *e.g.* mimicking photosynthetic reaction centres. Finally, the concept of addressability is concretized using triplex recognition. Paper II includes an illustration of how triplex forming oligonucleotides can be employed to functionalize a preformed addressable grid. A study of sequential energy transfer based on triplex recognition is presented in the last part of chapter 4.

2. Fundamental Matters

This chapter aims at giving a framework to the work and results presented in the thesis. The DNA molecule, which is the heart of this work, will be described, and recent advances in DNA nanotechnology will be briefly reviewed. Furthermore, the important concepts of click chemistry and self-assembly will be discussed, and some elements of photophysical theory, needed for understanding parts of the results in chapter 4, will be presented.

2.1 DNA

DNA (deoxyribonucleic acid) is the molecule containing “blue-prints” for all living systems, with the exception of some RNA-based viruses. A paradigm shift took place in 1953 when Watson & Crick^{III} discovered the helical structure of DNA.^{3,4} For over 50 years, the structural features of DNA have been the focus of extensive research trying to answer questions concerning the correlation between structure and function. By altering the sequence of bases, *i.e.* the four letters A, T, G & C, a manifold of different genes can be created, each corresponding to a particular protein having a specific function in the cell.

2.1.1 DNA Structure

DNA is a biopolymer built up of nucleotides. Each nucleotide consists in one part of a 2-deoxyribose sugar that is linked to another nucleotide *via* a phosphodiester bond (Figure 2.1). The polymeric alternation of sugar and phosphate constitutes what is entitled the backbone of a DNA molecule. The other part of a nucleotide is one of four possible bases: adenine (A), guanine (G), thymine (T) and cytosine (C). By changing the sequence of these four bases that different genes can be created. All four bases are nitrogen containing aromatic molecules, either one-ring systems as for the pyrimidines (T & C) or two-ring systems for the purines (A & G). An absolutely central feature of the bases is their ability to form hydrogen bonds. The specific pattern of hydrogen bonding donor and acceptor sites on each base give rise to a complementary relation between A & T and G & C, the former by two hydrogen bonds and the latter by three. These are known as the Watson-Crick base pairs (Figure 2.2). Because DNA is asymmetric, the biopolymer has directionality, determining how a sequence of bases should be read. The direction is determined by how two adjacent sugars are connected *via* the phosphate

^{III} Francis H. C. Crick & James D. Watson was awarded the Nobel Prize in Physiology or Medicine 1962 together with Maurice H. F. Wilkins "for their discoveries concerning the molecular structure of nucleic acids and its significance for information transfer in living material" (www.nobelprize.org/nobel_prizes/medicine/laureates/1962/)

groups in the backbone, from the fifth carbon of the first sugar to the third carbon of the second one. The direction is therefore denoted 5' to 3'.

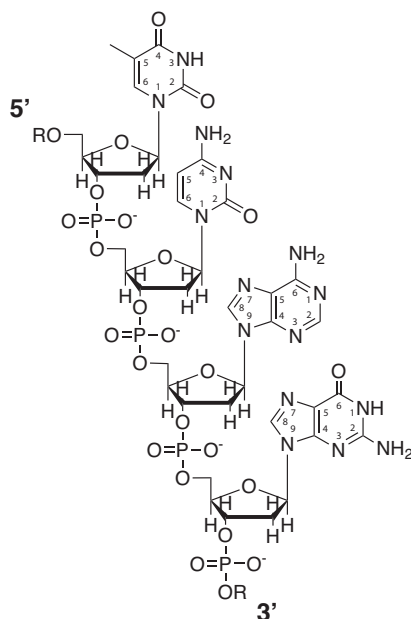


Figure 2.1. The four nucleotides connected by the phosphodiester groups of the backbone. Starting from the 5'-end: Thymine, Cytosine, Adenine and Guanine.

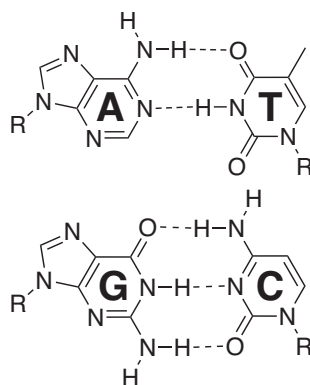


Figure 2.2 The Watson-Crick base-pairs. (Top) Adenine (A) & Thymine (T). (Bottom) Guanine (G) & Cytosine (C).

Due to the base-pair formation possibility, two DNA molecules can interact *via* the specific hydrogen bonds between the bases forming a helical duplex. In the double helix the bases stack on each other in the centre of the helix, forming a hydrophobic core. The two sugar-phosphate backbones wind around each other wrapped about the hydrophobic centre, shielding it from the surrounding water. The phosphate group has a pK_a around 1, meaning that the proton is dissociated under most conditions, resulting in a negatively charged backbone. The two DNA strands repel each other in the absence of salt. However, at physiological conditions the effective net charge is lower because of associated counter ions, such as Na^+ , decreasing the repulsion between the strands and facilitating the duplex formation. The helix normally has a right-handed pitch of 10 bases per turn, denoted B-DNA (Figure 2.3). The stacking of the bases in the core of the helix arises from π - π

interactions due to the aromatic character of the bases. The distance between two adjacent base pairs in the stack is 3.4 Å and the width of the helix is 22 Å, in B-DNA. The asymmetric character of the helix gives rise to two different grooves one wider than the other, referred to as the major and minor groove, respectively. Both play key parts in the interactions between DNA and other molecules, influencing the binding mode of any associated target. Aside from B-form, DNA can also adopt an A- or Z-form under certain conditions. The former is a right-handed helix with a much wider pitch than B-form and can occur in AT-rich regions of DNA or dehydrated samples. The wider pitch of A-DNA makes the minor groove wider and shallower and the major groove narrower but deeper, compared to their counterpart in B-DNA. The Z-form of DNA is on the other hand a left-handed helix and can arise in presence of high salt concentrations. Although the existence of these forms of DNA is evident, their biological relevance is disputed.⁸

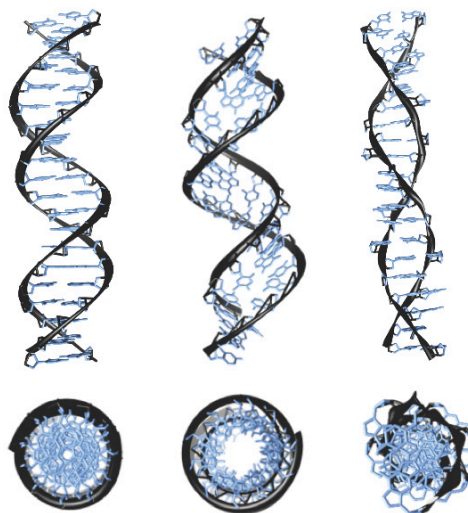


Figure 2.3. The helical structure of double stranded DNA, viewed perpendicular and through the helical axis. B-DNA (left), A-DNA (centre) & Z-DNA (right).

2.1.2 Triplex DNA

Soon after the discovery of the double helix, a three-stranded DNA structure was found.⁹ In this structure a third strand is situated in the major groove between the two other strands forming a double helix. This three-stranded structure has been denoted a DNA-triplex.¹⁰ In addition to the common Watson-Crick base pairs, other hydrogen bonding patterns between the DNA-bases can form, which is especially interesting for the purines. The N7 position can act as a hydrogen bond acceptor to both guanine and adenine. Guanine also has an acceptor position at O6, whereas adenine has donating hydrogen on the corresponding N6. These positions are situated in the major groove in a double stranded DNA, making them easily accessible for molecular interactions with incoming agents, such as amino acids or other nucleotides. The molecular interactions between nucleotides involving these positions give rise to a recognition pattern equivalent to the

Watson-Crick base pairing; called Hoogsteen base pairing after its discoverer (Figure 2.4).¹¹ Both purines and pyrimidines can form Hoogsteen interactions with guanine and adenine. For example, an oligonucleotide of polypyrimidines can, *via* Hoogsteen-binding in the major groove of a polypurines-polypyrimidines double helix, form a triplex. This triplex forming oligonucleotide (TFO) binds with the same directionality as the polypurine strand. A strand of polypurines may also form a triplex with a polypurines-polypyrimidines double helix, albeit with opposite directionality. In this project, TFOs of polypyrimidines have been used and the focus will therefore be on these. Interested readers may seek more information about polypurine TFOs in review articles by Duca *et al.*¹² and Frank-Kamenetskii *et al.*¹³.

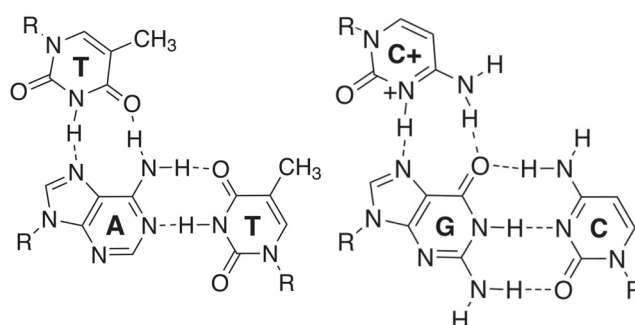


Figure 2.4. Hydrogen-bond pattern of Hoogsteen base pairing. T*AT (left) and C*GC (right).

Both cytosine and thymine can form Hoogsteen base pairs with guanine and adenine, respectively. A prerequisite for cytosine to bind to guanine *via* this interaction is protonation of the N3 position, enabling hydrogen bonding to guanine at the O6 position. The pK_a is about 4.5, depending on its position in the base sequence.¹⁴ At pH below this, the triplex forming affinity is induced by the positive charge of the protonated cytosine. The positive charge partially neutralizes the repulsion between the negatively charged backbones and thereby stabilizing the triplex structure. No protonation is necessary for thymine to bind to adenine *via* Hoogsteen-binding, but the affinity to form a triplex structure is lower compared to cytosine.¹⁵ The reason for this is the unfavorable positioning of three negatively charged polyions close in space due to electrostatic repulsion.

The ability of TFOs to target specific regions of DNA has made it subject for extensive research for possible use in gene therapy.¹² Chemical modifications of nucleobases to improve the triplex forming features are an interesting part of this endeavor. The low pK_a of cytosine suppresses formation of stable triplex structures under physiological conditions (pH 7.5). Finding improvements that solves this problem have therefore been of interest. Methylation at C5 position of cytosine (^MC) raises the pK_a and thus also binding affinity (Figure 2.5). 3-methyl-2-aminopyridine (^MP), which is one of the bases also used in this work, has a more basic character compared to cytosine, due to the removal of the 2-oxo functional group (Figure 2.5).^{16, 17} The result is an increased triplex affinity at physiological

pH.¹⁸ The low affinity of thymine to form Hoogsteen bonds has also been addressed. One solution is the addition of multivalent counter ions, such as Mg^{2+} , which facilitate triplex formation by shielding the negative charges of the backbone. The drawback is the high salt concentration needed, dissimilar to physiological conditions. 2'-aminoethoxythymidinide (^AT) has a modified sugar with the addition of a positive charge (Figure 2.5). The positive charge interacts with the negative charge of phosphate in the backbone, thereby increasing the affinity through electrostatics.^{19, 20} ^AT is the other modified base used in this project. A lot of focus has been on developing different bases matching the pattern of adenine and guanine. The advantage of purines compared with the pyrimidines is better positions for hydrogen bonding in the major groove. But in order to achieve a more versatile system, the ability to recognize all four bases is of considerable interest. Recently, candidates able to form triplex structures at physiological pH were synthesized.²¹ These results bear promise to the use of triplex recognition in the field of biomedicine as well as DNA nanotechnology, creating more possibilities of addressability based on third-strand targeting.

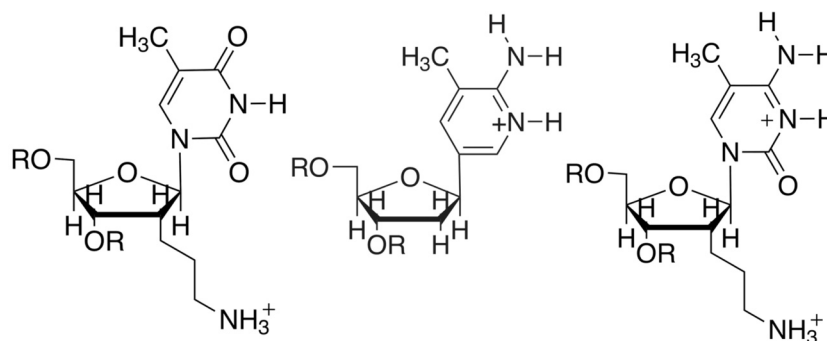


Figure 2.5. Synthetic base analogs with high triplex forming affinity. (Left) 2'-aminoethoxythymidinide (^AT), (middle) 3-methyl-2-aminopyridine (^{Me}P) and (right) 2'-aminoethoxy-5-methyl-cytosine (^{Me}C)

2.2 DNA Nanotechnology

The unique structural features of DNA have expanded the perspective of the potential applications of the molecule outside the arena of bioscience. A combination of a reliable system for information storage with sub-nanometre resolution makes DNA ideal for molecular nanotechnology. This section will discuss some advances that have been made in the field.

2.2.1 DNA Crystalline Arrays

This thesis aims at constructing a two-dimensional non-repetitive DNA nanonetwork. Though conceptually disparate from periodic pseudo-crystalline DNA nanoarrays, there are structural similarities. Being acquainted with these assemblies is therefore important for the understanding of the nanostructures studied in this thesis.

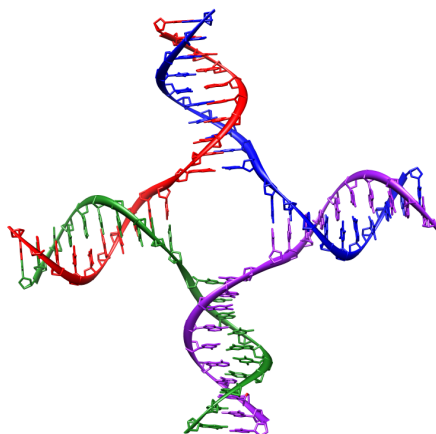


Figure 2.6 Holliday junction. Four DNA-strands form a four-way junction.

Seeman postulated the use of DNA as a structural material in the beginning of the 1980s.²²⁻²⁶ Inspired by the naturally occurring Holliday junction (Figure 2.6), oligonucleotides can be assembled into structural motifs by careful design of the base sequence. The Holliday junction is a four-way junction, first discovered in fungi, playing a role in for example gene recombination.²⁷ The structure found in biological systems is a transient state, with a moving junction in a palindromic sequence. However, to be used as a structural motif the junction must manifest stability, why algorithms for sequence design must follow certain criteria.²⁸ This led to the development of the double crossover (DX) motif (Figure 2.7), which joins two DNA helices in a tight parallel arrangement.^{29, 30} Since the motif involves two junction points, the resulting unit exhibits the desired structural rigidity. By adding single stranded overhangs, *i.e.* sticky-ends, multiple motifs may be connected (Figure 2.8). A number of different crossover motifs have been developed based on the principles of the DX junction: triple- (TX), paranemic (PX) and the juxtaposed paranemic (JX) crossover.^{31, 32} Crossover junctions have become the architectural basis in many DNA-based structural designs, also in the folding logic of DNA origami (*vide infra*). But it was as tiles in the formation of self-assembled repetitive lattices that they were developed and first introduced.

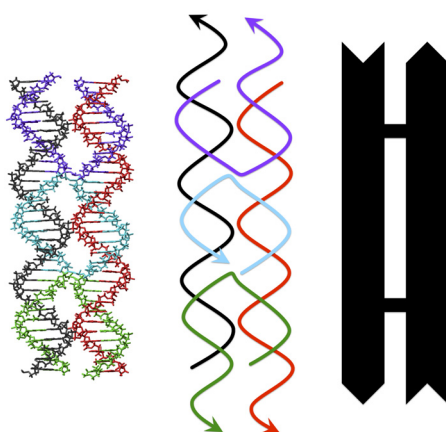


Figure 2.7. The double-crossover motif (DX). (Left) A molecular model of the motif. (Middle) A schematic representation of the same structure, with single-stranded extensions transform the motif to a tile. (Right) A representation of a DX tile, which may assemble into a periodic array according to Figure 2.8.

The first DNA-based 2D pseudo-crystal lattice was presented in 1998 by Seeman and coworkers.³³ Based on the crossover motifs, the following years a number of different arrays were presented.^{31, 34-42} This branch of DNA nanotechnology has relied heavily on atomic force microscopy (AFM) for visualization of the assembled structures. The geometry of the pseudo-unit cell of the 2D crystal-like structure will depend on the constitution of the underlying DNA building block, thus creating *e.g.* a square pattern³⁵ or different hexagonal patterns^{36, 38}. That structural properties of the building blocks influence the features of the final assembly is obvious, and an analogy with macroscopic architectural design was underlined when Mao and coworkers introduced the structural concept of tensegrity in the DNA nanofabrication context.⁴³ Tensegrity^{IV} is to combine compression and tension, *e.g.* with bars and wires respectively, resulting in rigid, though lightweight, structures. Building on early attempts of incorporating these architectural principles of combining two opposite forces for rigid constructs, the group of Mao managed to design a triangular DNA building block where double- and single-stranded regions of DNA were positioned according to this logic. With the conventional use of sticky-ends, these building blocks could be assembled into one- & two-dimensional arrays. Furthermore, Seeman *et al.*⁴⁴ demonstrated that it was possible to create a 3D crystal through self-assembly of DNA molecules, having postulated this in the early 1980's,²² by adopting the tensegrity triangle. The triangular building block had three years earlier also been used to organize Au-nanoparticles in a two-dimensional array,⁴⁵ bordering another application of structural DNA nanotechnology that Seeman had envisioned, *i.e.* as a scaffold for protein organization. Principles of DNA mediated protein organisation have been demonstrated with biotin/streptavidin in various studies by Yan *et al.*,^{35, 46} a group

^{IV} A contraction of tensional integrity.

that also has exploited aptamers^V in order to position thrombin.⁴⁷ A study, closer to Seemans original vision, was done by Turberfield *et al.*^{48,49} where they demonstrated that visualization of proteins in transmission electron microscopy could be facilitated using a two dimensional DNA nanoarray.



Figure 2.8. A 2D periodic DNA nanoassembly of DX-tiles.

Organization of proteins is a target for applications in molecular biology, equivalently there could be an interest of organizing metallic nanoparticles into specific patterns for nanoelectronic or optical devices. The principles of DNA-templated organization are the same, which the group of Yan has utilized, forming repetitive arrays of Au-nanoparticles in the same manner as with proteins.^{50, 51} An important aspect, concerning the arrangement of functionalizations, such as nanoparticles, in DNA networks, is the precision with which they can be positioned. The spatial separation between particles can be controlled by the size of the unit-cell. However, the structures so far discussed are all repetitive arrays, which prevent further precision in the positioning. To enable total freedom in localization the nanostructures need to be fully addressable, with unique building blocks in a controlled arrangement. In the groups of Yan and LaBean, advancements have been made in this aspect, creating DNA nanoarrays of finite size. The former first illustrated that the number of unique tiles and consequently the number of unique addresses could be controlled in a 5×5 array, by varying the symmetry of the building block.⁵² Shortly thereafter they also constructed a molecular pegboard with precise positioning of streptavidin in a 3×3 array, with 9 unique addresses.⁵³ A similar system was demonstrated by LaBean and co-workers in a 4×4 fully addressable lattice of 16 unique building block, spelling out the letters “D”, “N” & “A” by arrangement of streptavidin.⁵⁴ Finally, by connecting multiple DNA helices in a tight parallel arrangement, mediated by the use of crossover motifs, it is possible to roll the helices into a tube or bundle. The formation of DNA nanotubes is interesting from both a biological and technological perspective, due to similarities with the filaments in the cytoskeleton, and the possibility of forming electronic, magnetic or photonic nanowires.

It is likely that all systems forming 2D periodic arrays have a tendency to form helical bundles. The competition between intra- and inter-structural associations

^V A short sequence of a nucleic acid that binds to a specific target, such as a protein. From the Latin word “aptus” meaning fitting or suitable.

presents two different assembly pathways. The former leading to a thermodynamic less favorable barrel structure compared to the latter sheet structure.^{vi} Albeit a system at non-equilibrium, intra-structural bundles may be stable due to slow kinetics. The antagonism of thermodynamic and kinetic forces in the self-assembly process may be shifted with clever system design, creating a bias in the assembly pathway. The first reported observation of DNA nanotubes was in 2003 by LaBean and co-workers,⁵⁵ in a system based on tiles of four-way junctions. They followed up this study with a system of TX motifs with repetitive thiol moieties, which could stabilize the tubular structure by forming disulfide bonds on the inside, thus causing a structural bias.⁵⁵ In two separate reports, Winfree *et al.*⁵⁶ and Turberfield *et al.*⁵⁷ demonstrated tube formation in systems through bending of the DX motif, the latter could also display chirality by using streptavidin functionalizations. The Seeman group was later able to achieve even greater control of the DNA nanotube formation. Bundles of a controlled number of helices could be preferentially assembled by carefully designed DX tiles. The crossover junctions were positioned in respect to the helical pitch of the DNA duplex such that a desired angle between neighboring tiles was achieved.⁵⁸⁻⁶¹ The same principle was utilized by LaBean *et al.*⁶² to assemble a three-helix bundle, which similarly to their earlier study could be metalized through Ag deposition, forming a conductive nanowire. The same group also developed another high-precision method of assembling monodisperse DNA nanotubes with controlled circumference.⁶³ The fundamental building block was a single stranded 42mer sequence that could be kinetically trapped in a tube of varied number of helices. Yan *et al.*⁶⁴ followed up on an earlier study, where they investigated the dependence of geometric features of the tiles on tube formation, with a report of Au nanoparticles integrated in DNA nanotube assemblies.⁶⁵ The study showed that the integrated nanoparticles influenced tube formation. The bulky nanoparticles promoted tubular folding through steric hindrance and furthermore, the size of the particles could shift the distribution of tube conformation from stacked rings to more twisted spirals, which display chirality. Assemblies such as this could have interesting properties for technological applications, *e.g.* nanoelectronics.

2.2.2 DNA Solitaires

The DNA nanostructures presented in this thesis are of same size as many objects reported in the DNA nanotechnology field. This section gives a brief overview of the DNA nanostructures of varied geometric shapes that has been published so far.

Even though Seeman originally envisioned DNA-based structural self-assembly as a tool to create pseudo-crystalline nanomaterials, the first published DNA nanostructure was a 3D cube, in 1991.^{5, 66} Each edge of the cube consists of a double-stranded stretch of 20 base pairs, corresponding to a length of approximately 7 nm. The structure was assembled in a number of ligation steps, resulting in a covalently closed nanostructure. Though the final yield was low,

^{vi} We will later see that intra-structural association can be thermodynamically favorable in systems that are studied in this thesis, related to the effect of ring-closure (chapter 4).

around 1%, it was an important first step for the architectural DNA nanotechnology field. Seeman presented another three-dimensional DNA-based object, a truncated octahedron in 1994,⁶⁷ before turning to his main focus of pseudo-crystalline assemblies.

An impressive range of DNA solitaires have been demonstrated during the two decades since the original publication, from a tetrahedron⁶⁸ to a buckyball⁶⁹. Assemblies may either be based on edges of single DNA duplexes^{66-68, 70} or have more complex structural motifs as building blocks^{69, 71}. The latter bears resemblance with the rigid tiles designed for 2D periodic arrays discussed in the previous section and have been developed by Mao and co-workers. They have designed a tunable star-motif that may form any type of polyhedral DNA-cage.^{69, 72-74} Interestingly, the same motif may either be directed toward formation of 3D solitaires or 2D periodic arrays.^{38, 41} Similar to the competitive bundle formation of periodic tiles mentioned earlier (*vide supra*), the process is highly governed by building block concentration, such that low concentration promotes intra-structural folding.⁶⁹ Another important factor influencing direction of the assembly process is the flexibility of the building blocks. It has been shown that greater flexibility in the structural motif promotes preferential formation of 3D constructs over 2D periodic networks.⁷² Related to this topic is the extensive study of a truncated octahedral DNA cage, formed with unpaired thymines at the vertices providing conformational flexibility.^{70, 75-77} By varying the number of thymines it was concluded that three unpaired bases at the vertex constituted the minimal linker length necessary to allow formation of the desired nanostructure.⁷⁰ This study has an interesting correlation with the hexagonal DNA nanostructure featured in this thesis (Paper I). The successful formation of this construct, with two unpaired thymines, may be assigned the lower level of structural complexity.

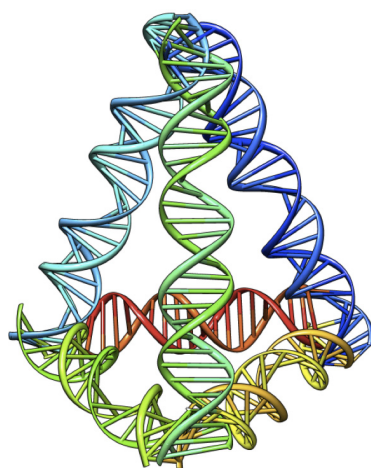


Figure 2.9. DNA tetrahedron. The vertical edges are 30 bases long and the horizontal edges are 20 bases long. Adapted from Turberfield *et al.* (2005).⁶⁸

The construct that has gotten the most recognition of the 3D solitaires published so far is perhaps the DNA tetrahedron (Figure 2.9), which was presented by Turberfield and co-workers for the first time in 2004.⁷⁸ The group later showed

that the assembly could be made chiral specific, in a study also including an imposing AFM-based test of mechanical compression.⁶⁸ The construct was formed at high yield (95%) in a one-step annealing process of four oligonucleotides, rendering edge-lengths of either 20 or 30 bp. Enzymatic ligation could, after hybridization, covalently seal this 3D nanostructure with sides on the order of 10 nm. The relative facile path to a 3D nanostructure with substantial structural complexity has made other scientist adopt the tetrahedron as a model system for functionalization studies of DNA nanostructures. Alivisatos *et al.*⁷⁹ demonstrated 3D arrangement of gold nanoparticles (AuNP) and Armitage *et al.*⁸⁰ created a highly fluorescent nanostructure using the intercalating dye YOYO, both based on the tetrahedron nanostructure. Yan *et al.*⁸¹ showed that a tetrahedral DNA nanostructure could be amplified using in vivo replication. The construct has also been subject to a number of systems with switchable character, including photo-responsive azobenzene⁸² and hybridization energetic “DNA-fuel”⁸³ (*vide infra*).

The main focus of these DNA solitaires has been in terms of nanoscaled cages. Various polyhedra have been utilized as molecular capsules, encapsulating single proteins⁸⁴ or AuNP⁸⁵. In a recent study, the potential of employing DNA nanocages as delivery vectors to mammalian cells was investigated.⁸⁶

All structures discussed so far have exclusively been based on normal oligonucleotides of various lengths. However, with chemical tools it is possible to synthesize artificial junctions that can direct the geometry of assemblies, based on the symmetry of the chemical motif. Especially Sleiman and co-workers has successfully developed this strategy, closely related to traditional supramolecular chemistry.⁸⁷ Using various rigid organic vertices, DNA nanostructures ranging from a 2D hexagon⁸⁸ to 3D prisms⁸⁹ have been assembled. The latter could also be expanded into tubular structures with adaptable cage sizes.^{90, 91} A similar approach has been followed in the group of von Kiedrowski. Simplistic nanostructures resembling small organic molecules, hence denoted nano-acetylene & nano-cyclobutadiene, could be assembled by creating synthetic branched oligonucleotides.⁹² The group later developed trisoligonucleotides with C_{3h} -linkers, which could assemble into a dodecahedron.⁹³ These systems involving chemical junctions are closely related to the strategy on which this thesis is based.

2.2.3 DNA Origami

The development of DNA origami is the closest to a paradigm shift this young research field has seen. The concept of addressability is a central part of this strategy, as well as in this thesis. The following section will present some recent progress in DNA origami.

DNA origami is a fabrication approach to nanotechnology made famous by Rothemund in 2006.⁶ It is based on controlled folding of a long scaffold DNA molecule into a predetermined shape, much like the Japanese paper art tradition from which it gotten its name. Though Rothemund coined the concept of origami in a nanotechnological context, the term has been used before in relations to nucleic acids. In 1994 Williamson referred to RNA origami concerning an algorithm to predict folding of a HIV binding sequence.⁹⁴ Despite the fact that both used the

same term, the expressions are conceptually different. The concept of folding a scaffold strand has also been exploited in structural nanotechnology previously. In 2003 Yan *et al.* constructed a 1D barcode from building blocks based on folded scaffold strands.⁹⁵ Furthermore, less than a year afterwards, Shih *et al.* presented an octahedron folded from a single-stranded 1.7 kilobase sequence.⁹⁶ Both these studies illustrated the principle of nanoconstruction through means of controlled scaffold folding. Nevertheless, none of them can compete with the impact of the assemble strategy of DNA origami as demonstrated by Rothemund.

The self-assembly approach of DNA origami, as presented by Rothemund, use viral DNA as a scaffold. The scaffold molecule most often used is the genomic DNA of the bacteriophage M13, or more specifically a circular single-stranded sequence of approximately 7.3 kilobases from the virus M13mp18. The folding process is governed by addition of numerous short oligonucleotides, “staple” strands that, by being complementary to specific regions on the scaffold, mediate the transition from a randomly ordered molecule into a desired shape (Figure 2.10). The size of the folded surface is on the order of $100 \times 70 \text{ nm}^2$.

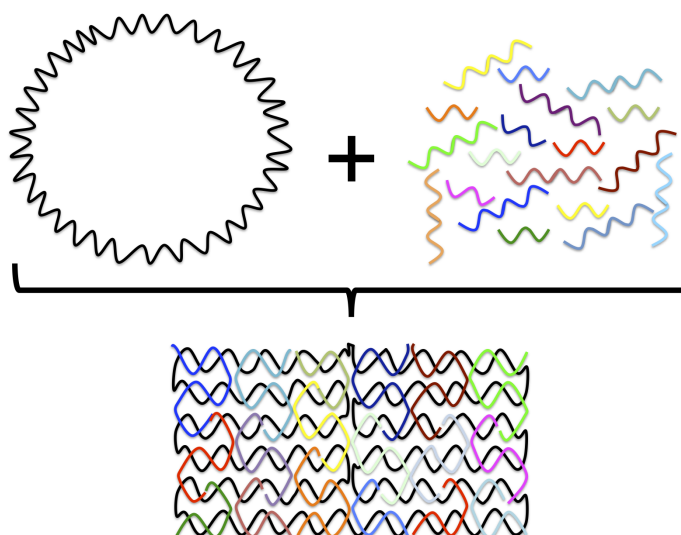


Figure 2.10. Illustration of DNA origami. Addition of numerous staple strands direct folding of a random-coiled single-stranded scaffold into a well-defined geometric shape. This schematic shape has a “seam” in the middle of the sheet. The equivalent structure presented by Rothemund (2006)⁶ is approximately $100 \times 70 \text{ nm}^2$ and utilizes 226 unique staple strands.

Already in the original DNA origami paper several remarkable shapes were assembled, including various triangles, stars, a smiley face and a structure resembling the western hemisphere. This assembly strategy has since then become more spread and a large variety of structures have been constructed based on the same principle of scaffold folding, *e.g.* a dolphin, similar to the 2D shapes of the original paper, was assembled by Andersen *et al.*⁹⁷ It has also been shown that it is possible to extend the assembled surface area by combining multiple folded DNA origami sheets in a tile like manner.^{98, 99} Furthermore, the origami approach is not restricted to single stranded scaffold molecules. Double-stranded scaffolds may also be curbed into

desired patterns by tuning the annealing process and taking advantage of a kinetic bias towards folding as opposed to rehybridization of the fully complementary original scaffold duplex.¹⁰⁰

As more scholars in the field of bottom-up nanoscience have adopted the approach of DNA origami, the knowledge and “nano-engineering” skill has increased and with that also the structural complexity of what has been manufactured. Extending the structural complexity in three dimensions has been achieved by a number of different groups, using slightly different approaches. The group of William Shih has developed a strategy for structural design in 3D involving packing the DNA helices of the origami sheet in pleated multilayers. With this design they have been able to assemble various bundle-type 3D geometries with a more or less solid composition.¹⁰¹⁻¹⁰³ In contrast to these compact constructs, it has also been shown that it is possible to assemble hollow containers using the folding technique of the M13 genome. The principle is the same as in the original origami paper, but the governing staple strands directs the architectural folding into sections, making up the sides of the final 3D structure. Adopting this approach, a tetrahedron has been manufactured in the group of Hao Yan,¹⁰⁴ as well as a cubic box, presented by two groups independently, one in Japan¹⁰⁵ and the other in Denmark¹⁰⁶. The architectural complexity of these structures is quite remarkable and the structural control on the molecular scale is still increasing. In 2010, Yan and his coworkers demonstrated formation of a Möbius strip using the origami approach and furthermore illustrated subsequent topological reconfiguration through strand displacement, analogous to the Japanese paper cutting technique “kirigami”.¹⁰⁷ Despite the progress of DNA origami from 2D to 3D, one should also bear in mind that the octahedron presented by Shih *et al.*⁹⁶ in 2004 was an example of scaffolded folding in 3D, assembled before Rothemund made the concept of DNA origami famous.

The addressable features of DNA-sheets folded by the origami technique have become the focus of many studies involving site-specific localization of functional units. Knowing the relative position of all 226 unique staple strands used in the $100 \times 70 \text{ nm}^2$ “seamed” sheet, presented in the original origami paper,⁶ provides an enormous opportunity for high-precision functionalization. Tinnefeld and coworkers positioned fluorophores on an origami structure and thus generated a nanoscopic ruler for calibration of super-resolution microscopy.¹⁰⁸ Later, a photonic pathway across a sheet was demonstrated, based on the same idea of precise fluorophore localization.^{109, 110} The principle of addressability in the context of DNA origami has also been utilized to position protein entities¹¹¹ and AuNP¹¹², at specific targets. Site-specific integration of AuNP has also illustrated strong plasmonic circular dichroism, which arises when nanoparticle-dressed sheets are rolled up forming chiral bundles.^{113, 114} Yet another example where addressability has been employed is the demonstration of assembly line for chemical reactions on the single-molecule level. This principle was illustrated by Gothelf *et al.*¹¹⁵ and Seeman *et al.*¹¹⁶ in two related studies. The latter involved a so-called DNA walker, which will be discussed in the following section (*vide infra*).

2.2.4 DNA Nano-Machines & Mechanical Devices

This section is intended to shed light on dynamic DNA-based systems aiming at nanomechanical devices, since this thesis also include a switchable function using triplex recognition.^{VII}

The structural DNA nanotechnology focuses on static constructs with features such as stability, integrity and rigidity, following in the footsteps of Seeman. Alongside this pathway scientist have investigated the possibility of using DNA in dynamic systems, as molecular mechanical devices or motors. This is yet another aspect of the DNA molecule as a functional unit, *i.e.* as an agent of change. Even though it is the structural features that make the biopolymer ideal for rigid architectures, they may also be used to create motion. Only a few years after Seeman had demonstrated the use of crossover junctions as structural motifs, he presented one of the first DNA based nanomechanical devices, where motion was induced by a structural shift of the double helix.¹¹⁷ By changing the ionic composition of a solution, it is possible to convert DNA from the normal right-handed B-DNA to a left-handed Z-DNA conformation. Thus, by switching the ionic strength it was shown that a twisting motion could be induced in a simple device, based on this conformational shift. This device was a DNA based nanomachine driven by changes in ionic composition as fuel. However, DNA may in itself also function as fuel, driving molecular motors. Nature relies on the nucleotide monomer adenosine triphosphate (ATP) as the universal “fuel of life”, to power the molecular machinery in the cell. It is not merely the chemical energy in the phosphodiester bond that makes DNA a potential fuel. The free energy of hybridization associated with two complementary DNA polymers engaging in helix formation may be utilized as driving force in dynamic processes. Strand displacement plays an important part in genomic regulation of living systems, *e.g.* in gene repair through genetic recombination (recombinases).

^{VII} The related topic concerning DNA computers & logics will not be discussed. Interested readers are encouraged to seek out the work of Leonard M. Adleman, Erik Winfree and Milan N Stojanovic, as well as ‘The Molecular Programming Project (MPP)’ (molecular-programming.org).

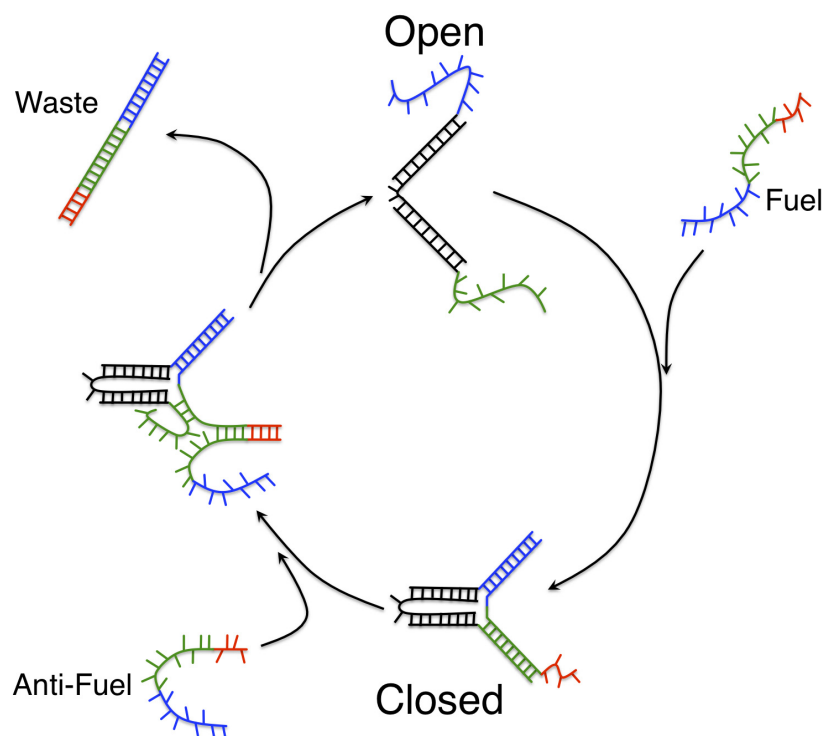


Figure 2.11. Schematic of a device driven by “DNA-fuel”. The molecular tweezers shift from “open” to “closed” state upon addition of the “fuel” strand that is complementary to the dangling ends of the “open” structure (green and blue). The “closed” structure contains a “toehold” sequence (red) that promotes hybridization with the “anti-fuel” strand, resulting in release of a totally double-stranded “waste” product and a return to the “open” state of the device. Adapted from Yurke *et al.*¹¹⁸

The nanotechnological employment of DNA as fuel relies on the same principle of strand displacement. If a DNA sequence is hybridized with its complementary but truncated counterpart, the single-stranded overhang or “toehold” that is created may be used as a driving force for strand displacement. By introducing the fully complementary sequence to the system, a new equilibrium will be reached where this sequence will replace the truncated counterpart. By designing a series of similar states of non-equilibrium, movement may be generated. The first illustration of this concept was in a device of “DNA-tweezers” that was presented in 2000 (Figure 2.11). The tweezers could be switched between the “open” and “closed” state by sequential addition of “fuel” and “antifuel” strands.¹¹⁸ From each step there is an accumulation of “waste-product”, *i.e.* the fuel-antifuel duplex. The approach of using toehold to drive conformational change was also employed by the Seeman-group to power a topological switch in a crossover motif, illustrating the possibility to create both robust and dynamic nanostructures using DNA.^{119, 120} Since then other metastable conformations of DNA have been investigated as hybridization driven molecular machines. The equilibrium balance between hairpin and linear duplex from the perspective of fuel in molecular machines has been explored in studies by Turberfield and co-workers.^{121, 122} The results suggest among other things that there are kinetic variations of the strand displacement reaction dependent on *e.g.* loop length and toehold position, differences which could be

exploited in DNA based machines. The idea of utilizing the energetic difference between a hairpin and a linear duplex in an application had been shown in another context before. A fluorescent molecular beacon for gene detection, based on opening of a hairpin structure, had been presented in 1996.¹²³ It may be seen as the first DNA device based on hybridization energy, though the purpose of that study was different.

DNA-based nanodevices that run on other sources of “fuel” have been explored as well. With incorporation of photochromic functionalities, *i.e.* units that isomerize upon absorption of photons, conformational change may arise through the irradiation of light. One example is a photon-driven version of the DNA-tweezers, which change state due to the photo-controlled cis-trans isomerisation of azobenzene moieties’. The planar trans-form of this photochrome intercalates in the base-stack and stabilizes the double helix. Upon irradiation of UV-light the photochromic molecule isomerizes to cis-azobenzene, which due to steric reasons destabilizes the duplex. The conformational change may be reversed with irradiation of blue light, thus a photon-driven nanomechanical device is created.¹²⁴

Another pathway in the development of DNA nanomachines follows the same principal as the B/Z-switch, *i.e.* conformational change induced by ionic interactions. The molecular properties of a polyelectrolyte like DNA are highly influenced by ionic interactions, *e.g.* the persistence length of the polymer is inversely dependent on the ionic strength of the solution. Furthermore, there are some specific structural conformations that DNA can adopt dependent on ionic interactions, such as the G-quadruplex.¹²⁵ By controlled variations in the environment of a DNA construct and the consequential conformational transition, molecular motion may be induced. There are several examples in the literature of devices where addition of specific ions induces conformational change, which is reversed with the addition of chelating agents, *e.g.* Sr^{2+} regulated duplex to G-quadruplex transition and sequential addition of EDTA reversing the motion.¹²⁶ Another example of an ion-dependent conformational change that has been explored is Mg^{2+} induced DNA supercoiling, which has been used to control geometries of DNA-nanoparticle networks.¹²⁷ Analogues to the possibility to form G-quadruplexes with guanine-rich sequences, cytosine-rich sequences may form tetraplex structures known as I-motifs, based on C-C⁺ basepairing.^{128, 129} This is a pH-sensitive conformation, because one cytosine base has to be protonated in order to form a stable pair with another cytosine. Thus, it may constitute a mechanism for a conformational driven DNA nanomachine, fueled by protons. The concept of the I-motif based machine was first demonstrated in 2003 by Balasubramanian *et al.*¹³⁰ and has since then been further explored by Simmel *et al.*^{131, 132} and Krishnan *et al.*¹³³. The former developed autonomous motion through pH oscillations and the latter demonstrated a pH-sensitive molecular device that could probe acidic conditions *in vivo*. Another pH-dependent conformational change that has been used in this context is the duplex-triplex transition, which also depends on the protonation of cytosine. At low pH, cytosine is protonated and able to bind to guanine *via* Hoogsteen base-pairing (*vide supra*), forming a CG*C⁺ triplet, while binding through

normal Watson-Crick base-pairing at elevated pH. A machine based on transition between these two states was presented by Mao *et al.*¹³⁴

The DNA nanomachines so far discussed are all examples of devices with repetitive changes of state in a back and forth manner, but there are also examples where a DNA based nanomechanical apparatus has induced propagating movement. DNA walkers are a class of nanodevices that have been used by a number of groups to demonstrate concepts of unidirectional motion. In 2004, three separate groups presented different versions of this specific device.¹³⁵⁻¹³⁷ The first two publications (Seeman *et al.* & Pierce *et al.*), though different in structural design, both involved a path-dependent movement of a bipedal walker along a track driven by sequential addition of DNA strands, equivalent to the principle of fuel/antifuel. The third study by Reif *et al.*, on the other hand, demonstrated a walking device that rather than being propelled by hybridization force was under enzymatic control, with alternating use of restriction enzymes and ligases. Hydrolysis of ATP drove the unidirectional motion of this walker autonomously. Since these early proof-of-principle illustrations of propagating DNA transporters, there has been further development of the concept of unidirectional autonomous motion of DNA devices, both with enzymatic^{138, 139} and hybridization driven¹⁴⁰⁻¹⁴² mechanisms. There are specific oligonucleotides that, similarly to DNA cleaving enzymes, can hydrolyze the phosphodiester backbone of DNA, a phenomenon that also has been utilized to drive molecular motion, by incorporation of this sequences in the structure of a device.¹⁴³ The approach of using DNAzymes has also been incorporated in multipedal walkers, denoted “DNA-spiders”,¹⁴⁴ which recently have been shown to move along a specific pathway in two dimensions on a DNA-origami sheet.¹⁴⁵ The DNA spiders were shown to be able to autonomously carry out sequential robotic action such as “start”, “follow”, “turn” and “stop”. Finally, it has also been demonstrated that the principle of directed molecular transportation *via* DNA walkers may mediate multistep organic synthesis analogous to a manufacturing assembly line.¹⁴⁶

2.3 Click Chemistry

This thesis demonstrates how Click Chemistry can be used in DNA nanotechnology to incorporate a fixation strategy for creating robust nanostructures. This section presents the background to this concept.

In 2001, Sharpless^{VIII} introduced a new concept for organic synthesis. The background was trying to direct focus away from research on reactions creating carbon-carbon bonds, and instead aiming at creating C-X-C links, as easy and efficient as possible. The idea was entitled *Click Chemistry*.¹⁴⁷ Sharpless stated a number of criteria for reactions to fulfill in order to be labeled “click reactions”, all dealing with the effectiveness and handling of the chemistry involved. High yield, clean, one-step, and harmless solvents are a few of the stated criteria. Furthermore, the possibility of generalization, *i.e.* to be able to use a reaction as module in molecule creation, is a key element.

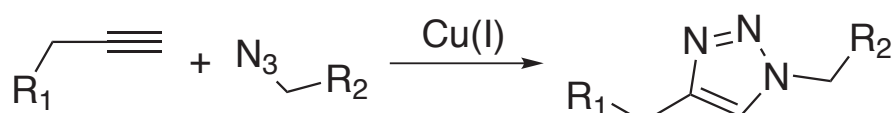


Figure 2.12. Copper(I)-catalyzed [1,3] cycloaddition (CuAAC reaction).

The challenge of finding a reaction fulfilling all criteria may be impossible, but there are candidates sufficiently close in doing just that. The copper(I)-catalyzed [1,3] cycloaddition, between an azide and a terminal alkyne producing a 1,2,3-triazole (CuAAC reaction), is perhaps the most interesting candidate, approaching near-perfect reliability (Figure 2.12). The CuAAC reaction was developed by Sharpless¹⁴⁸ and Meldal¹⁴⁹, independently, and has since then been adopted in a variety of contexts. The exact mechanism is not completely understood despite extensive research, including theoretical calculations and crystallographic studies, but a suggested plausible mechanism is presented in Figure 2.13.^{150, 151}

^{VIII} K. Barry Sharpless was awarded the Nobel Prize in Chemistry 2001 "for his work on chirally catalysed oxidation reactions". The prize was divided, and the other half was jointly awarded William S. Knowles and Ryoji Noyori "for their work on chirally catalysed hydrogenation reactions". (www.nobelprize.org/nobel_prizes/chemistry/laureates/2001/)

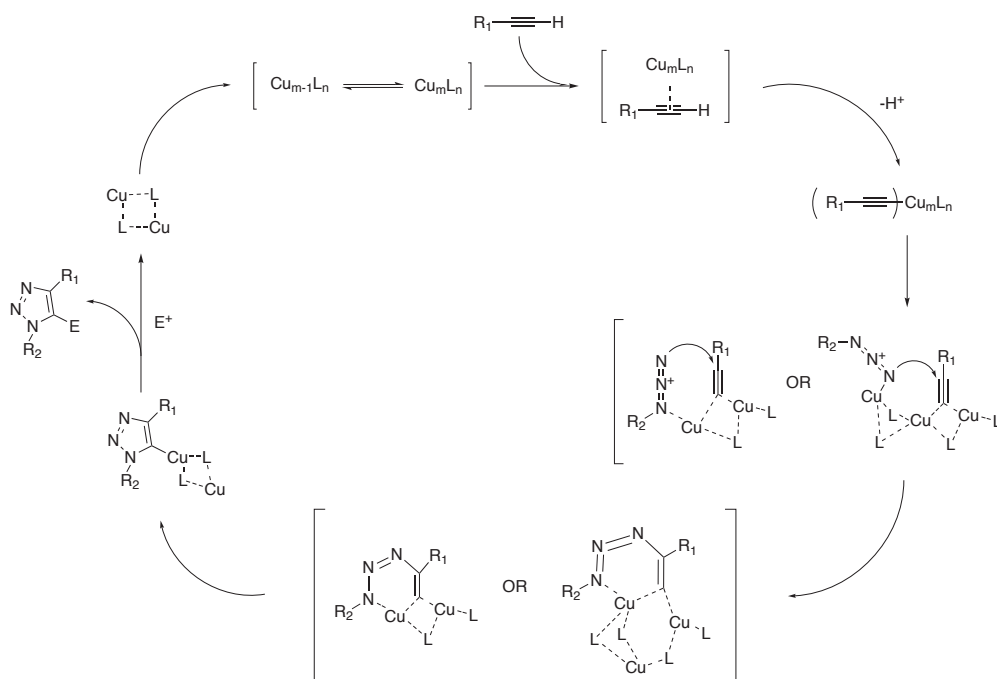


Figure 2.13. Plausible mechanism of the CuAAC reaction. Adapted from Meldal (2008).¹⁵⁰ Though the reaction works with bare Cu(I), either by direct addition (e.g. CuI) or indirect by reducing Cu(II) (e.g. CuSO₄ and NaAsc as reduction agent), advantages with coordinated ligands have been reported. Ligands have been seen to enhance the rate as well as protect the Cu(I) from oxidation into the inactive Cu(II) in contact with oxygen.¹⁵²

The diversity of areas where the CuAAC reaction has been applied spans an impressive collection of applications. Many applications of click chemistry can be found in the field of drug discovery, as Sharpless envisioned.¹⁵³ However, there are other interesting examples worth mentioning. For instance, by designing branch points of azides and alkyne impressive triazole-based dendrimers have been created.¹⁵⁴ ¹⁵⁵ The click chemistry approach has also been adapted for peptide modifications, especially in the field of peptidomimetics, replacing naturally occurring groups by synthetic counterparts.¹⁵⁶ The triazole can link amino acids together, replacing the amide bond or be used to functionalize the peptide or connect it to some other structure. Among the more important advantages of using the CuAAC reaction in this context is the insensitivity towards amino acid side chains. Click chemistry has even been carried out *in vivo*. One example is protein labeling done in mammalian cells for activity-based profiling.¹⁵⁷ Although the reaction mostly has been carried out in solution, there are also studies of surface modifications using click chemistry. Surfaces have been successfully functionalized *via* triazole linkages on a variety of materials (e.g. polymers, glass and gold). Both azide and alkyne modified templates can be used, but there seems to be a slight advantage in placing the alkyne on the surface.¹⁵⁸ Various biomacromolecules have also been immobilized on surfaces using click chemistry, e.g. oligonucleotides, creating functional microarrays.^{159, 160} A thorough and extensive summary of the research on click chemistry, including the variety of usages, can be found in the review by Meldal & Tornøe 2008.¹⁵⁰

The use of CuAAC on DNA has already been mentioned in the framework of surface modifications. However, there are other areas worth broaching in the field of nucleic acid research where click chemistry has been applied. Various functionalizations, such as fluorophores, can be attached using triazole linkages,^{161, 162} with azide or alkyne modifications at the desired location an obvious prerequisite. For instance, click chemistry was used to attach the Alexa dyes to oligonucleotides in the energy transfer study of this project. Energy transfer will be discussed in the next section (*vide infra*).

The approach of using click chemistry as a fixation strategy in DNA nanotechnology used in this thesis is based on the work of Tom Brown's group in Southampton. Different covalently linked oligonucleotides have been created by combining azide and alkyne modified oligonucleotides, either in the backbone (5' or 3') or on a nucleobase. Two complementary end-labeled oligonucleotides were assembled and by sequential CuAAC reaction sealed, forming a DNA catenane.¹⁶³ A very stable cyclic DNA miniduplex of just two base pairs has also been formed¹⁶⁴ and a site-specific cross-linking between two complementary oligonucleotides, markedly increased the duplex stability.¹⁶⁵ A more general result about the CuAAC reaction that the studies also show is that positioning the reactants close together in space, minimizing diffusion, maximizes the kinetics of the reaction.

2.4 Photophysics

Understanding the interaction between light and matter is crucial for spectroscopic investigation of molecules. This section introduces some basic concepts and, furthermore, theory regarding Förster resonance energy transfer (FRET), a method utilized in this thesis.

The wave-particle duality of light, arising from the failure of classical physics to explain empirical phenomenon such as black body radiation, is necessary in understanding how light interacts with matter. Light can on one hand be depicted as a travelling sinusoidal wave, classically described as electromagnetic radiation. As the name entails there are two contributions: one electric (E) and one magnetic (B), fundamentally interconnected. The two components form perpendicular waves propagating through space at the speed of light.

$$E(x,t) = E_0 \sin(kx - \omega t) \quad (2.1)$$

$$B(x,t) = B_0 \sin(kx - \omega t) \quad (2.2)$$

On the other hand, light is also a discrete unit of energy, *i.e.* a photon behaving like a particle. This description of light arose from empirical findings that the electromagnetic field is quantized, with the energy (E) of the quanta proportional to the frequency (ν) of the radiation field. The factor h is known as Planck's constant.

$$E = h\nu \quad (2.3)$$

Light can under certain conditions interact with matter, *e.g.* a molecule, causing a perturbation in the distribution of electrons, leading to a change of states in that system. The interaction depends first and foremost on the oscillating electric field of the photon and the contribution of the magnetic field may therefore be neglected in this context. A constructive interaction induces an excitation of the molecule, which reaches a state at a higher energy level. The first criterion for a constructive interaction leading to such an excitation is that the energy of the photon corresponds to the energy gap between the initial (i) and the final state (f). This is called the Bohr frequency condition.

$$\Delta E = E_f - E_i = h\nu \quad (2.4)$$

The condition tells us that interactions between light and matter are quantized and take on discrete values. However, the Heisenberg uncertainty principle naturally makes the transition between states less distinct.

The transition between states can be treated quantum mechanically using perturbation theory, where the electromagnetic field is considered a small disturbance causing a shift in the electronic state of the molecule. If the molecule is small compared to the wavelength of the radiation, one can assume that the electric field is uniform over the molecule, and the transition dipole moment may be used to describe the transition.

$$\bar{\mu}_{fi} = \langle \Psi_f | \hat{\mu} | \Psi_i \rangle \quad (2.5)$$

Ψ_f and Ψ_i are the wave functions of the final and initial state, respectively; μ is the electric dipole operator.

$$\hat{\mu} = -\sum_i e_i r_i \quad (2.6)$$

i.e. the sum of all electronic charges (e) at position (r), assuming the nuclei are fixed. Using the transition dipole moment, the probability of transition from an initial state to a final, according to first order perturbation theory, is

$$P_{fi}^{(1)}(t) = \frac{\pi I(\omega_{fi})}{\epsilon_0 \hbar^2 c} |\bar{\mu}_{fi}|^2 t \cos^2 \theta \quad (2.7)$$

$I(\omega_{fi})$ is the intensity of radiation, c is the speed of light, ϵ_0 is the permittivity in free space and θ is the angle between the transition dipole moment and the electric field. The probability of a transition is clearly dependent on the dipole strength as well as its orientation. Connecting the theoretical probability with the observable process of absorption can be done by introducing the molar extinction coefficient, $\epsilon(\nu)$. The molar absorptivity, as it also is called, is a function dependent on the radiation frequency and can be derived by relating the absorption in a cross-section with the energy flux of photons passing it. Not surprisingly the extinction coefficient turns out to be proportional to the transition dipole strength.

$$\int \epsilon(\nu) d\nu = \frac{\pi N_A}{3\epsilon_0 \hbar c} \nu_{fi} |\bar{\mu}_{fi}|^2 \quad (2.8)$$

2.4.1 Excited State Processes

Upon absorption of a photon the molecule is excited to an electronic state of higher energy, most often a singlet state (S_n) since the ground state usually is a singlet. The process of absorption is very fast, in the femtosecond (10^{-15} s) regime, after which a number of processes may be involved relaxing the molecule to its ground state. These processes can be visualized in a Jablonski diagram (Figure 2.14).

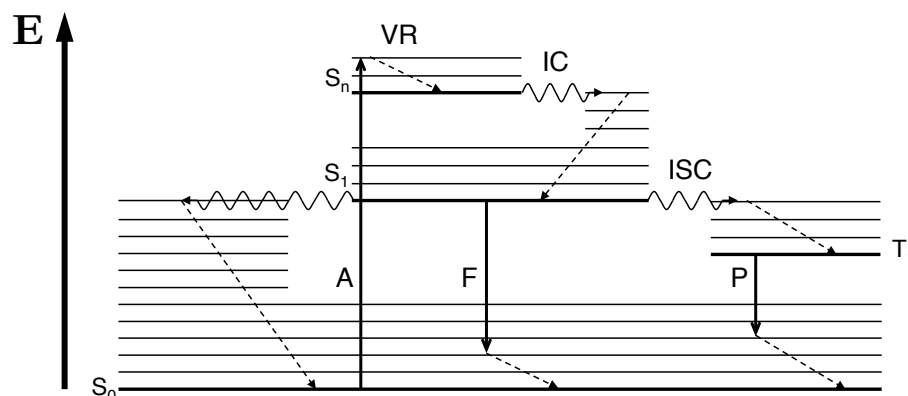


Figure 2.14. Jablonski diagram. All radiative processes are indicated by straight arrows; A represent absorption, F fluorescence and P phosphorescence. Non-radiative processes are represented by dotted arrows or waves; IC is internal conversion, VR is vibrational relaxation and ISC is intersystem crossing. S_n are singlet states and T_n are triplet states, respectively.

There are both radiative, *i.e.* a photon is emitted, and non-radiative processes involved when energy is dissipated from the excited molecule. Non-radiative relaxation processes are usually faster than radiative, which is why most molecules are non-emissive. Vibrational relaxation (VR) occurs when the molecule loses energy by going from higher to lower vibrational levels within a given electronic state. Through internal conversion (IC) a molecule may pass from an excited state (S_n) to a lower state (S_{n-1}) if there is a constructive interaction between them. There is no intrinsic energy change in internal conversion, *i.e.* no energetic driving force, however it is coupled with sub-sequential vibrational relaxation within the lower electronic state. Intersystem crossing (ISC) is another non-radiative process by which an excited molecule can change multiplicity, passing from a singlet (S_n) to a triplet (T_n) state, and vice versa. Changing from a singlet to a triplet state involves a quantum mechanically forbidden spin change. Though a process is denoted forbidden it does not mean that it never occurs just that the probability and therefore the rate is considerably slower. A luminescent molecule may emit a photon after excitation, which involves a radiative process when relaxing to the ground state. The radiative process of passing from S_n to S_{n-1} is known as fluorescence (F). Due to the fact that non-radiative processes are orders of magnitudes faster, fluorescence normally occurs from the lowest vibrational level of S_1 to several vibrational levels of S_0 . This leads to the common mirror image relation between absorption and emission. When passing from the triplet state (T_1) to the

singlet ground state (S_0), phosphorescence can occur, an analogue to fluorescence, involving a change in spin. Since phosphorescence involves a quantum mechanically forbidden spin change, it is considerably slower than fluorescence.

There are rate constants associated with all processes, related to molecular parameters as well as the surroundings. This can be used to determine the quantum yield and lifetime, used to characterize fluorescent molecules. The quantum yield of fluorescence (ϕ_f) relates the amount of photons emitted by a molecule through fluorescence to the amount of photons absorbed and it can be calculated by comparing rate constants.

$$\phi_f = \frac{\text{Photons emitted}}{\text{Photons absorbed}} = \frac{k_f}{\sum_i k_i} \quad (2.9)$$

The lifetime (τ) refers to the average time a molecule occupies an excited state. As for quantum yield, the fluorescence lifetime can be expressed in terms of rate constants of the processes involved in the transition from excited state to ground state.

$$\tau_f = \frac{1}{\sum_i k_i} \quad (2.10)$$

2.4.2 Förster Resonance Energy Transfer

Förster Resonance Energy Transfer (FRET) is a specific pathway by which an excited molecule (donor) can lose energy by transferring it to another molecule (acceptor) in the close vicinity. The excitation energy of the donor molecule (D) is transferred to an acceptor molecule (A) *via* dipole-dipole coupling of the transition dipole moments involved. It is important to stress that this is a non-radiative process, *i.e.* no photon is emitted in the process. The process of energy transfer is highly dependent on the spectral overlap between the emission of the donor and the absorption of the acceptor. The overlap is described by the J-integral.

$$J(\lambda) = \int_0^{\infty} F_D(\lambda) \epsilon_A(\lambda) \lambda^4 d\lambda \quad (2.11)$$

F_D is the normalized fluorescence intensity of the donor, ϵ_A is the extinction coefficient of the acceptor and λ denotes wavelength. The rate at which the energy transfer proceed (k_T) strongly depends on the distance between the species (r), reflecting the sharp shift in transfer efficiency (E_T) at a characteristic distance. The Förster distance (R_0) is the characteristic distance of a donor-acceptor pair at which the efficiency is 50%. The rate constant can be calculated in the following manner.

$$k_T = \frac{1}{\tau_D} \left(\frac{R_0}{r} \right)^6 = \frac{\phi_D \kappa^2}{\tau_D r^6 n^4} \left(\frac{9000(\ln 10)}{128\pi^5 N_A} \right) J(\lambda) \quad (2.12)$$

N_A is Avogadro's number, n is the refractive index of the medium, τ_D and ϕ_D are the lifetime and quantum yield of the donor, respectively. κ^2 is the orientation factor, describing the angles between the transition moments of the donor and acceptor. If the involved molecules have complete rotational freedom the factor is $2/3$; r corresponds to the distance between donor and acceptor. As r is raised to the power of 6, the strong distance dependence of the process is indicated. By measuring the transfer efficiency it is possible to calculate the distance between the donor and acceptor with their characteristic Förster distance. The transfer efficiency is given by comparing the emission intensity of the donor molecule, in the presence (I_{DA}) and absence (I_A) of the acceptor, but it may also be calculated using the lifetimes of the system.

$$E_T = \frac{R_0^6}{R_0^6 + r^6} = 1 - \frac{\tau_{DA}}{\tau_D} \quad (2.13)$$

τ_{DA} and τ_D are the lifetimes of the donor, in the presence and absence of the acceptor, respectively.

The strong distance dependence of the efficiency enables the use of FRET as a "molecular ruler". Typically, R_0 varies between 20 and 60 Å, setting the limit of measurable distances to about 90 Å using standard FRET-pairs.

2.5 Lipid Membranes

Lipid membranes are used in this work as part of soft-surface nanotechnology, where DNA nanostructures is tethered to a surface using molecular anchors.

Lipids are a class of amphiphilic molecules, including cholesterol, triglycerides, fatty acids and phospholipids, with a hydrophilic head-group and a hydrophobic tail-group. These naturally occurring surface-active molecules are the main constituents of cell membranes. Through self-assembly in solution they form structural aggregates with a wide morphological spread. Like all molecular self-assembly, it is the structural features of the molecule that govern the morphology of formation. The packing parameter (PP) is an especially important factor, linking the geometry on the molecular level with the shape of the final assembly. This parameter explains the size difference between the two functional groups of a lipid. It is the ratio between the volume, on one hand, and the effective head-group area \times tail-group length, on the other ($PP=v/a_0l$). Lipids may be divided into three classes according to the packing parameter: cone-shaped ($PP<1$), cylindrical ($PP=1$) and inverted cone-shaped ($PP>1$). The two versions of cone-shaped lipids preferentially form assemblies with high curvature, albeit with the opposite orientation. Self-assembly of cylindrical lipids favors formation of flat structures, such as bilayers, and thus also are the most frequent class in cellular membranes (Figure 2.15). Phospholipids are almost exclusively part of this class. The molecular structure of these lipids is often a diglyceride, with varied hydrocarbon chain length, as the hydrophobic tail-group. The hydrophilic head-group is usually composed of a phosphate in combination with another small organic unit, *e.g.* choline. The combination with the phosphate-group affects the size of the head-group as well as its charge. Phosphocholine lipids are zwitterionic at physiological pH and an example of this type of lipid is 1,2-dioleoyl-sn-glycero-3-phosphocholine (DOPC), exclusively used in this project. The thickness of the assembled bilayer is correlated with the chain length of the hydrophobic tail-group, yielding in the case of DOPC a thickness of roughly 4.5 nm. The degree of saturation of the hydrocarbon chains also affects the nature of the bilayer. It is important to keep in mind that self-assembled structures such as lipid bilayers are highly dynamic, rendering fluctuating boundaries.¹⁶⁶

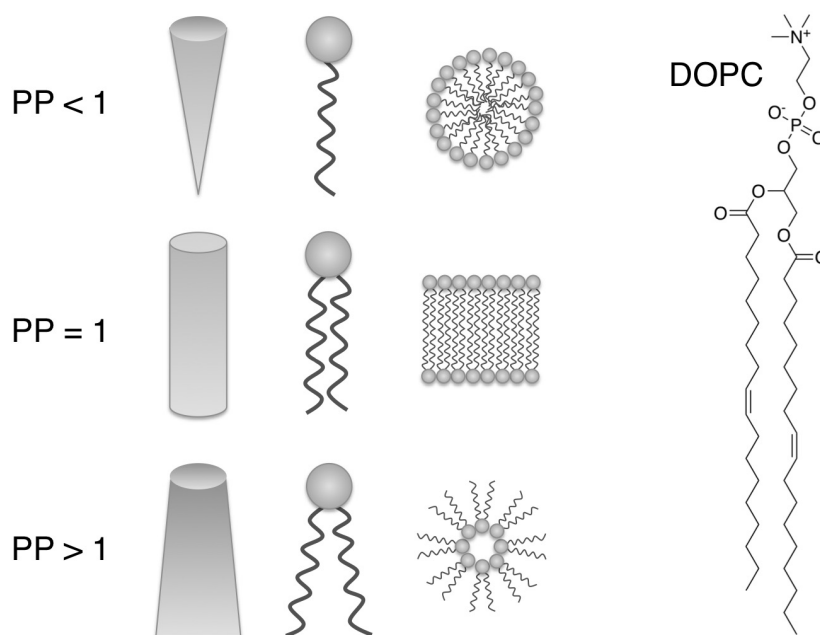


Figure 2.15. (Left) Illustration of the interplay between shape of a lipid (*i.e.* packing parameter, PP) and the geometry of the assembly. $PP < 1$ promotes micelles; $PP = 1$ lamellar phases such as bilayers; $PP > 1$ inverted micelles. (Right) Chemical structure of the zwitterionic phospholipid used in this thesis, 1,3-bis(sn-3'-phosphatidyl)-sn-glycero-3-phosphocholine (DOPC).

The morphology of lipid assemblies depends on one hand on the packing parameter of the lipid, but also on other system parameters such as lipid concentration. Lipid systems may exist in a number of different phases, such as micelles, lamellar, hexagonal or cubic. The lipid bilayers of the lamellar phase may, under certain conditions self-enclose, forming spherical unilamellar lipid vesicles, *i.e.* liposomes. The structural analogy with cell membranes makes liposomes a reoccurring model system in biophysical studies. Liposomes may be divided into three size regimes, though there is a lack of consensus concerning dimensional limits of these regimes in the literature: small (SUV, < 100 nm), large (LUV, > 100 nm) and giant unilamellar vesicles (GUV, $> 1 \mu\text{m}$).

2.6 Self-Assembly

The concept of self-assembly is an important topic and absolutely central for this thesis. This section will provide a brief discussion about this subject.

Variations of the term self-assembly (*e.g.* self-organization, self-construction, self-creation) have appeared in a number of different scientific contexts such as astrophysics (galaxies, solar systems), meteorology (weather patterns) and economics (market organization), with the common denominator being description of an emergence of spontaneous order in a system. Though related, these phenomena are not equivalent with self-assembly from a molecular science perspective.

Self-assembly is a process where an ordered structure is spontaneously formed from a disordered system of subunits, directed by specific interactions between the components in absence of external interference. It is important to bear in mind that the spontaneous organization of the components is an apparent decrease of disorder of the system; self-assembly must obey the second law of thermodynamics. There are a number of keystones describing a self-assembling system, characteristics that distinguish this process from general formation (adapted from Whitesides (2002)¹⁶⁷). (1) The components that are involved in the process are initially in a state of disorder but have specific properties that favor constructive interactions between the components at a local level. The components need not be separate entities, randomly linked units forming a final state of higher order is also a process of self-assembly, *e.g.* protein-folding. (2) Interactions between the components are of relatively weak nature, *e.g.* hydrogen bonds, van der Waals and dispersion forces. Furthermore, (3) the assembly processes must be reversible which is correlated with the weaker interactions between components. (4) The environment of the process plays a key part, mainly for entropic reasons. The solvent, in which the process occurs, pays the entropic cost of spontaneous organization of the subunits. Finally, (5) components must have free mobility in order to interact properly. Motions towards possible self-assembly are driven by diffusion. *E.g.* aggregation as a result of sedimentation should not be considered a process of self-assembly according to this criterion. On a chemical level, the subunits are molecules that interact through non-covalent forces based on the structural properties of the molecular entities. The strength of these non-covalent interactions are of the same order of magnitude as the thermal fluctuations that may disrupt the formation, resulting in an assembly with structural integrity yet dynamic motion on the molecular level. The solution in which molecules may self-assemble is an integrated part of the process. Brownian motion allows molecules to come into contact and the solvent directly affects the constructive interaction between the molecules, particularly apparent in the hydrophobic effect of non-polar solvents. The free energy gain of the system by caging lipophilic entities together in solvent shells, originates from the entropic and/or enthalpic favorable state of solvent molecules avoiding direct contact with the assembly of these moieties. Structural assembly of amphiphilic lipids in aqueous solution is one example driven by the hydrophobic effect.

Self-assembly on the molecular level is closely related to other important concepts of chemical science, *i.e.* molecular recognition and supramolecular chemistry, shifting from the traditional emphasis on covalent bonds in chemistry. The former is the phenomenon describing specificity of non-covalent interactions between molecules, yielding distinct intermolecular coupling. The complementarity of the Watson-Crick base pairs in nucleic acids is one example of molecular recognition, which is central for this thesis. The latter is a term, coined by Jean-Marie Lehn^{IX}, defining a research field driven by chemical design utilizing molecular recognition as a tool, providing higher orders of structural complexity.^{168, 169} Molecular recognition patterns may be studied as well as employed with supramolecular chemistry, understanding the connection between chemical structure on the molecular level and the geometric properties of the final structure. Intelligent molecular design can direct self-assembly processes in desired directions towards predetermined structures.

All systems in the realms of biology are governed by principles of self-assembly, from compartmentalization to macromolecule folding. The lipid bilayer (*vide supra*) of the cell membrane is a good illustration of this phenomenon, as is protein folding where primary sequence of covalently linked amino acids set the inception, but it is the intermolecular forces between these entities that induce folding into the final functioning structure. Molecular recognition is especially important in the nucleic acid domain. The high fidelity of the hydrogen bond pattern between adenine and thymine on one hand, and guanine and cytosine on the other is the basis of the precision in DNA duplex formation, a reason for the reliable information-storage of the genetic code.

Inspired by the structural precision of biological self-assembly, the ideas of supramolecular chemistry have expanded in molecular science, striving towards large-scale systems assembled from the bottom-up with potential nanotechnological applications. Understanding of the connection between chemical structure and molecular recognition patterns, intermolecular assemblies can be controlled with high precision. This is the guiding principle of this thesis. The next chapter will demonstrate how this principle is put into practice, using self-assembly to construct of an addressable DNA nanonetwork.

^{IX} Awarded the Nobel Prize in Chemistry 1987 together with Donald J. Cram and Charles J. Pedersen "for their development and use of molecules with structure-specific interactions of high selectivity" (www.nobelprize.org/nobel_prizes/chemistry/laureates/1987)

3. Methodology - The Daily Matters

Analytical tools used to gain insight in the studied systems are briefly described in this chapter. More detailed information regarding reaction conditions and other technical aspects related to the presented results can be found in the experimental sections of the appended papers.

3.1 Spectroscopy

The interaction between electromagnetic radiation and matter is utilized in the powerful analytical technique called spectroscopy. Characterization, quantification and the dynamics of processes are examples of what may be studied by analyzing the absorption and/or emission of a sample at different wavelengths. Spectroscopy can be carried out at steady-state conditions or be time-resolved, providing different information about a system. Steady-state measurements of both absorption and emission, in the region of ultraviolet (UV) and visible (Vis) spectral regions, have been used in this project.

3.1.1 Absorption

Chromophores^x are molecules (or part of molecules) that absorb light in the UV-Vis region, responsible for the perceived color of a molecule. Allowing monochromatic light to pass through a sample cell containing one or multiple chromophores, and comparing the intensity before and after the cell at each wavelength, it is possible to extract systematic information, from concentration determination to monitoring dynamic process involving spectral shifts. For example, by continuously measuring absorbance at 260 nm during a temperature increase of a sample containing nucleic acids, the transition from double- to single-stranded form can be investigated.

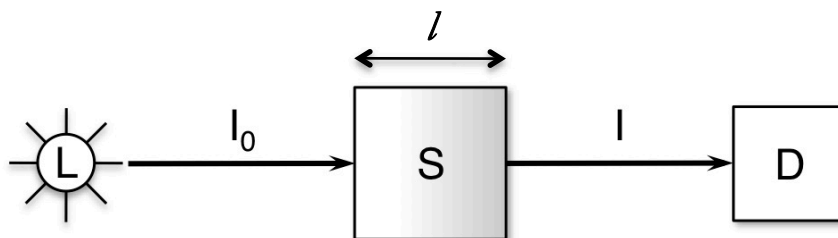


Figure 3.1. Schematic of absorption spectroscopy. Radiation originates from a light source (L) and passes through a sample (S) where some light is absorbed before the beam finally reaches the detector (D). I_0 and I are the intensity of light before and after absorption of the sample, respectively, and l is the path length.

^x Etymology: Greek, 'chromo-' meaning 'colour' and '-phore' meaning 'bearing'

The absorption of a chromophore is measured in the unitless quantity absorbance (A), which is related to the intensity of the incident and transmitted light.

$$A(\lambda) = \log \frac{I_0}{I} = \varepsilon(\lambda)cl \quad (3.1)$$

$A(\lambda)$ is the absorbance at a given wavelength (λ) and I_0/I is the ratio of the intensity before and after the sample, respectively. The relation between the absorbance and the absorbing species, stated above, is known as the Beer-Lambert Law. $\varepsilon(\lambda)$ is the molar extinction coefficient ($M^{-1}cm^{-1}$) related to the transition dipole moment of the molecule, c is the concentration of the chromophore (M), and l is the path length of the sample cell (cm).

The sample is normally isotropic and the radiation unpolarized leading to directionally randomized interactions. There are, however, other techniques that analyze samples using circular or linear polarized light. Linear dichroism (LD) is such a spectroscopic technique where orientation is the important parameter (*vide infra*).

3.1.2 Fluorescence

The corresponding term to chromophore for fluorescent molecules is fluorophore. An emission spectrum of a sample is generated by recording the fluorescence intensity as a function of wavelength, upon excitation of the fluorophore. The basic setup is similar to that of absorption, but the emission is normally collected at an angle perpendicular to the excitation light path to avoid stray light.

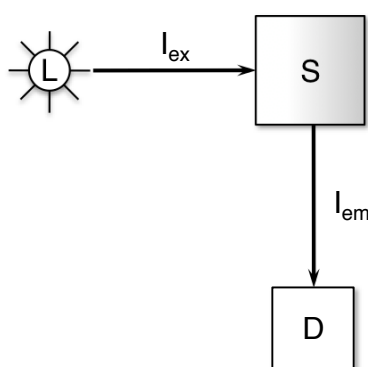


Figure 3.2. Schematic of emission spectroscopy. Radiation originates from a light source (L) and excites the sample (S) which emits if the species is emissive. The emitted light is collected perpendicular to the excitation light by a detector (D). I_{ex} and I_{em} are the intensity of excitation light and emission light, respectively.

The fluorescence quantum yield (ϕ_f) is a characteristic property of a fluorophore determining how efficient an emitter is, relating the amount of photons emitted through fluorescence to the amount absorbed. The quantum yield for an

unknown fluorophore can empirically be determined by comparison with a known specimen (subscript R^{XI}).

$$\phi_f = \phi_R \frac{I}{I_R} \frac{A_R}{A} \frac{n^2}{n_R^2} \quad (3.2)$$

Similar to absorption spectroscopy the system is normally isotropic, as in all fluorescence experiments in this thesis. Though, by orientation of samples and the use of polarized light, information about structural features can be extracted. This is called fluorescence anisotropy.

3.1.3 Linear Dichroism

Linear dichroism (LD) is the differential absorption of two perpendicular planes of linearly polarized light.

$$LD = A_{\parallel} - A_{\perp} \quad (3.3)$$

A system must display anisotropy in order to preferentially absorb light in a certain direction; randomized (isotropic) systems display a net zero LD. If the sample lacks intrinsic alignment, it must be oriented by application of external force. Macroscopic orientation of a system can shift the organization of molecules into ordered arrangements resulting in preferential absorption of either light vector. If the transition dipole moment is known, linear dichroism can give information on molecular orientation within the aligned system. There are a number of ways to obtain molecular alignment.¹⁷⁰ Small asymmetric molecules (*e.g.* anthracene) may orient in stretched films, trapped in the matrix of the polymer (*e.g.* polyvinyl chloride). Electric or magnetic fields, depending on molecular susceptibility, are other examples of ways to induce alignment. Orientation due to shear forces is the most versatile method for alignment of macromolecules with high aspect ratios, and also the modus used in the LD experiments of this thesis.

The sign of the LD-signal gives a first estimation of molecular orientation in an aligned sample. However, in order to obtain quantitative data of the angular orientation of a specific molecule, LD needs to be made independent of concentration and path length. The reduced linear dichroism (LD^r), *i.e.* LD normalized with the isotropic absorption, relates the direction of the transition dipole moment to the orientation axis.

^{XI} The reference fluorophore should have similar spectroscopic properties as the unknown specimen

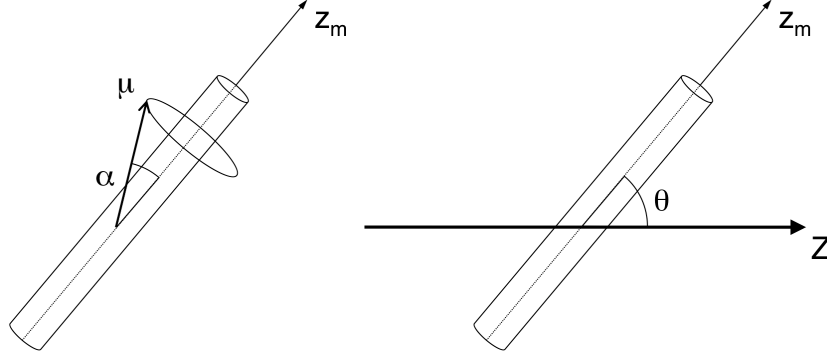


Figure 3.3. Geometry for uniaxial orientation of a rod-like molecule. Z is the macroscopic orientation axis; z_m is the molecular orientation axis; μ is the transition dipole moment.

For a sample with uniaxial orientation, where the molecular transition moment is at an angle, α , from the macroscopic orientation axis and where orientations with respect to the azimuthal angle are equally probable (Figure 3.3), the LD^r can be expressed in the following way:

$$LD^r = \frac{A_{\parallel} - A_{\perp}}{A_{iso}} = S(\theta)O(\alpha) = \frac{3}{2}S(3\cos^2 \alpha - 1) \quad (3.4)$$

where S is the orientation factor. The factorization of LD^r and introduction of S is a convenient method to account for imperfect alignment, separating the degree of macroscopic alignment (S) from molecular orientation (O). The orientation factor is defined based on an angle, θ , between the macroscopic orientation axis and the molecular orientation axis (Figure 3.3).

$$S = \frac{1}{2}(3\langle \cos^2 \theta \rangle - 1) \quad (3.5)$$

S is 1 for perfect orientation and 0 for isotropic samples. It should also be pointed out that the brackets indicate orientational average of an ensemble, due to dynamic systems. The same approach may be applied on equation 3.4, depending on if the molecule is rigid with a well-defined transition moment orientation or flexible with conformational freedom motivating an ensemble approach (*e.g.* DNA).

Many aligned systems are complex, preventing their description in terms of a uniaxial arrangement around the macroscopic orientation axis. Lipid vesicles oriented in shear flow is one example of special interest in this context, as it was studied in Paper VI. Lipid vesicle orientation in shear flow originates from deformation of the vesicles into ellipsoidal shapes.¹⁷¹ This deformation is small but renders the system oriented enough to enable measurement of preferential absorption of chromophores associated with the membrane. Figure 3.4 depicts a model of a deformed lipid vesicle. The vesicle is separated into a perfectly aligned cylinder and two isotropic half-spheres. In a lipid bilayer, the membrane normal

defines the axis around which molecular orientation is related. This can be accounted for considering a biaxial system.¹⁷² A system of this nature may be described by defining two angles. Firstly, the angle between the transition moment and the membrane normal is denoted α . Secondly, β is the angle between the membrane normal and the long-axis of the deformed vesicle. The latter assumed parallel to the macroscopic orientation axis.

$$\begin{aligned} LD^r &= 3S\left(\frac{1}{2}(3\langle\cos^2\alpha\rangle-1)\right)\left(\frac{1}{2}(3\langle\cos^2\beta\rangle-1)\right) \\ &= \frac{3}{4}S(1-3\langle\cos^2\alpha\rangle) \end{aligned} \quad (3.6)$$

The right equality holds for $\beta=90^\circ$, rendering the second factor in equation equal $-1/2$. This is true assuming an infinitely elongated vesicle (*i.e.* tube) and that any deviation of membrane plane from this geometry can be condensed into the orientation factor S .

The orientation factor may be experimentally calibrated using a probe with known membrane orientation. Retinoid chromophores (vitamin A derivatives) can be utilized for this purpose, having slightly red-shifted absorption compared to biomolecules, such as nucleic- and amino acids ($\lambda_{\max} \sim 350$ nm). Retinoic acid in particular has been shown to bind parallel with the membrane normal. By aligning with the lipids in the bilayer, $\alpha=90^\circ$ and the degree of orientation in the system is directly determined by LD^r of the probe.¹⁷³

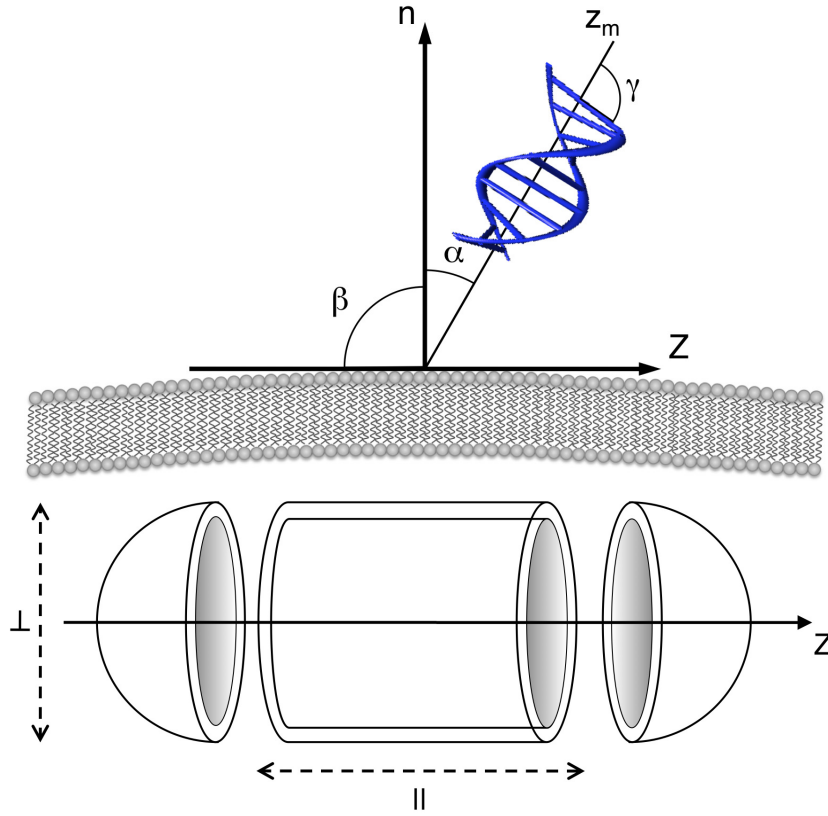


Figure 3.4. (Top) Angles describing DNA in respect to an oriented lipid vesicle surface. Z is the macroscopic orientation axis; z_m is the molecular orientation axis; n is the membrane normal. The long-axis of the deformed liposome is assumed parallel to Z . (Bottom) Model of a deformed lipid vesicle. The vesicle is separated into a perfectly aligned cylinder and two isotropic half-spheres. Dashed lines represent orientation of parallel and perpendicular polarized light in respect to the deformed vesicle.

In the specific case of DNA oriented with respect to the surface of a macroscopically aligned lipid vesicle, as studied in Paper IV, additional formalism needs to be introduced (Figure 3.4). The reason is that the transition moment of the chromophores in DNA is disparate from the molecular axis of its helix, since it is the nucleobases that absorb light. To account for this, a third angle between the DNA helix axis and the base-stack, denoted γ , is introduced. The angle α in equation 3.6, now denotes the angle between the helical axis and the membrane normal, *i.e.* the orientation of DNA that one wishes to determine. This results in the following expression:

$$\begin{aligned}
 LD^r &= \frac{3}{4} S(1 - 3\langle \cos^2 \alpha \rangle) \left(\frac{1}{2} (3\langle \cos^2 \gamma \rangle - 1) \right) \\
 &= \frac{3}{8} S(3\langle \cos^2 \alpha \rangle - 1)
 \end{aligned}
 \tag{3.7}$$

The second equality holds for the same assumption as in the equation above and with the new factor also set to $-1/2$ ($\gamma=90^\circ$). This is a good approximation, as the effective angle γ between the helix axis and the various in-plane transition moments in nucleobases^{xii} is 86° in the helical stack of B-DNA.^{174, 175}

One can consider two extreme cases where the DNA molecule is either protruding from or perfectly aligned with the membrane surface ($\alpha=0^\circ$ and 90°). This gives rise to the following theoretical LD^r values:

$$\alpha = 0^\circ \quad \Rightarrow \quad LD^r = \frac{3}{4}S \quad (3.8a)$$

$$\alpha = 90^\circ \quad \Rightarrow \quad LD^r = -\frac{3}{8}S \quad (3.8b)$$

Notable is the asymmetric relation in LD^r values, where the positive signal of the protruding arrangement gives rise to twice the value of the opposite arrangement.

Specific instrumentation is needed in order to obtain shear flow alignment, enabling LD measurements of this nature. Shear can be induced in a Couette cell¹⁷⁶ consisting of two concentric quartz cylinders (Figure 3.5). One cylinder rotates with a certain shear rate, while the other is stationary. This motion creates a laminar shear flow in the gap between the cylinders (0.5 mm in the cell used in Paper VI) resulting in alignment of the sample, due to the shear forces. An addition of sucrose (50% w/w) to the sample buffer plays an important role in flow alignment of lipid vesicles. First and foremost, light scattering is substantially reduced due to matching of refractive indices between sucrose buffer and lipid vesicles. An additional effect is an increased viscosity resulting in augmented orientation of the vesicles.¹⁷¹ The orientation factor is typically on the order of 0.05 for deformed vesicles.

^{xii} Averaged by their \cos^2 values

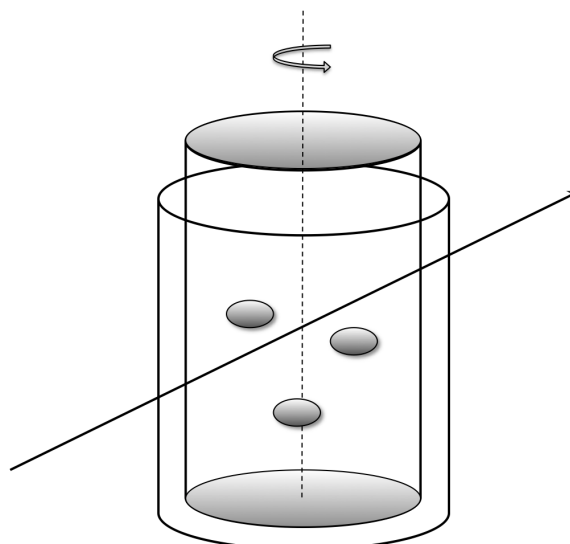


Figure 3.5. Schematic of a Couette cell. Orientation of lipid vesicles by the laminar shear flow between two concentric cylinders, where one rotates and the other is stationary. The arrow passing through the cell represent the incident polarized light.

3.2 Dynamic Light Scattering

Dynamic light scattering (DLS) is a method used to determine particle size and distribution of colloidal systems. The principle is measuring the intensity fluctuations of scattered light that arise when a particle suspension in Brownian motion is radiated with coherent, monochromatic light^{XIII}. A difference between refractive index of particles (n_p) with that of the solvent (n) renders elastic scattering of the incident light, *i.e.* Rayleigh scattering, in all directions. Upon interaction with the particles, the originally uniform phase of the photons will shift depending on the interparticle positions and the relative direction to the detector, *i.e.* the scattering angle θ ^{XIV}. The difference between incident and scattered wave is referred to as the scattering wave vector, denoted q . The magnitude of this vector depends on the refractive index, the wavelength of the incident photon and the scattering angle related by Bragg's law.

$$|\vec{q}| = \frac{4\pi n}{\lambda} \sin\left(\frac{\theta}{2}\right) \quad (3.9)$$

Fluctuations in interference of the scattered light arise when diffusion causes variation in interparticle positions, resulting in time-dependent scattering intensity by the interplay of constructive and destructive interference. By monitoring these alterations in the coherence pattern at the detector, correlated with particle

^{XIII} Typically He-Ne laser light with $\lambda=633$ nm

^{XIV} Between 0° and 180° .

movement, the diffusion coefficient of the system may be extracted. To this end, an intensity autocorrelation function for the fluctuating light intensity is constructed, finding repeating patterns in the signal itself.

$$g^{(2)}(q, \tau) = \frac{\langle I(t)I(t + \tau) \rangle}{\langle I(t) \rangle^2} \quad (3.10)$$

Brackets represent an average over time and τ denotes the time delay. The intensities are almost the same for small τ when the interparticle positions are nearly conserved, yielding high correlation. In contrast, for large τ the particles have diffused to a point virtually independent of their initial positions, hence low correlation. The diffusion coefficient of a system is an important parameter determining this time-dependent exponential decay. The Siegert equation relates a measured $g^{(2)}$ -function to the level of diffusion:

$$g^{(2)}(q, \tau) = 1 + |g^{(1)}(q, \tau)|^2 = 1 + e^{-2q^2 D \tau} \quad (3.11)$$

where $g^{(1)}$ is the field correlation function and D is the diffusion coefficient. The second equality is valid for spherical particles and short time decays.

Knowing the diffusion coefficient of a monodisperse particle suspension, the particle size can be estimated. The Stokes-Einstein equation correlates the Brownian motion of particles with the hydrodynamic radius, R_H . Assuming particles are perfect spheres and keeping the system sufficiently dilute, avoiding interparticle interactions, yields the equation:

$$D = \frac{k_B T}{6\pi\eta R_H} \quad (3.12)$$

where k_B is Boltzmann's constant, T is absolute temperature and η is solvent viscosity.

3.3 Gel Electrophoresis

Electrophoresis utilizes the electrokinetic motion of charged particles or molecules in an electric field. By applying an external electric field to a sample containing charged species, a movement towards the corresponding electrode will be created, *i.e.* positively charged particles will move towards the cathode and negatively charged particles will move towards the anode. The electrophoretic mobility describing this motion is determined by the ratio between the speed of the analyte (v) and the applied electric field strength (E); as well as by the ratio between the charge of the analyte (q) and the friction with the medium (f).

$$\mu = \frac{v}{E} = \frac{q}{f} \quad (3.13)$$

Differential electrophoretic mobility is used to separate biological macromolecules such as nucleic acids and proteins, with either positive or negative net charge. To get efficient separation, a gel matrix is used as transportation medium. The gel matrix consists of a system of polymers forming a porous material in which the movement of the molecule is restricted dependent on size and shape. The two most commonly used polymers are agarose and polyacrylamide. Agarose is an uncharged linear polysaccharide creating a hydrogel with a continuous system of pores between the fibres. The fact that agarose is unbranched and that there is no cross-linking in the matrix makes the pores relatively large and therefore well-suited for separation of larger macromolecules (>1 kb for DNA). Polyacrylamide is made by polymerizing acrylamide monomers into a gel matrix. The pore size is usually smaller than in agarose gels, making separation of smaller molecular fragment possible. The difference in pore size is largely dependent on the ability to cross-link the polyacrylamide fibres. The pore size can therefore be controlled both by the concentration of acrylamide and by the degree of cross-linking.

Many biological macromolecules are charged and can therefore be subject to electrophoretic motion. Proteins have a net charge dependent on the composition of amino acids. It is possible to separate proteins depending on their isoelectric point using a pH gradient in the gel matrix. The electrokinetic motion stops when the protein becomes uncharged. Nucleic acids display negative charge at physiological pH due to the deprotonation of the phosphate in the backbone and can therefore be subject to electrophoretic mobility. The separation of DNA is highly dependent on the size of the molecule, *i.e.* how long the base sequence is. Using appropriate composition of gel matrix, separation with single base resolution is possible. There are two regimes of motion for longer, natural occurring DNA molecules: either in random coil or stretched form. The former describes motion in matrices with large pore size and at low field strength, the latter to the opposite situation when the DNA molecule is forced to adapt a stretched conformation in order to pass through the matrix. Two descriptive models can be applied to the two situations: the Ogston and Reptation model, respectively.^{177, 178} The main difference

between the two models is the shape that the linear polymer of DNA adapts when subject to electrokinetic motion. Shape is also the separating parameter when analyzing DNA nanostructures with gel electrophoresis, making it possible to distinguish assembled structures with the same number of base pairs.

4. Construction of an Addressable DNA Nanonetwork

This chapter aims at giving an overview of some interesting conclusions based on experimental discoveries made during the course of this project. The discussion is sectioned into four separate parts focusing on different aspects of the results: (i) creating an addressable DNA polycyclic nanostructure, (ii) development of a fixation strategy, (iii) controlling integration with lipid surfaces, and (iv) site-specific functionalization by triplex recognition. The intention is not to present all experimental details, but rather to highlight some interesting perspectives and findings. Apart from some yet unpublished data in section iv, results have been thoroughly discussed in the published papers, on which this thesis is based. Readers are encouraged to read the appended papers to get a conclusive representation of all results.

4.1 Introduction – AMNA

The aim of this work is to create a structural platform that enables control over molecular processes on the nanometer scale. Based on principles of bottom-up fabrication, a fully addressable non-repetitive network for non-trivial molecular nanotechnology is envisaged, for applications in molecular electronics (electron transfer), information technology (energy transfer) and single molecule chemical engineering (assembly lines of catalysts).

The framework of which this work is a part of goes under the abbreviation AMNA, Addressable Molecular Node Assembly.¹⁷⁹ It started in 2004 with the goal of constructing a DNA based molecular grid for controlling diverse processes at the highest precision. The project is conceptually grounded in principles of bio-inspired molecular nanoscience, focusing on utilizing chemical tools to engineer molecular recognition patterns governing self-assembly for bottom-up fabrication. The inherent recognition pattern of DNA places it in the centre of this development and the project as a part of the DNA nanotechnology research field.

A number of important ideas have guided the structural design of AMNA. First and foremost, addressability, which is a prerequisite for precise positioning of functionalities with well-defined interspatial localization. This concept has been explored in non-repetitive lattice structures with assembly of unique tiles⁵²⁻⁵⁴ but, more importantly, it has recently become an integral part of structures based on the DNA origami approach. Numerous studies have illustrated the localization precision that can be achieved using the unique addresses on an origami sheet.^{108, 111, 112, 115, 116} Orthogonal sequence design is an essential part of addressability, enabling unique positions in a structure.

Another fundamental concept of AMNA is a network of finite-size. The desired grid should be of known size and shape, assembled by unique building blocks, thus in dichotomous relation with the crystal-like repetitive lattices developed by Seeman.⁵ Additionally, it is desirable to assemble a structure of smallest possible size. Stretches of 10 bases in length were therefore chosen as the geometric basis of the construct. A sequence of 10 bp constitutes approximately one turn in normal B-DNA, 3.4 nm in length, and was perceived to be the shortest practical unit to use. This results in assembled nanostructures of minute size, compared with the relatively large sheets of the origami approach. Furthermore, the structure size may potentially be varied depending on purpose, as opposed to the folding of the genomic scaffold in DNA origami, limited by the size of the M13 macromolecule. Finally, the last pillar of the AMNA project is to utilize chemical tools to achieve sophisticated building blocks, combining the inherent properties of biomolecules with advanced molecular engineering. This has so far been a relatively rare approach in DNA nanotechnology, with some notable exceptions, *e.g.* the work of von Kiedrowski and Sleiman.^{88,93} Molecular engineering has, in AMNA, provided development of the synthetic three-way oligonucleotide, which constitutes the structural basis of the assembled network, as well as incorporation of functional units such as fluorophores for energy transfer purposes or amphiphilic moieties for membrane conjugation.

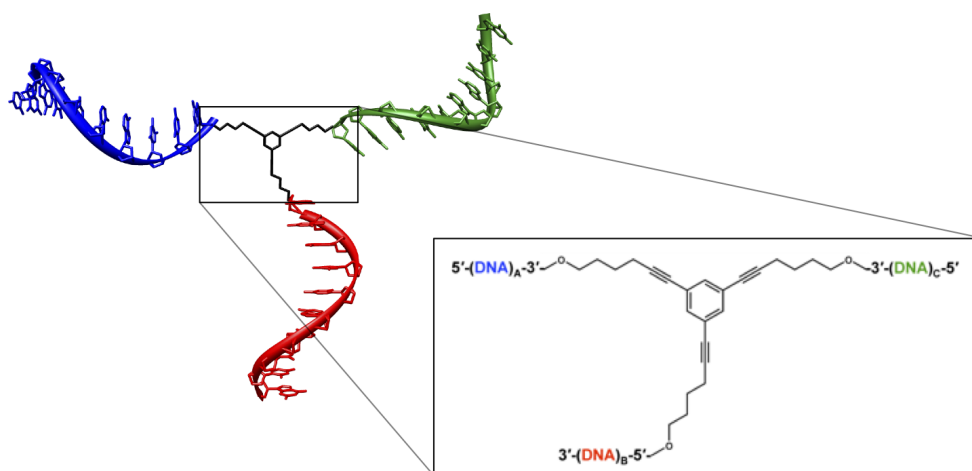


Figure 4.1. Schematic of the synthetic three-way oligonucleotide, with the 1,3,5-trisubstituted benzene node in the box to the right.

The pathway that was set out in order to reach this goal is the basis for this thesis. A non-repetitive two-dimensional DNA network as the structural template, assembled by three-way oligonucleotides, which form hexagonal unit cells. The three-way oligonucleotides are synthesized using a 1,3,5-tri-substituted benzene node, made compatible with standard solid-phase synthesis (Figure 4.1). The D_{3h} -symmetric node gives rise to the hexagonal geometry of the unit cell. However, a non-repetitive network demands unique sequences on all three positions, which can be achieved by incorporating intelligent choices of protection groups in the synthetic process (Paper I). This enables not only the necessary freedom in base sequence design but also directional freedom of the strands. In the construct of this

study, all nodes are connected to the 5' end of one strand and the 3' end of the two other strands. The reason for this geometry is simplicity and optimization of the reaction yields in the solid-phase synthesis. The chemical links connecting the oligonucleotides to the node have been made flexible by a four carbon alkane chain, making the network more adaptable, *e.g.* to avoid possible distortions due to the 10.5 bp helical pitch of B-DNA. Earlier studies on similar nodes illustrates possible problem with successful assembly using more rigid linkers.⁸⁸ Sequences are designed to be complementary to just one other sequence in the system and orthogonal to all others, ensuring addressability in a non-repetitive structure (Figure 4.2).

Creating predetermined assembly patterns and also to enable addressability, all sides in the structure must be made unique. Thus, sequence design needs careful consideration. Using stretches of 10 bases per side and maintaining the four Watson-Crick nucleotides of the genomic alphabet, it is possible to create well over one million (4^{10}) unique variations. A more strict evaluation process of appropriate sequences needs to be enforced to maintain robust self-assembly and structural integrity. Orthogonal sequence design ascertains that interference from other than fully complementary sequences is minimized. The orthogonality condition used in this project is a mismatch criterion of ≤ 4 (for any strand alignment) between two non-complementary 10 base sequences. This reduces the number of suitable sequences substantially, resulting in merely 84 possible duplexes. The limited number of possible unique sides in this system can be compared with the 226 individual staple strands used to fold the “seamed” origami rectangular sheet.⁶ Furthermore, to ensure sufficient duplex stability throughout the network, each sequence must contain at least 4 G-C pairs to sustain the melting temperature of all sides. Bearing in mind that the correlation between duplex stability and base sequence is more complex than the number of G-C pairs, especially in short oligonucleotides such as this where nearest-neighbor effects are predominant,¹⁸⁰ it is an adequate stability criterion. To enhance stability further, and also decrease fraying ends, sequences with G-C at the ends of the sequence were chosen over sequences ending with A-T, though this has not been a strict requirement. In the final step, sequences were assigned to nodes in sets of three, generating the three-way oligonucleotide building blocks. These sets were chosen so that numbers of intra-node base matches are minimized, since the covalent connection may promote formation of undesired secondary structures. A design where all three strands on one node have the same directionality would avoid these effects, since parallel base matching is much less favorable. A compromise in favor of optimized yield in solid-phase synthesis resulted in the chosen design used on all nodes in the network of this project.

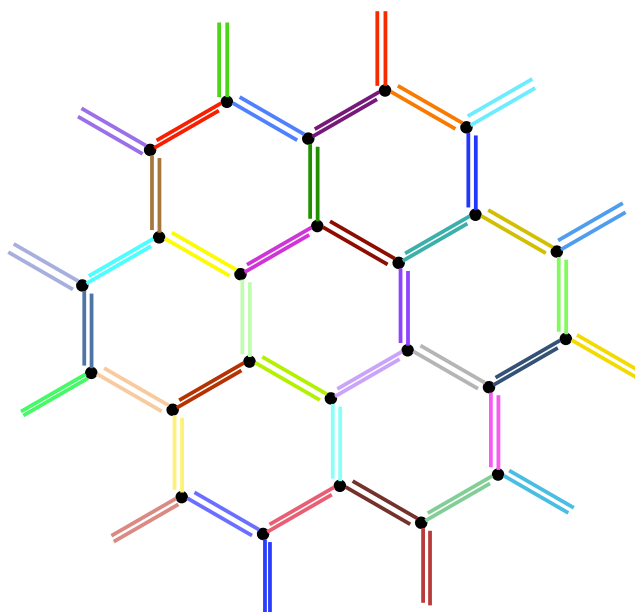


Figure 4.2. A fully addressable non-periodic network assembled by 24 unique three-way branched oligonucleotides, with 42 exclusive sides as indicated by the color-coding. The structure is called DNA-coronene by the nomenclature adopted in this work.

With these careful considerations for optimal molecular design, the desired DNA nanostructures may be manufactured with minimal effort, according to principles of self-assembly. All constructs are assembled in a one-step hybridization reaction, by standard nucleic acid annealing. Each oligonucleotide of the structure should be present in equimolar amounts, though sequential mixing of building blocks is unnecessary. As the desired network becomes larger, alternative fabrication strategies may however be preferred, which is shown in Paper III.

The symmetry of the three-way building blocks result in assemblies of honeycomb geometry, with hexagonal unit-cells. Though due to the non-repetitive nature of the network, each unit-cell is unique. The first hexagonal unit-cell was presented in Paper I, followed by the bihexagonal structure in Paper II, and larger structures in Paper III. Since there is a geometric analogy of these hexagonal DNA nanostructures with polycyclic aromatic hydrocarbons, a nomenclature was developed inspired by von Kiedrowski.⁹² The single hexagonal nanostructure is thus referred to as “DNA-benzene”; the bihexagonal extension is equal to “DNA-naphthalene”. The three-ring structure “DNA-phenalene” is not a perfect analogue due to a saturated carbon breaking the conjugation. The four-ring structure of Paper III lacks aromatic analogue for the same reason^{xv}. The schematic structure depicted in Figure 4.2 (“DNA-coronene”) would render a fully addressable nanostructure of approximately 25 nm in diameter and with 42 exclusive sides assembled from 24 unique three-way oligonucleotide nodes. A system of such high information density is an exceptional platform for controlling processes on a molecular scale.

^{xv} In hindsight, “DNA-benzoanthracene” or “-pyrene” would have been preferred, maintaining linguistic stringency.

The simplistic version of the hexagonal unit-cell that is presented in Paper I, where the synthetic benzene-node is replaced by two unpaired thymines (TT, Figure 4.8), is an important reference system and has proven to be an appropriate model system for gaining more fundamental understanding of the system.^{181, 182} Furthermore, it is the structural basis of the DNA nanostructures used in the “proof-of-principle” studies of Paper IV-VI in this thesis. Having a system based on normal linear oligonucleotides provides many advantages, also from a synthetic point of view.

4.2 Part I – Assembly of Polycyclic DNA Nanostructures

The focus of this section is on the actual fabrication process of fully addressable polycyclic DNA nanostructures, assembled by synthetic three-way oligonucleotides. Each side constitutes a unique sequence of 10 bases, i.e. 3.4 nm in length, and can be considered the smallest practical unit of DNA in a nanotechnological context. Figure 4.3 show the largest structure yet assembled (Paper III).

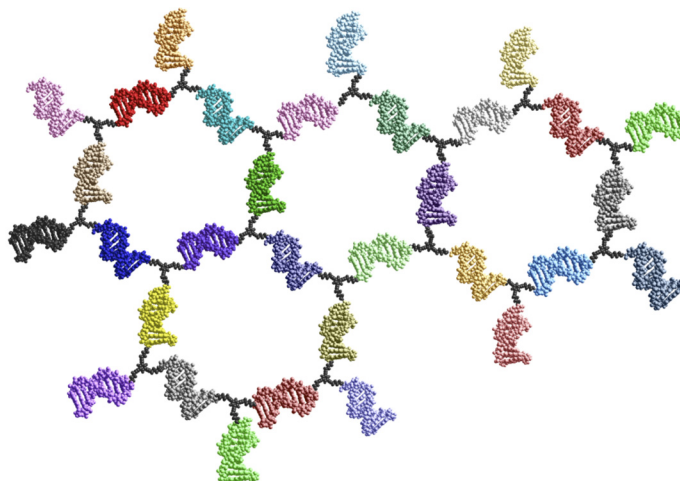


Figure 4.3. The four-ring DNA nanostructure presented in Paper III. The structure consists of 17 synthetic three-way oligonucleotides. Each side corresponds to a 10 nucleotide long DNA duplex, and the color-coding indicates unique, orthogonal sequences. In addition, complementary 10-mer oligonucleotides are added to all blunt arms, making all sequences in the system double-stranded.

Gel electrophoresis has been the main tool for characterization of the assembled DNA nanostructures throughout this work. As a separation technique with high size and shape sensitivity, it is ideal for analysis of small individual DNA assemblies with incremental structural discrepancies. The discriminatory possibilities of this technique have enabled identification of different constructs, based on either geometric differences between constructs of same size and charge or logic mobility retardation corresponding to step-wise structural size increase. The former was the basis for determination of the hexagonal structures in Paper I, where successful formation of a ring-closed structure could be shown by an electrophoretic retardation compared with a linear DNA assembly of same number of bases but without ring-closing possibility. The desired DNA hexagon and its linear reference construct differ solely in their geometric shape, which causes a distinct shift in molecular mobility through the porous gel matrix, analogous to the mobility difference between a circular DNA plasmid and its linear counterpart. This relation holds for both the hexagonal construct with hinges of unpaired thymines and for the three-way junctions, where the difference is even more pronounced.

When the network was expanded beyond the single ring structure, a comparison with ring-opened equivalents was insufficient as structural determination. DNA-naphthalene in Paper II and the larger structures in Paper III

were, hence, verified through incremental size increases, starting from DNA-benzene. The rationale of this experimental setup was that every addition of a building block result in slightly larger structure with a corresponding decrease in electrophoretic mobility. However, several “structural isomers” (Figure 4.4 & 4.5) have less predictable electrophoretic mobility, from a geometric point of view. A general trend of step-wise retardation with increased structural size can be seen in all gel images, going from DNA-benzene to the largest four-ring structure (Figure 4.3). Albeit that the separating resolution become less prominent in each step as the construct increases and one additional building block constitutes a decreasing subset of the entire assembly. The four-ring DNA nanostructure may approach the upper limit of what is experimentally feasible to resolve in this experimental setup of gel electrophoresis, using MetaPhor agarose. Changing setup to native PAGE is one possibility that could increase the separation between different substructures further, having a potential resolution on the level of individual base pairs. Another plausible approach is analysis by visualization techniques such as atomic force microscopy (AFM) or electron microscopy (EM). AFM has been a reliable tool in many studies of DNA nanostructures, first and foremost of periodic crystal-like arrays³⁴⁻⁴² and 2D DNA origami arrangements^{6, 97, 99, 112, 183, 184}. EM has been used to visualize smaller DNA nanostructures, *e.g. via* positioned metallic nanoparticles^{65, 79, 185} and even 3D DNA nanostructures in cryoEM^{73, 96, 106, 186}. The four-ring structure in this study approaches a size where microscopic techniques could provide useful information, though the fine structure of the constructs may be hard to distinguish (as evident from the AFM image of DNA-naphthalene in Paper II). A reason for the choice of this particular asymmetric design of four-ring construct was that these features could potentially be resolved in AFM.

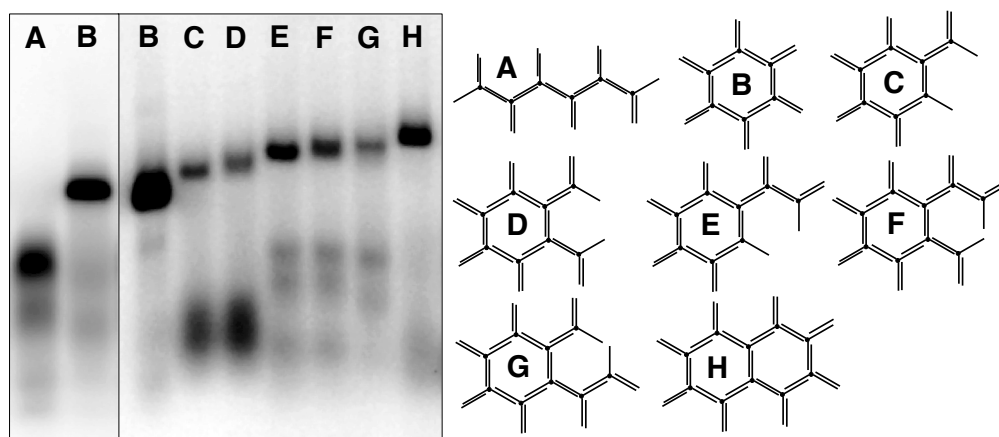


Figure 4.4. Gel demonstrating formation of DNA-benzene (Paper I) and DNA-naphthalene (Paper II). (Left gel) The closed form of DNA-benzene (B) is proven in comparison with its open structural analogue (A), illustrating the importance of molecular shape as separating factor. (Right gel) Stepwise construction of DNA-naphthalene (H) following the schematic on the right. Electrophoresis was performed in 4.5% MetaPhor agarose and phosphate buffer (pH 7.5, 200 mM Na⁺). Cy3 was the fluorescent probe used for visualization in the gel scanner.

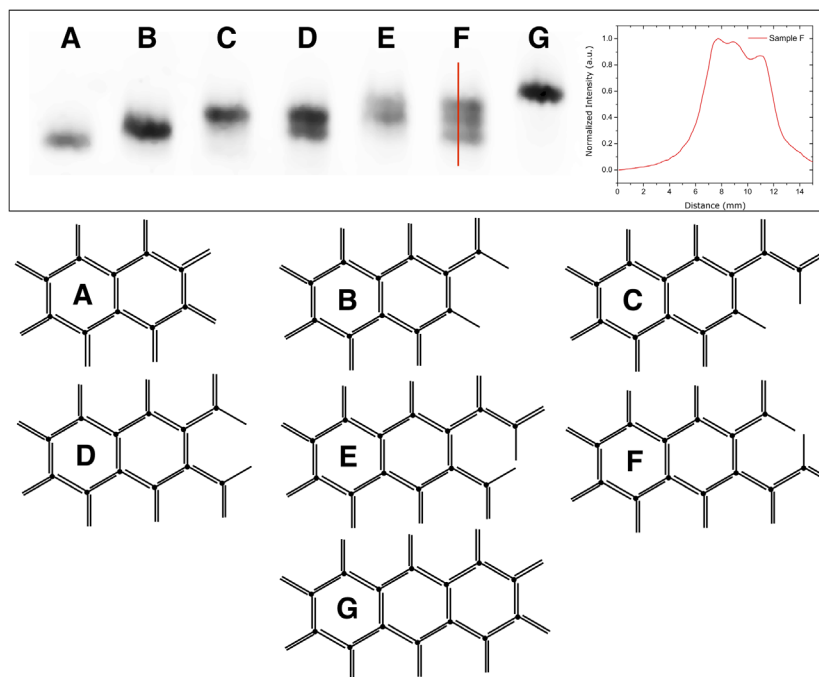


Figure 4.5. Step-wise assembly of DNA-anthracene (G) following schematic below, with the same experimental conditions as in Figure 4.4. The line on sample F gives the intensity profile (Right inset). Three strongly overlapping bands can be seen, corresponding to binding of one, two and three nodes to the two-cell construct. The presence of multiple bands illustrates difference between ring-closed structure and intermediates.

All gel results indicate a consistent difference between fully ring-closed structures and the other intermediate sub-structures, having one or more single-stranded branch. The yield of the desired construct is significantly higher in all cases where the structures are cyclized and all sides double-stranded, which can be seen in that the bands on the gel are more distinct for all closed structures. The intermediate structures display, in contrast, a less distinct pattern, both in terms of barely separable bands and also in a more undefined smear in the lanes of the gel (illustrated by the inset on intensity profile of sample F in Figure 4.5). This indicates poor binding of some individual three-way oligonucleotides. There are a number of possible explanations for this behavior, none of which are mutually excluding. Interference effect of secondary order within the specific sequence, that is, semistable hairpin-like structures of a few base pairs could give rise to this behavior. Even if the sequence design strives to minimize undesired secondary structures, potential distorting effects of the tripodal arrangement are difficult to predict. However, the free energy of these structures should not be higher, compared with the free energy when all sequences are perfectly matched. Another explanation could be that constructs with considerable conformational flexibility are destabilized by the close proximity of dangling regions with a high density of negative charge. Such regions will be more mutually repulsive compared with the more rigid conformation of fully ring-closed structures. There seems to be a correlation between the number of uncyclized flexible branches and structure stability, such

that more flexible branches result in lower yield of that particular construct, which could support an explanation based on electrostatic repulsion. The consistent difference between fully cyclized structures and the intermediates can also be discussed within the context of another perspective, *i.e.* the thermodynamic effect of ring closure. We will soon have reason to return to this discussion. Figure 4.6 shows all polycyclic DNA nanostructures of Paper III.

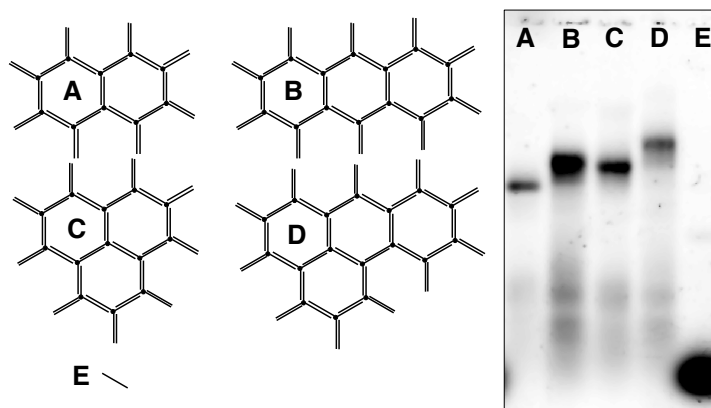


Figure 4.6. Four completely ring-closed DNA nanonetworks of Paper III, following the schematic outline to the left of the gel. DNA-naphthalene (A), DNA-anthracene (B), DNA-phenalene (C), four-ring structure (D) and Cy3-labeled 10-mer reference (E).

Systematic yield analysis of the assembled constructs provides an opportunity to determine the efficiency of the chosen fabrication strategy. Gel electrophoresis with fluorescence detection combines structural separation with a reliable tool for quantitative analysis. Covalent labeling with a fluorescent probe (Cy3 in this work) used for visualization of the gel-separated nanoconstructs enables quantification of relative fluorescence intensities associated with each band of interest on the gels. A yield analysis of all ring-closed nanostructures, from DNA-benzene to the four-ring network, was done in Paper III (Figure 4.7). The result revealed a somewhat discouraging trend: as the network becomes larger, the formation yield of the desired structure decreases. The yield drop can be described by an experimental model, based on the same principle as total yield of multi-step synthesis:

$$Y = y_{duplex}^n \quad (4.1)$$

where Y is the final yield of n number of hybridization events, y_{duplex} , *i.e.* number of duplexes in the construct. The latter is assumed to be uniform over the system of interest. Even though experimental indications of weak sides in the system, both from the gel results and from melting studies¹⁸², might seem to contradict this assumption, an average treatment of all sides can describe the observed yield. Using this method to model the data resulted in an average hybridization reaction yield of 96%. An estimation of the expected single-stranded concentration at equilibrium can only account for less than 0.5% of the deviation

from uniform hybridization conversion^{xvi}. Another possible explanation for lack of uniform conversion could be deviations from perfect 1:1 stoichiometry. This is of particular interest since it is a prerequisite for DNA nanostructures based on this assembly approach, dissimilar from the origami approach where a large excess of staple strands drives the equilibrium towards the desired folded state of the M13 scaffold.

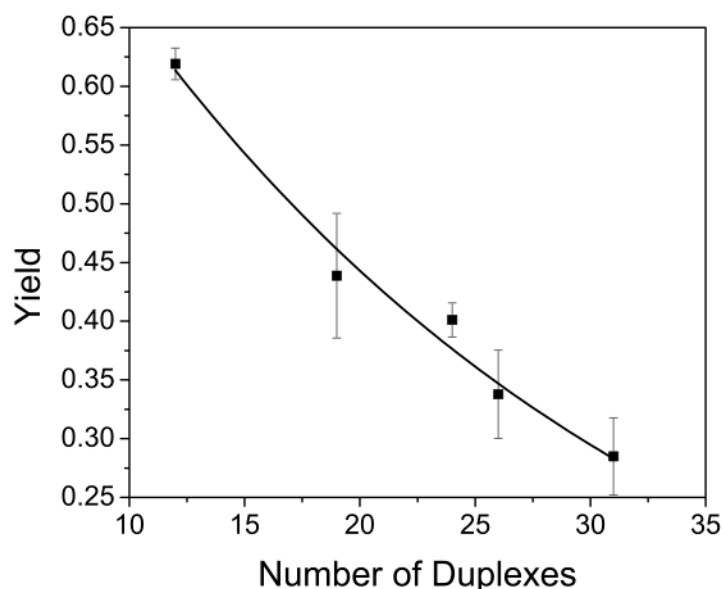


Figure 4.7. Yields for the ring-closed structures, plotted against the number of duplexes involved in forming one specific structure. DNA-benzene ($n = 12$), DNA-naphthalene ($n = 19$), DNA-phenalene ($n = 24$), DNA-anthracene ($n = 26$), and the final four-ring network ($n = 31$). Error bars show standard deviation for the particular structure, from repeated experiments carried out under the same conditions. The number of repeated experiments is 21 for DNA-naphthalene, 6 for DNA-anthracene, and 3 for each of DNA-benzene, DNA-phenalene, and the final four-ring network. The solid curve corresponds to the statistical yield model (eq 4.1)

Dependence on equimolar stoichiometry illustrates a fundamental problem of nanoconstruction based on self-assembly of unique building blocks. The fabrication yield may very well be sufficient for many potential applications but an alternative approach based on scaffolded folding seems to be preferable from this perspective. However, one factor that could potentially counteract the exponential yield decay is if the network-formation is thermodynamically favorable. Although ring closure is expected to increase electrostatic repulsion and decrease conformational entropy, compared to linear polymerization, it also provides a higher apparent concentration of the two ends closing the circle, in the end resulting in a thermodynamically favored process. This phenomenon was investigated in a related report, studying the thermodynamic aspects of the hexagonal DNA nanostructure with unpaired

^{xvi} This estimation is based on equilibrium of DNA hybridization at 4 °C, assuming $K \approx 1.2 \times 10^{12} \text{ M}^{-1}$ (from Sandin *et al.*) and concentration of duplex $\approx 10^7 \text{ M}$.

thymines as hinges.¹⁸² Ring closure thermodynamically favored process is based on conclusions from Paper I, associated with melting data of this construct. Comparing the melting trace of the cyclized construct with the linear reference unable to ring-close revealed a clear difference (Figure 4.8). The former displayed a distinct shift in absorbance, manifested as a sharp peak in the first derivative of the melting function. This behavior stems from co-operative ring opening due to the stabilization effect of an intramolecular event. The weakest link in the chain of 10mer duplexes is stabilized in a ring-closed structure because the higher apparent concentration of building blocks in this arrangement favors intramolecular ring-closure, as opposed to intermolecular chain-growth. The polycyclic network of three-way oligonucleotides may be seen as an extension of this hexagonal unit-cell and thus exhibit similar features. The equilibrium model of hexagon formation from the previous report may be expanded to a ring of an arbitrary number of building blocks. Assuming that deviations of oligonucleotide concentration from the mean value follow a normal distribution with standard deviation σ , the overall yield can be expressed as an exponential relation:

$$Y = 1 - \alpha = \kappa e^{-\frac{n}{\sqrt{\pi}} \left(\frac{\sigma}{\alpha} + \frac{5}{6} \left(\frac{\sigma}{\alpha} \right)^3 + \frac{43}{20} \left(\frac{\sigma}{\alpha} \right)^5 \right)} \quad (4.2)$$

The non-trivial derivation of equation 4.2 can be found in the supporting information of Paper III and will not be further discussed in this text. Instead, what is the implication of this relation? First of all, the dimensionless parameter κ is the ratio between equilibrium constant of ring closure and the average oligonucleotide concentration, thus, gauging the strength of ring closure. This means that a large κ , *i.e.* an effective thermodynamic driving force for ring closure, could counteract the influence of stoichiometric deviations on the overall yield. The model, albeit too simplistic to explain all interconnecting aspects in the branched geometry of the network, illustrates that a favorable process of network-formation can, to some extent, counteract the exponential yield decay of the growing network. Treating the polycyclic system as rings of different sizes, the magnitude of the ring closure efficiency can be estimated. Fitting equation 4.2 to the experimental data for the different structures^{xvii} rendered $\kappa = 3.6$ over all polycyclic constructs, which can be compared with $\kappa = 6$ for the simple hexagonal ring-system.¹⁸²

The hierarchical construction of the addressable DNA network, from DNA-benzene in Paper I to the four-ring nanostructure in Paper III, shows that fully addressable nanogrids can be assembled from synthetic three-way oligonucleotides of smallest practical size in one-step. Quantitative analysis of assembly yields revealed discouraging indications on the fabrication efficiency. However, with a better understanding of the interplay between branched building blocks and the

^{xvii} If one assumes a standard deviation of 10% given by the uncertainty in concentration determination relying on the nearest-neighbor approximation (ref. Bloomfield)

assembly process, aspects promoting more favorable network-formation could potentially be integrated in the system design, maximizing self-assembly efficiency.

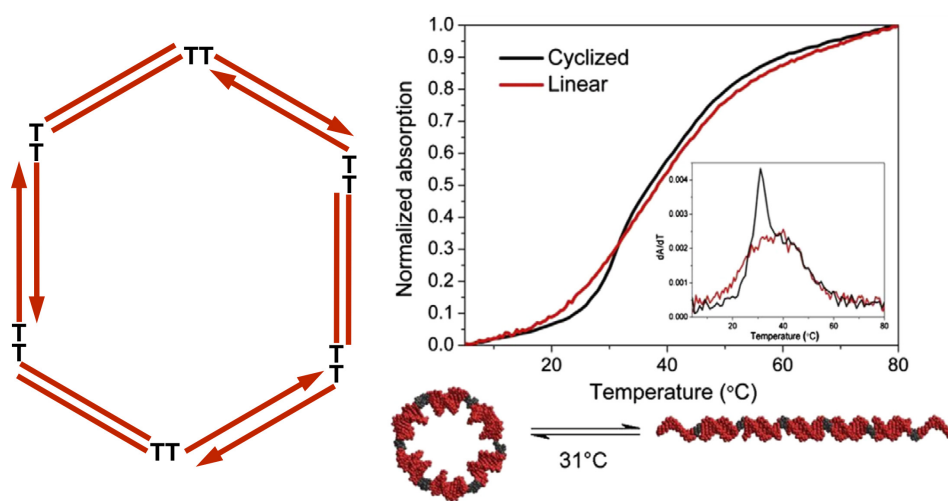


Figure 4.8. UV-melting experiment from Paper I on the hexagonal unit-cell with TT-hinges (black line) and its non-cyclizable linear analogue. Inset shows first derivative of the melting functions. Ring-opening occurs at 31 °C. The characteristic melting profile of the closed structure has been utilized as a footprint confirming the structural integrity of the hexagonal DNA nanostructure (Paper VI), and also on a theoretical level in yield analysis of the polycyclic network (Paper III).

4.3 Part II – Click Fixation Strategy for Modular Build-up

The non-covalent forces maintaining structural integrity of DNA assemblies make the constructs fragile. We have therefore developed a fixation technology, based on click chemistry, creating robust structures. This could potentially enable an alternative fabrication strategy of modular build-up.

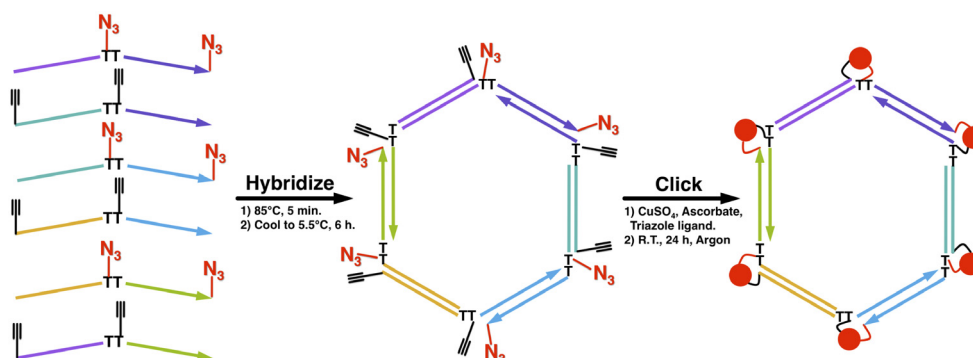


Figure 4.9. Reaction scheme of the site-specific click-fixation strategy of a hexagonal DNA nanostructure. Firstly, six alkyne and azide modified 22-mer oligonucleotides are hybridized to form a hexagonal construct with edge length 10 bases. Color-coding shows strands that are complementary. Secondly, the nanostructure is locked covalently by six simultaneous click reactions in which azide and alkyne form a triazole in presence of Cu(I). Upon formation of the hexagonal nanostructure, azide and alkyne modifications are situated to enable the site-specific click reactions of the fixation step. The first step is reversible, whereas the second is irreversible.

Using nucleic acids as material for nano-scale fabrication has many advantages, as illustrated by the progress of DNA nanotechnology. The assembly and stability of such nanostructures relies on precise hydrogen bonding as well as base stacking. The minute dimensions of the addressable DNA nanogrid in this work are a product of the mere 10 oligonucleotide stretches that constitute the sides of the network. Working with units of this length scale ensures a system fit for molecular nanotechnology, having dimensions suitable for many interesting processes, *e.g.* energy transfer. However, there is an intrinsic trade-off between smaller building blocks and the stability of the construct. The non-covalent nature of the Watson-Crick base pairing makes the system delicate, which is true for all supramolecular DNA assemblies, and even more so if the oligonucleotides are short. A solution to this problem is to develop strategies that reinforce the constructs after the assembly process. We have therefore developed this fixation technology, based on click chemistry (Figure 4.9), creating robust structures that will be necessary for many future applications. Ligase enzyme has previously been used in DNA nanotechnology to join together ends of strands.¹⁸⁷ However, the enzymatic approach is limited because it is only possible to seal nicks in linear sequences on a small scale. Finding chemical alternatives that are both versatile and suitable for large-scale production is the motivation for the fixation strategy developed in this thesis.

The development of a fixation technology is also interesting from another perspective, associated with the assembly process. One approach could be to apply fixation on a final assembly, providing a more robust nanostructure. Another approach involves an alternative fabrication platform to one-step assembly. Analogous to civil construction based on mounting of ready-made larger units, as opposed to brick-by-brick-construction, a modular build-up approach can be applied on hierarchical self-assembly as well. With the incorporation of a fixation step in the assembly process, larger molecular modules may be created that can be purified and stored before subsequent assembly into even larger structures.

The strategy that we developed was site-specific cross-linking, based on the principles of click chemistry, of each side in an assembled DNA structure. This was demonstrated in Paper IV, a proof-of-principle study on the hexagonal DNA nanostructure. Providing further insight on the behavior, the analysis was expanded in Paper III.^{xviii} Site-specific cross-linking of the hexagonal nanostructure is made *via* azide and alkyne modifications on the six oligonucleotides constituting the assembly. Azide and alkyne are the reactants in the most prominent of click reactions, *i.e.* the copper(I)-catalyzed cycloaddition (CuAAC)^{148, 149} producing a triazole link between molecular units one wants to connect. To covalently lock the complete structure, all six strands have to be linked together, requiring six individual reaction sites. The positioning of the azide and alkyne modifications on the oligonucleotides ensures that only the desired cross-linking takes place. In Paper IV we show that all six click reactions can be performed simultaneously on the annealed hexagonal DNA nanostructure.

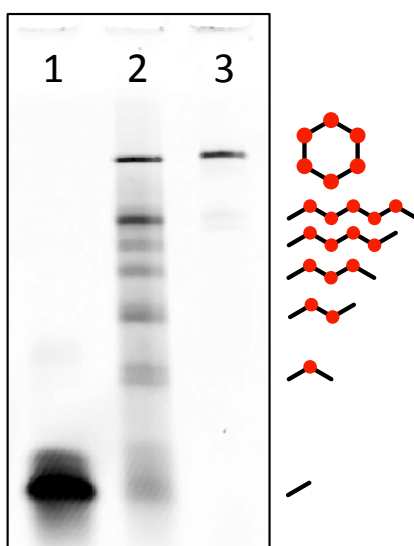


Figure 4.10. The click fixation reaction analyzed with 10% denaturing PAGE. (1) Control sample without Cu(I); (2) crude click reaction sample; (3) the cross-linked hexagon extracted from crude reaction mixture. The sketches indicate the constructs of the corresponding bands and the number of successful click reactions involved.

^{xviii} This may seem anachronistic, but Paper III was actually published after Paper IV.

The result after the click reaction is performed on the hybridized hexagonal nanostructure is shown in Figure 4.10, analyzed with denaturing polyacrylamide gel electrophoresis (PAGE). Lane 2 is the crude reaction mixture containing a distribution of the different sub-structures, from monomer (bottom) to the desired hexagon (top). Comparing this with lane 1, containing the same hexagonal DNA sample without addition of Cu(I), it is evident that the click reaction has successfully created a covalently cross-linked DNA nanostructure. The different substructures in lane 2 correspond to all possible structures formed when one or more of the six reactions fail. Another important result is also demonstrated in Figure 4.10, *i.e.* the possibility to extract the desired construct from a crude reaction mixture (lane 3). The efficient purification suggests that large-scale production is plausible. Furthermore, the procedure illustrates that the cross-linked DNA nanostructures are robust and maintain their composition even after freeze-drying and addition of denaturing agents such as formamide.

We investigated if these reaction sites interact with each other or if they proceed independently, through yield analysis of the electrophoresis results. Positioning multiple reaction centers on a nanoscale template may present conditions different from unrestricted reactions. For instance, given the high electrostatic surface charge of a DNA nanostructure, the activity of the catalytic Cu(I) could be affected in a way that differs from freely diffusing reaction sites, leading to interference effects. Local catalytic depletion is an imaginable effect of chemical reactions on nanoscale templates. Looking at the resulting fractions of substructures formed after the fixation step, it is apparent that the probability of a click reaction to occur is below unity. The effect of this non-ideal behavior is that instead of one single end product (one totally covalently locked DNA hexagon) there will be a distribution of various substructures corresponding to species where one, two, or more click reactions have not taken place. Furthermore, the range of substructures formed is not only due to the number of reactions but also dependent on where in the structure these reactions occur, something that adds extra complexity. Nonetheless, the analysis is possible to conduct, which was done in Paper III, mapping out all combinatorial possibilities of the process.

Based on the assumption that each of the six click reactions constitutes a Bernoulli experiment^{xix}, dependency may be tested by adopting a binomial model on the system. If the reactions occur independently then the resulting outcome of the six sequential, independent events should follow a binomial distribution. A comparison between the experimental outcome and the theoretical estimation of the binomial model^{xx} is displayed in Figure 4.11.

^{xix} A binary option of success or failure. Flipping a coin is a typical Bernoulli experiment.

^{xx} The model is a weighted sum of binomial terms, originating from every starting template structure with its corresponding distribution (Table S3 in SI of Paper III). The experimental yield data from the hybridization reaction are the coefficients (Table S4 in SI of Paper III) used for the different substructures in the weighted sum.

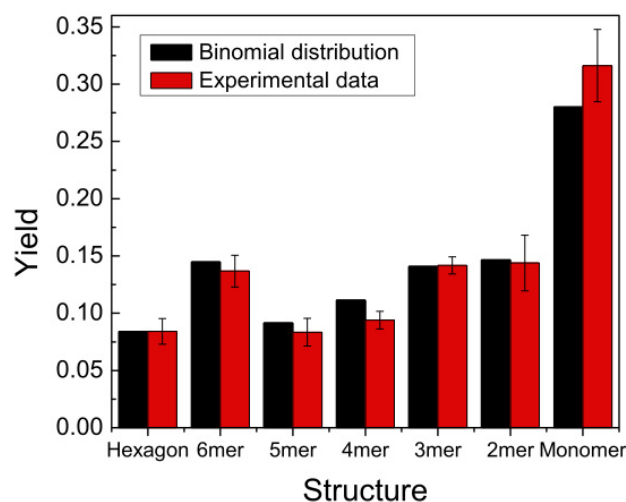


Figure 4.11. Yield analysis with binomial model. Yield data for click fixation of the DNA hexagon. Experimental distribution of possible substructures shown as red columns, error bars indicating standard deviation (14 samples). Experimental data taken from Paper IV. Black columns show binomial model, *i.e.* weighted sums of binomial distributions for each substructure of all possible starting materials. The probability, p (yield of one click reaction), is deduced to be 0.82 from the observed yield of totally cross-linked DNA hexagon.

As seen in the figure, the pattern of the model corresponds well with the experimental results, within experimental error in all but two cases (4-mer and monomer). The fact that the binomial model can predict the fractions of substructures to this degree is an indication that all click reactions proceed independently. This conclusion implies that the binomial distribution can function as a test of cooperativity between chemical reactions on the confined template of the DNA nanostructure. Deviations from this model would indicate positive or negative chemical interference, potentially of general interest.

The probability of one click reaction to occur, deduced from the experimental results, is 82% in this system, which is a reasonable value in the range of what has been reported.¹⁵⁰ But the fact that the yield of the final cross-linked product of interest is below 10% is unsatisfying from a manufacturing point of view.^{XXI} A low yield from the hybridization reaction is a major problem in this regard. Further optimization of this process would be necessary in order to increase the yield of the final product. Despite the low yield, the possibility of easy purification of these larger molecular modules may nonetheless make the alternative assembly approach of modular build-up worthy for serious consideration. Combining multiple and orthogonal fixation strategies could be a useful asset in nano-construction of this nature. One example could be a site-specific photo-induced cross-linking approach.¹⁸⁸

^{XXI} Although, one should bear in mind the widespread range of reported yields in the literature, from 1% to 95%, for different DNA nanoassemblies. 10% is not despicable in this context.

In conclusion, we have developed a click fixation strategy that provides robust and easily purified DNA nanostructures, aiming at modular build-up of larger structures. We have also demonstrated that there is no interference between the six simultaneous click reactions, since they follow a binomial distribution model.

4.4 Part III – Soft-surface Nanotechnology

Surface-integration is an important aspect of nanotechnology and soft-surfaces provides interesting prospects in applications such as artificial photosynthesis. We have therefore explored two molecular anchors for controllable membrane integration of our DNA nanostructures.

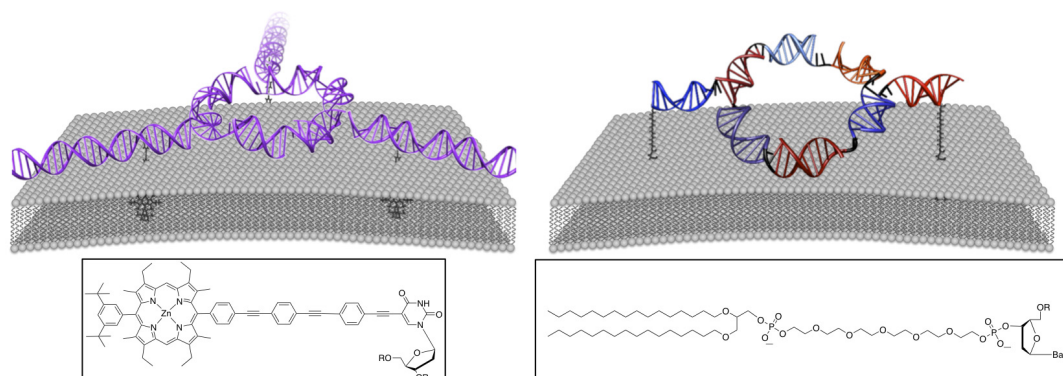


Figure 4.12. DNA nanostructures tethered to lipid membranes. (Left) Porphyrin anchor (Paper V). (Right) Lipid anchor (Paper VI).

One of the endeavors outlined in the AMNA project was development of immobilization strategies for controllable surface integration of the DNA based nanogrids. Nature extensively utilizes membranes in the organization of biochemical processes, from the cell surface to the organelle compartments in its interior. Lipid bilayers have many valuable properties from the perspective of molecular science. Fluidity, structural flexibility, bifacial separation and a water/oil interface are just some properties making lipid bilayers highly interesting. Furthermore, self-assembly in aqueous solutions is an ideal feature in this context. By integrating controllable structural scaffolds with lipid membranes, a surface-based nanotechnological platform is created. Soft-surface nanotechnology has potential use in molecular assembly lines for chemical synthesis or as a framework for artificial photosynthesis, mimicking the organization of photosynthetic reaction centre in the thylakoid membrane^{xxii}.

Both Paper V and VI explore this topic, focusing on conjugating a DNA nanostructure with lipid bilayers, using two different molecular anchoring motifs. The main focus of both studies has been on membrane surfaces in the form of lipid vesicles, typically 100 nm in diameter. Such a system is interesting from a fundamental point of view. The bifacial membrane separates two volumes, one of which is enclosed in the interior. The lumen is a confined entity that could for instance pool substrate or product in chemical synthesis. The large size difference between particle and construct, results in the radius of curvature to be virtually negligible on the dimensions of the DNA nanostructure.^{xxiii} The use of a colloidal

^{xxii} Membrane-compartment of chloroplast in photosynthetic organisms, where all proteins involved in photosynthesis are embedded (e.g. photosystem II).

^{xxiii} A nanostructure with radius 5 nm experience a height-difference between center and edge of $<3 \text{ \AA}$, when adsorbed on the surface of a 100 nm vesicle.

system also renders the opportunity to apply spectroscopic techniques in the characterization of the system.

The two anchoring motifs that have been studied in this thesis are a porphyrin moiety and a two-tailed lipid unit (Figure 4.12). The molecular properties of these two entities are diverse, as can be seen in Figure 4.12, but the common denominator of high hydrophobic affinity makes both ideal as molecular anchors in the context of soft-surface nanotechnology.

The design of the lipid anchor (glyceryl-bis-C16-hexaethyleneglycol) was based on a desire to mimic the phospholipids of a membrane to which the anchor should penetrate, thus the amphiphilic molecular structure. The hydrophobic alkane chains (C16) associate with the interior of a membrane, whereas the hydrophilic hexaethyleneglycol-based (HEG) linker enables more structural flexibility of the attached oligonucleotide molecule in solution, minimizing undesired interference between the tethered DNA and the membrane.

Porphyrins are considerably more complex, with multiple functionalities, having both energy- and electron-transfer properties. These features of the porphyrin moiety in the context of DNA nanotechnology have been extensively studied in several publications by Börjesson *et al.*¹⁸⁹⁻¹⁹¹ The porphyrin motif used in Paper V has a triphenylethylenylene spacer separating the macrocycle and the oligonucleotide to which it is attached. Apart from being a linker with rigid molecular structure, its conjugated nature also renders a hydrophobic character. Thus, the porphyrin anchor is not amphiphilic in itself as the lipid anchor in Paper VI. Another difference between the two anchoring motifs that has been examined in this thesis is the position of the attachment to each modified oligonucleotide. The triphenylethylenylene of the porphyrin anchor is covalently bound to the C5 position of a uracil, located in the middle part of the base sequence, whereas the lipid anchor is situated at the end of the sequence, at 5' and 3' position, respectively. This difference has impact on the arrangement of the DNA nanostructure afloat on the membrane surface.

The DNA nanostructures that were investigated in the two related studies of this thesis are both based on the hexagonal core-unit established in Paper I (Figure 4.8). The structural design differs by the positioning of the anchoring units. In the case of porphyrin anchors, three protruding arms were set in a tripodal arrangement separated by a 120° angle. The orientation was altered when the lipid anchors were used, where the protruding anchoring arms were positioned on opposite sides of the hexagonal unit, 180° apart. Another difference is the length of the protruding arms, 39 bases in the case of porphyrin anchors and 10 bases for the lipid anchors.^{xxiv}

^{xxiv} The porphyrin modified uracil was the 9th base of the arm, starting from the hexagonal core, *i.e.* almost on the same distance as for the lipid modification at the end of base 10.

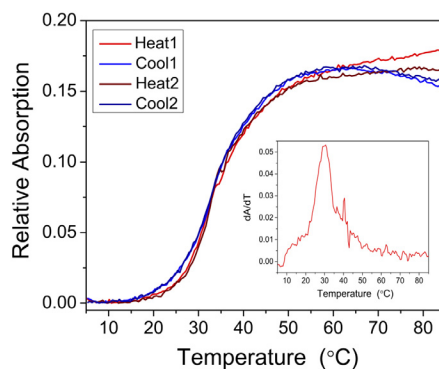


Figure 4.13. UV-melting results of the hexagonal DNA nanostructure with two lipid anchors (HexA2) tethered to a lipid vesicle. Inset is first derivative of the initial melting curve (Heat1). Melting temperature (T_m) according to peak value of derivative is 30 °C for DNA nanoconstruct bound to liposomes. The sample has been subject to 2 heat/cool cycles. The consistent shape of the profiles indicates reversibility.

An advantage of soft-surface nanotechnology is the dynamic properties of the system, which can be illustrated by the maintained reversibility in self-assembly when the nanostructure is tethered to a lipid membrane by molecular anchors. This was demonstrated by melting experiments on the studied DNA nanostructures. In the case of the construct tethered with lipid anchors in Paper VI, the melting profiles displayed the distinct characteristic of a ring-closed structure established in Paper I, manifested as a sharp peak in the first derivative of the melting function (comparing Figure 4.13 with Figure 4.8). This confirmed the structural integrity of the system. Furthermore, the persistent shape of the melting traces over sequential melting and annealing steps was an indication of total reversibility of the self-assembled nanostructure.

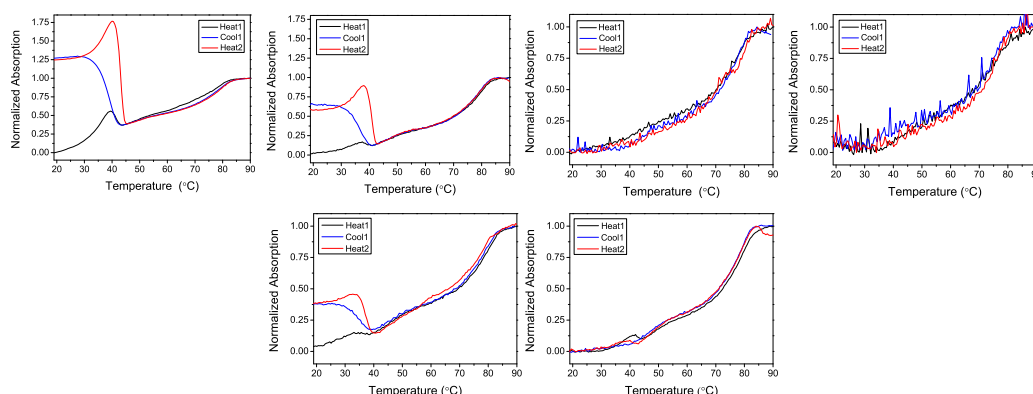


Figure 4.14. UV-melting results of the hexagonal DNA nanostructure with three porphyrin anchors (HexP3), illustrating effects of irreversible assembly. (Black) First temperature increase; (blue) temperature decrease; (red) second temperature increase. (Top row) Melting curves with constant DNA:liposome ratio ($[\text{HexP3}]:[\text{lipid}] = 1:1200$) but at different total concentrations. From left to right: $[\text{lipid}] = 400 \mu\text{M}$, $200 \mu\text{M}$, $40 \mu\text{M}$ & $20 \mu\text{M}$. (Bottom row) Melting curves with varied DNA:liposome ratio: (left) $[\text{HexP3}]:[\text{lipid}] = 1:300$, (right) $[\text{HexP3}]:[\text{lipid}] = 1:3000$ ($[\text{HexP3}] = 167 \text{ nM}$).

The situation was slightly more complex in the case of porphyrin anchors, but on the other hand illustrates some interesting features of the system. First, it should be pointed out that this system displays two separate melting regions: one minor transition associated with the dissociation of the hexagonal unit at low temperatures (40 °C) and a second major transition at elevated temperature associated with the melting of the protruding anchoring arms (80 °C). The larger hypochromicity correlated with the longer base sequence of the arms (39 bases compared to 10 bases per hexagonal side), makes the transition at high temperature dominate. Looking at the melting traces in Figure 4.14, the most striking effect is the lack of reversibility, dissimilar from the lipid anchor (Figure 4.13). When the constructs are rehybridized on the lipid membrane an increase in the optical density (OD) is seen at low temperatures. Subsequently, when the temperature is increased again an initial rise in OD is seen, followed by a sharp descend in OD. This transition occurs in the temperature region where the hexagonal core melts and the explanation for this behavior is a bridging effect between separate lipid vesicles, forming aggregates that scatter more light. When the hexagonal construct is reassembled in the colloidal solution of lipid vesicles it has the possibility of connecting anchoring arms situated on separate liposome surfaces, thus forming aggregates. The phenomenon has been studied in a related context of controlled lipid vesicle aggregation¹⁹² and it is also the basis of DNA directed vesicle fusion.^{193, 194}

This undesired effect can be avoided, as seen in Figure 4.14. It is also interesting from a fundamental perspective, illustrating the interplay between the restricted lateral diffusion on a membrane surface on one hand with the free diffusion of lipid vesicles and DNA in solution on the other. The top series in Figure 4.14 demonstrates one way to circumvent the bridging effect, *i.e.* by system dilution. This means that the concentration of bound DNA on the liposome surface will be the same for all samples, but the dilution of the system will affect the average interparticle distance. Thus, by diluting the system the number of interparticle contacts will decrease, rendering less linking possibilities and consequently diminishing light scattering. It is the competition between diffusion on the membrane surface and the diffusion of the liposomes that governs if the DNA constructs will link liposomes together. This can also be demonstrated by altering the DNA:lipid ratio (Figure 4.14, bottom row). At low lipid concentration the tethered oligonucleotides are more closely packed on the surface, leading to higher apparent concentration. This means that even if diffusion is slow on the surface, the building blocks making up the hexagon have a greater probability of meeting each other on the same lipid vesicle compared to building blocks on other vesicles. Hence, light scattering is substantially decreased at low lipid concentration.

Interestingly, the bridging effect was not present in the system with lipid anchors. Either depending on the fact that the DNA:lipid ratio used in Paper VI is in a concentration regime avoiding undesired intervesicle-linking or that this system is less prone to promote aggregation.

One method to assess the arrangement of the nanostructures when tethered to liposomes is to monitor the hydrodynamic size of the particle as a function of

number of anchors. This was done using dynamic light scattering (DLS) for both the porphyrin and lipid systems. Both systems displayed the same, predicted, pattern in that additional anchors resulted in smaller particle size, originating from the DNA nanostructure becoming more aligned with the membrane surface through multiple anchoring points (Figure 4.15).

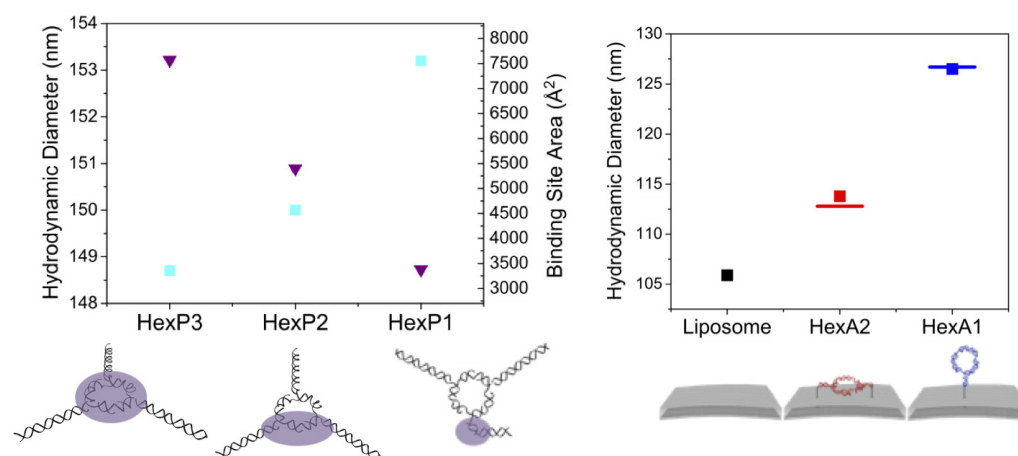


Figure 4.15. Estimations of how tethered DNA nanostructures arrange on the membrane as a function of number of anchoring points. Hydrodynamic diameter measured by DLS for both systems: (left) Porphyrin and (right) Lipid. The binding site area of the constructs are given by purple triangles and particle size by cyan squares, for the porphyrin system (left). The diameter of liposomes in the absence of DNA was 130 nm in this system. (Right) Horizontal bars mark expected diameter values for the hypothetical structures deduced from angles given by linear dichroism for the lipid system (Figure 4.16).

Additional structural information was collected for both systems, using different methods. The spectroscopic properties of porphyrins enable structural information deduced from photometric titration. The effective area of tethered DNA nanostructure on the lipid surface could be estimated based on the surface coverage at equilibrium given by the binding isotherm. The estimated footprint of the nanostructure increased with increasing number of anchoring points, with an effective surface area for the tripodal anchored construct (HexP3) on the same order as the hexagonal core area.

In contrast, the optically transparent lipid anchor, in Paper VI, calls for another technique to provide more detailed conformational information. Linear dichroism (LD) was applied on flow-aligned lipid vesicles to which the DNA nanostructure had been attached. By comparing the LD spectra of a construct tethered with a single anchor (HexA1) with the case of two opposite positioned anchors (HexA2), a clear structural difference could be concluded (Figure 4.16). When the construct is anchored at a single point it protrudes from the membrane, positioning the nucleobases in predominately parallel arrangement to the orientation axis, resulting in a positive LD-signal at 260 nm. HexA2 displays a mirrored spectrum and the bases are consequently more perpendicular in respect to the orientation axis, thus showing that the construct itself is more aligned with the membrane surface.

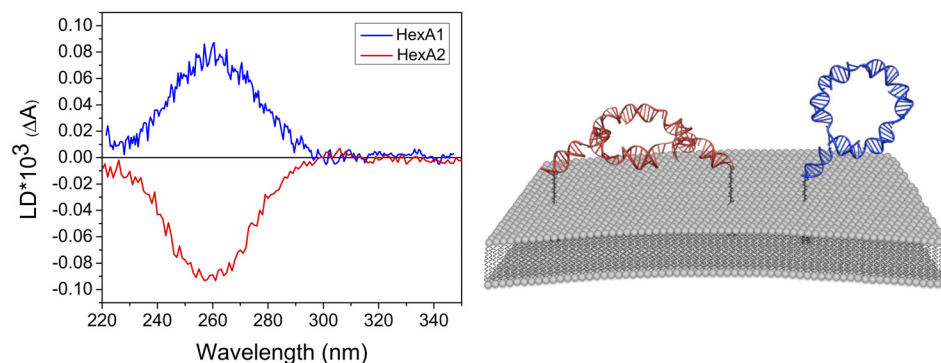


Figure 4.16. LD spectra of the DNA nanostructure tethered to lipid vesicles. (Left) Hexagonal DNA nanostructures, tethered with one (HexA1, blue) or two anchors (HexA2, red). (Right) Schematic of the DNA nanostructure in arrangements suggested by the LD results. The hexagonal unit-cell is viewed as totally isotropic in both cases and in contrast the double-stranded 10mer stretch of the anchors are anisotropic, yielding an LD signal. The LD^r at 260 nm of HexA1 (blue) and HexA2 (red) is 0.00668 and -0.00469, respectively. The corresponding angles, relative the membrane normal, are 49° and 59°.

More defined angular information about how the tethered DNA nanostructure orients when anchored to the membrane of a vesicle can be obtained from the reduced linear dichroism (LD^r). Several experimental indications (Paper VI) on this system suggest that a large portion of the nanostructure remains isotropic even when tethered to a membrane. This lead to the conclusion that only the protruding anchoring arms orient and subsequently yield a detectable LD-signal, whereas the hexagonal unit is isotropic and thus invisible for differential polarized light. This was based on analysis of LD signal strength of various related single anchored DNA assemblies and the interpretation of these findings has been extensively discussed in Paper VI. How the hexagonal DNA core structure may be viewed as totally isotropic even in the restricted conformational state of two opposite anchoring points, needs to be clarified. The structural freedom of the isotropic core in the confined environment of this arrangement is not interpreted as total rotational flexibility. Rather, a wobbling flexibility of a semi-planar structure that yields no net orientation of the bases and consequently no LD-signal. Based on the assumption that it is merely the nucleotide stretches of the anchoring arms that orient and render a differential response to linearly polarized light, the angles of the two anchoring alternatives could be estimated. When tethered with a single anchor, the helical axis diverts with an angle of 49° from the membrane normal. The corresponding angle for the two-anchor arrangement is estimated to be 59°. On the basis of these angles, the structural arrangements illustrated in Figure 4.16 were suggested. Furthermore, with a simple geometric interpretation of these arrangements the effective height of each alternative may be estimated. With a single anchor the DNA structure protrudes approximately 10.5 nm from the membrane surface and the corresponding protrusion is 3.5 nm for the double

anchors. The bars in Figure 4.15 show the consequential effect on particle size that these protrusions would render.

The studies presented in Paper V & VI demonstrate how DNA nanostructures can be integrated with lipid bilayers and how the structural arrangement depends on anchoring positions as well as anchoring type. Soft-surface nanotechnology is an interesting concept creating new multifunctional interfaces. The high-precision organization potential of a fully addressable nanogrid pave the way for surface based applications controlled on the molecular level. Maintaining system dynamics is a prerequisite for many processes in this context.

In conclusion, the molecular moieties employed as anchors in this thesis should be viewed from the perspective of two similar instruments for membrane integration, but with complementary properties. The porphyrin motif is on one hand a multifunctional unit that could for instance be an integral cog in an energy transfer machinery. This feature may on the other hand be undesired in many systems and the synthetic complexity of the porphyrin modification uncalled for. The lipid motif is more suited for generic use, avoiding the synthetic and functional complexity of porphyrins. Furthermore, optically transparent anchors are desirable in general applications.

4.5 Part IV – Triplex Recognition for Site-specific Functionalization

We have developed triplex recognition as a unique method to add site-specific functionalizations to preformed addressable DNA nanostructures. In this section, triplex recognition is demonstrated in context of energy transfer aiming at photonic applications.

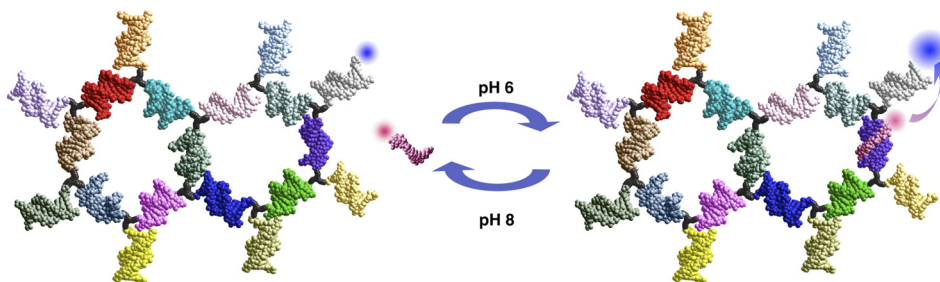


Figure 4.17. DNA-naphthalene with a pH-sensitive FRET switch. Protonation of the triplex forming oligonucleotide promotes binding at the specific address, upon which energy transfer may occur. The system constitutes a simplistic write-read-erase function.

A common approach to incorporate functionalizations into a DNA nanostructure is to use chemically modified oligonucleotides as an integrated part of the assembly, replacing one or more building blocks with functioning equivalents. Oligonucleotides can for instance be modified with linkers for nanoparticle attachment, *via* thiol or biotin/streptavidin association.^{79, 195} The latter may also be used to anchor protein motifs to DNA templates.^{35, 196} Fluorophore functionalization is another reoccurring topic in the literature, commonly used for energy transfer studies,¹¹⁰ demonstrating the potential of DNA based structural nanotechnology. However, being limited to incorporation of active units in the initial assembly process is unsatisfactory. The possibility of adding functionalities to a preformed DNA scaffold is a desirable property, providing opportunities of adaptability and evolved system dynamics. This led us to development of a hitherto unique strategy for site-specific targeting of DNA nanostructures using triplex forming oligonucleotides (TFO). This concept was demonstrated in Paper II, on the two-ring structure DNA-naphthalene (Figure 4.17).

To illustrate triplex addressability in the context of DNA nanotechnology, a sequence with high triple-strand binding affinity was incorporated into the construct. The address, to which the TFO adheres, relies exclusively on recognition pattern of Hoogsteen base pairs in the major groove of the double helix,¹¹ thus a polypurine stretch of 10 nucleotides was designed as part of the structural grid. It should be emphasized that even though the hydrogen-binding pattern in the major groove of polypurines is favorable for increased affinity, triplex addresses are not restricted to guanines and adenines. With the development of base analogues, candidates recognizing all four bases have been synthesized,²¹ expanding the number of available sequences suitable for triplex formation. Using a polypurine triplex address, the choice of TFO design is restricted to finding appropriate

thymine and cytosine analogues for T*AT and C⁺*GC triplets. The bases in the TFO used in Paper II were 2'-aminoethoxythymine (^AT) and 3-methyl-2-aminopyridine (^{Mc}P). The former promotes triplex stability by the amino modification on the sugar, which forms a coulombic interaction with the anionic phosphodiester backbone of the duplex, thus, decreasing the electrostatic repulsion. The cytosine analogue, ^{Mc}P, has higher pK_a than its Watson-Crick equivalent (above pH 6), making it more suitable in this context since low pH has a destabilising effect on the nanostructure itself.

The pH dependency of the TFO binding is useful and was utilized in Paper II to switch the triplex formation (Figure 4.17). It is first and foremost the N1 proton of ^{Mc}P that is the origin of this effect, being directly involved in Hoogsteen binding to N7 of guanine as hydrogen bond donor. ^AT also displays a pH dependent interaction, albeit less pronounced. Firstly, the cationic character of the protonated amino group only has an indirect effect on the binding affinity. Secondly, deprotonation of the group in question arise at elevated pH (above pH 8), at the limit of the regime used in Paper II. Gel electrophoresis run at pH 6.5 and subsequently pH 7.5 showed that the TFO bound at low pH and released at higher pH; meanwhile the structural integrity of the DNA-naphthalene was intact (Figure 3 in Paper II). Running the same gel at pH 7.5 proved that the TFO does not bind at higher pH since a band corresponding to the unbound TFO was observed. In contrast, no band migrating at the same rate as the nanostructure could be detected.

Triplex recognition has in this work been used to incorporate photonic functions in the nanostructure, demonstrated in Paper II by a basic write-read-erase function. This simplistic device was based on energy transfer between two cyanine dyes constituting a FRET pair: Cy3^{XXV} (donor) and Cy5^{XXVI} (acceptor).¹⁹⁷ The triplex forming strand, had been covalently modified with Cy3, infusing the photonic functionality to the construct upon binding. *Via* coupling to Cy5, already incorporated in the structure, energy transfer could be induced. As stated above, the pH sensitivity of the TFO binding provides an opportunity to switch the signal as a function of proton activity. By monitoring emission of the acceptor (Cy5) upon excitation of the donor (Cy3) at different pH, an estimation of the FRET efficiency was obtained. Reliable quantitative data of the efficiency could not be obtained since the stoichiometric relation between donor and acceptor bound to the same construct was difficult to estimate. Nevertheless, the FRET experiment showed two things. Firstly, that the TFO binds to the construct at low pH, since the presence of energy transfer correlates with the FRET-pair being in close proximity ($R_0=60 \text{ \AA}$ for Cy3: Cy5, according to Iqbal *et al.*¹⁹⁸). Secondly, that it is possible to turn this signal ON and OFF, by switching the pH from 6 to 8, at least for the duration of three cycles (Figure 4.18).

It is apparent when evaluating the estimated FRET efficiency as a function of pH that the process was not totally reversible. As expected, the initial high FRET at

^{XXV} Cy3: Abs $\epsilon_{\text{max}}=547 \text{ nm}$; Em $\lambda_{\text{max}}=564 \text{ nm}$

^{XXVI} Cy5: Abs: $\epsilon_{\text{max}}=648 \text{ nm}$; Em $\lambda_{\text{max}}=670 \text{ nm}$

pH 6 decreased significantly as the pH was increased to 8. The low FRET state is equivalent with the emission intensity of directly excited Cy5. This suggests complete dissociation of the TFO from the structure. The subsequent return to pH 6, causing TFO re-association, resulted in a corresponding increase in efficiency, which was again diminished at elevated pH. Though the system may be switched ON and OFF, each cycle displays a continuous loss of FRET efficiency, indicating inadequate reversibility. Control experiments indicated that the reason for this decrease is a gradual loss of material. Presumably the rather harsh treatment of strong acid and base, due to alternating additions of NaOH and HCl (1 μ l of 5 M), or undesired adhesion to pipette tips used in the experiment. The latter originates from nonspecific affinity of the TFO to such surfaces.

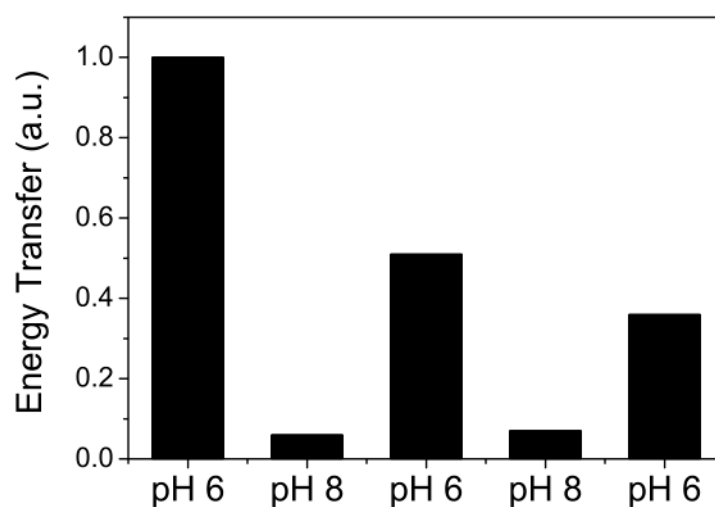


Figure 4.18. Switching between ON (pH 6) and OFF (pH 8). The output signal is the emission of Cy5 (670 nm) based on FRET from Cy3 upon binding of the TFO to DNA-naphthalene. The signal at pH 8 is equal to direct excitation of Cy5. Emission has been normalized so that the start value is unity.

We have, since the publication of Paper II, expanded the study of triplex recognition on a slightly altered system. The DNA template of the extended study is also a two-ringed structure but instead the two rightmost rings of DNA-anthracene from Paper III (Figure 4.5 & 4.6). The polypurine triplex address is thus positioned in the centre of the construct (Figure 4.19), as opposed to on the edge as in Paper II. Changing the conformation in this manner presents an opportunity of probing triplex targeting to a more structurally confined address, interesting from a versatility perspective. The design of this system also includes an additional fluorophore, suitable as energy donor in respect to Cy3 situated on the TFO. Furthermore, this arrangement has potential for two-step FRET process across the nanostructure, mediated by TFO in the bound state (Donor-Mediator-Acceptor system, Figure 4.19). Alexa488^{XXVII} is an appropriate choice of energy donor, since

^{XXVII} Alexa488: Abs ϵ_{\max} =495 nm; Em λ_{\max} =518 nm

its photophysical properties are insensitive to pH change. This system will here on be referred to as “DMA-naphthalene”.^{xxviii}

The binding constant of a triplex forming strand to a double helix is expected to be lower compared with the association affinity of the duplex itself. Addition of TFO in large excess is therefore not uncommon when studying triplex interactions (*e.g.* 12 equivalents in Rusling *et al.*²¹). To avoid undesired surplus of unbound TFO, an addition of only 1.25 eq. was used in Paper II. It is difficult to estimate the degree of labeling in this case, not knowing the binding constant of the triplex recognition to the nanostructure. A simple experiment varying the stoichiometric relation between the added TFO and the nanostructural target was therefore performed on the DMA-naphthalene system with the triplex address located in the middle of the structure (Figure 4.19).

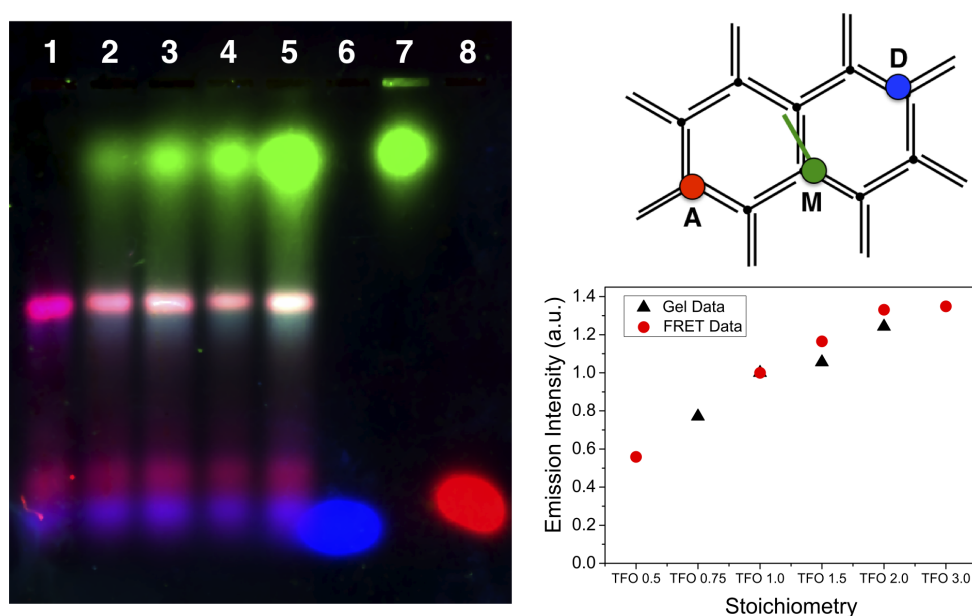


Figure 4.19. (Top right) Structure of DMA-naphthalene displaying positions of the photonic components: Alexa488 (Donor, D), Cy3-TFO (Mediator, M) & Cy5 (Acceptor, A). (Left) Gel showing TFO binding to DMA-naphthalene at different stoichiometric relations. (1) 0 eq TFO, (2) 0.75 eq TFO, (3) 1 eq TFO, (4) 1.5 eq TFO, (5) 2 eq TFO, (6) Alexa488 reference, (7) Cy3-TFO reference & (8) Cy5 reference. The figure is a compilation of three color-coded images corresponding to each dye in the system (D=blue, λ_{ex} =488 nm, filter=520 BP; M=green, λ_{ex} =532 nm/filter=580 BP; A=red, λ_{ex} =633 nm/filter=670 BP). The middle band on the gel corresponds to the desired DMA-naphthalene with the presence of all three dyes, in lane 2 to 5. Electrophoresis conditions are the same as described in Paper II, the gels were visualized using a Typhoon 9410 (GE Healthcare). (Bottom right) Combined emission data from gel (black triangles) and photometric titration (red circles) showing binding of TFO at different stoichiometry. Photometric titration monitoring the emission of Cy5 upon excitation of Alexa488 (ex : 470nm), as a function of TFO addition. The intensities have been normalized in respect to the intensity at 1 eq TFO.

^{xxviii} “DMA” is an abbreviation of Donor-Mediator-Acceptor, and “naphthalene” refers to the two-ringed DNA template.

The gel image in Figure 4.19 shows the result from an electrophoresis experiment with varied amount of TFO added to the structure. The middle band on the gel corresponds to the desired DMA-naphthalene with the presence of all three dyes, in lane 2 to 5. Interestingly, this is not the slowest migrating structure. The top band on the gel is equivalent with the unbound TFO (green). The reason why this short oligonucleotide of merely 10 bases displays the lowest electrophoretic mobility is due to its charge. At pH 6 both ^AT and ^{Me}C should be protonated resulting in a zwitterionic entity, with no net mobility in either direction. However, the pK_a may not be uniform over all bases in the TFO. It is plausible that some of the aminopyridine bases have become deprotonated in this pH regime, rendering slightly anionic species. The phenomenon was also observed and discussed in Paper II.

Going from left to right, the amount of added TFO is increased (from 0 eq. in lane 1 to 2 eq. in lane 5). Analyzing the emission intensity of Cy3 from the middle band, the level of bound TFO can be estimated. Evidently, the amount of triplex forming strand in the bound state increases with increasing addition of the oligonucleotide, indicating that the system has not reached saturation in this stoichiometric window (albeit the number of data points are rather limited). Combining this with data from a photometric titration experiment gives results in a more conclusive picture. Monitoring the emission of the energy acceptor Cy5 as a function of TFO addition upon excitation of Alexa488, the triplex forming efficiency can be estimated, based on the same principle as the FRET-experiment in Paper II. Relating the emission intensity of samples in both experiments to the sample with 1:1 stoichiometry, results in comparable data, given in Figure 4.19. The results indicate that the triplex address is saturated at approximately 2-3 eq. of TFO. Keeping in mind the large cohort of unbound TFO with modest anionic character visible on the gel, a minute decrease in pH could possibly increase binding affinity.

The idea of the DMA-naphthalene is to create a switchable photonic device, based on a two-step energy transfer process. To optimize the FRET efficiency and implement an alternative switch strategy, driven by hybridization energetic “DNA-fuel”^{121, 199}, the DMA-system was modified in two ways. (1) The fluorophores Cy3 and Cy5 were replaced by Alexa594^{XXIX} and Alexa647^{XXX}, respectively, resulting in a system based exclusively on Alexa dyes. The reason being that the overall energy transfer efficiency is expected to increase due to larger Förster distances (R_0). $R_0 \sim 60$ Å between Alexa488 (D) and Alexa594 (M) for the first step and 85 Å between Alexa594 (M) and Alexa647 (A) in the second step.^{XXXI} (2) The TFO was also modified. 5-methyl-cytosine (^{Me}C) with the same 2'-aminoethoxy-functionalization as ^AT was incorporated, instead of 3-methyl-2-aminopyridine (^{Me}P) recognizing guanine. This base-shift provides an alternative to the pH dependent switch. Since ^{Me}C, as opposed to its pyridine analogue, can form stable normal duplex it could

^{XXIX} Alexa594: Abs ϵ_{\max} =590 nm; Em λ_{\max} =617 nm

^{XXX} Alexa647: Abs ϵ_{\max} =650 nm; Em λ_{\max} =665 nm

^{XXXI} Invitrogen – Molecular Probes (www.invitrogen.com/site/us/en/home/References/Molecular-Probes-The-Handbook/tables.html)

potentially be used in a device driven by “DNA-fuel”. The basis of the switch would be a competition between triplex/duplex hybridization, driven by sequential addition of “fuel” and “anti-fuel” strands, similar to many toehold driven DNA machines.^{118-120, 200} The pK_a of ^{Me}C is expected to be slightly lower than ^{Me}P , potentially affecting triplex formation negatively, hence the addition of a stabilizing aminoethoxy-group at 2'-position. Furthermore, the mediating fluorophore Alexa594 was attached on opposite end of the TFO, positioned closer to the donor fluorophore (Figure 4.20).

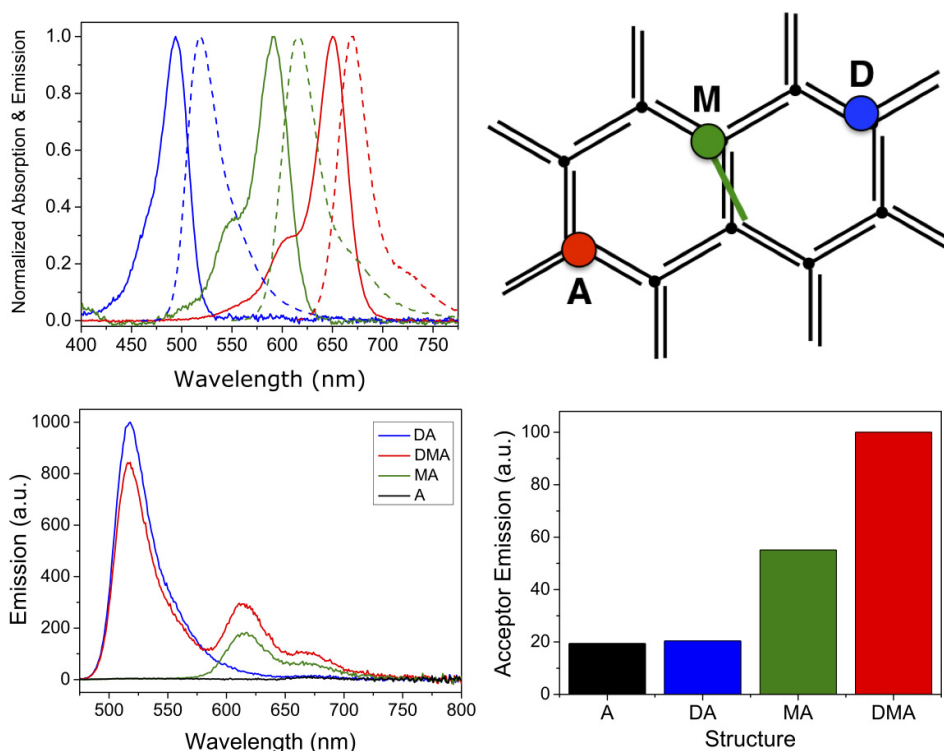


Figure 4.20. (Top left) Normalized absorption (solid lines) and emission (dash lines) spectra of the three Alexa dyes: Alexa488 (blue), Alexa594 (green) & Alexa647 (red). (Top right) Structure of DMA-naphthalene displaying positions of the photonic components: Alexa488 (Donor, D), Alexa594-TFO (Mediator, M) & Alexa647 (Acceptor, A). (Bottom left) Emission spectra of different dye combinations of the DMA system, excited at 470 nm. With the mediator TFO (M) bound to the construct, quenching of Alexa488 (D) is observed along with increased Alexa594 (M) and Alexa647 (A) emission (DMA vs DA). (Bottom right) Extracted acceptor emission coefficients from the spectrum to the left, using equation 4.3. Coefficients have been normalized so that the DMA value (red) is set to 100.

Before dynamic switching properties of the device are tested, the static ON and OFF states of the system need to be characterized. The energy transfer process from donor (D) to acceptor (A) was therefore studied, in the absence and presence of the mediating TFO (M). A theoretical prediction of the two-step energy transfer efficiency provides an idea of what experimental values to expect. The distances between the fluorophores can be estimated with a simple geometric interpretation of DMA-naphthalene. Assuming a distance of 70 Å in the first step and 80 Å in the

second, results in a total energy transfer efficiency of approximately 17%.^{xxxii} It should be clarified that this estimation presumes freely rotated fluorophores, *i.e.* $\kappa^2=2/3$, which may be an oversimplification on the crowded environment of the nanostructure.

Emission spectra of DMA-naphthalene samples containing different combinations of the fluorophores were recorded in order to evaluate energy transfer efficiency in the system (Figure 4.20), upon excitation of the donor ($\lambda_{ex}=470$ nm). The two primary constructs, representing ON and OFF, are constructs with both the donor and acceptor present, but with the difference of the mediator being present or not (DMA and DA, respectively). Furthermore, a sample containing only the acceptor was also assembled (A), to determine the effect of direct excitation of the dye. Another undesired pathway is the transfer to the acceptor from directly excited mediator, motivating the assembly of a construct with only these two fluorophores (MA). The resulting emission spectra are presented in Figure 4.20. The spectra of DA and DMA display clear differences. There is both a decrease in donor emission at 520 nm as well as an increase at 665 nm equivalent with acceptor emission, indicating energy transfer between the two upon binding of the mediation dye attached to the TFO. As seen from the MA spectra, there is a substantial contribution from energy transfer from directly excited mediator. On the other hand, there is minute effect from directly excited acceptor, evident from the A spectrum.

To estimate energy transfer efficiency the emission of the acceptor needs to be separated from the emission of the other fluorophores. Treating the recorded spectrum as a linear combination of spectra from individual fluorophores involved, can resolve the problem with spectral overlap of the participating dyes.

$$DMA(\lambda) = dD(\lambda) + mM(\lambda) + aA(\lambda) \quad (4.3)$$

DMA equals the recorded spectrum and the terms of the weighted sum correspond to the participating spectral components (Alexa488, 594 & 647, respectively). The same treatment has been utilized on similar systems.^{201, 202} The extracted contributions, *i.e.* coefficient in the linear combination, correlating with the acceptor emission from the different constructs are displayed in Figure 4.20. It is evident from the large difference between DA and DMA that the mediator indeed transfers energy across the nanostructure, a distance of approximately 15 nm. However, there is also a substantial contribution from energy transfer by undesired direct excitation of the mediator, as seen for the MA structure.

The overall yield of the process can be estimated by what portion of excitation energy from the donor that is emitted by the acceptor at the end. This black-box perspective on the two-step transfer process may be expressed as a fraction of spectral integrals (F), taken the corresponding quantum yield (Q) into account:

^{xxxii} $E_1=0.28$ and $E_2=0.59$

$$E = \frac{F_A/Q_A}{F_D/Q_D} \quad (4.4)$$

Important to note is that the emission of acceptor (F_A) in the numerator has been corrected for undesired secondary effect, *i.e.* transfer from directly excited mediator (substantial), direct excitation of the acceptor (minute) and direct transfer from the donor (negligible). The total efficiency is estimated to approximately 4% for the DMA-system presented in Figure 4.20, based on this analysis. This is significantly lower than the theoretically expected efficiency of 17%. There are a considerable number of reasons that could explain this deviation, including preferential orientation of the fluorophores or environmental variations affecting photophysical properties. However, the main reason for the low transfer efficiency is most likely the incomplete construct assembly. Based on the yield analysis in Paper III, the expected outcome of DNA-naphthalene assembly is less than 50%.^{xxxiii} The effective end-to-end energy transfer efficiency more than doubles, when taking the flawed self-assembly into account.^{xxxiv} It is plausible that the actual efficiency of the process is even higher, bearing in mind that the degree of triplex formation probably is below unity.

In conclusion, we have developed triplex recognition as a method of adding site-specific functionalizations to prefabricated addressable DNA-nanostructures. It has specifically been demonstrated in the context of photonics in this thesis, both in a simple pH-switchable FRET based device and a mediated two-step energy transfer system, potentially driven by “DNA-fuel”. These findings encourage further development of triplex recognition as a strategy for site-specific functionalization. The focus on energy transfer processes should not be viewed as merely a path towards photonic applications, but also an analytical method providing insight into system characteristics. Understanding triplex formation is vital for expanding high-precision functionalization to other arenas, *e.g.* reaction centers for synthetic assembly lines on the nanoscale.

^{xxxiii} $\gamma = 0.96^{19} = 0.46$ based on equation 4.1

^{xxxiv} By adding a loss factor in the denominator of equation 4.4, accounting for the fraction of excited donor molecules that is not part of a DMA-structure.

5. Concluding Remarks - Does this really matter?

In this thesis I have demonstrated how DNA can be employed as a structural material for molecular LEGO^{xxxv}, a construction process based on the principles of self-assembly. The work includes fabrication as well as functionalization of DNA-based nanoassemblies. Our development of the three-way oligonucleotide made it possible to assemble functional DNA nanostructures of minute size. This was demonstrated through the construction of a fully addressable DNA polycyclic nanonetwork (Papers I-III). We have also shown how application of a novel click fixation strategy can reinforce these constructs, creating robust structures that endure harsh conditions under which DNA normally is denaturated (Paper IV). We introduced triplex recognition as a method to add site-specific functionalizations to prefabricated structures, something that we demonstrated in terms of photonics (Paper II). Furthermore, this thesis also includes two studies that have taken us closer to useful applications. We have used a concept we call soft-surface nanotechnology, to achieve controllable integration of fabricated DNA nanostructures to lipid membranes (Paper V-VI). By the use of intelligent design on the molecular level, as well as clever use of chemical construction tools, we have demonstrated that it is possible to assemble non-mundane DNA nanostructures with built-in functions.

All the papers included in this thesis demonstrate concepts of great importance for the ongoing development of the DNA nanotechnology field. But, during the course of this work, we have also identified a few significant challenges related to the employed strategies. One example is relying on precise stoichiometric relations between the molecular LEGO-bricks in the assembly process. In this regard, the folding approach of DNA origami assembly provides a clear advantage, since the equilibrium is shifted towards the desired folded state by a huge excess of staple strands. Furthermore, it is plausible that there is an evolutionary advantage in avoiding extensive secondary structure formation of the M13 genome, *i.e.* evolution promotes inherent orthogonal sequence design in this case. To establish a detailed understanding of the elusive criteria of orthogonality that evolution has rendered could potentially help in future development of better algorithms. Another related topic, discussed in this thesis, is the assembly of networks through thermodynamically favorable processes, as manifested in effective ring-closure reactions. This is connected to recent reports about bundle formation of repetitive tiles, where a competition between intra- and inter-structural associations occurs,

^{xxxv} The Danish toy manufacturer coined the brand name LEGO® in the 1930s, based on the Danish phrase “leg godt” (“play well”). It was later realized that the word also had a Latin meaning: “I assemble”.

and where certain concentration regimes can promote the former. Gaining further insight in the thermodynamic and kinetic aspects of complex DNA self-assembly could hopefully provide more efficient future fabrication methods. An alternative assembly approach that has been discussed in this thesis is based on modular build-up. The formation of robust nanostructures that can serve as structural intermediates, and with long shelf-life, could provide a facile method of assembling larger nanostructures and provide an alternative to one-step formation if need be.

The last two papers included in this thesis demonstrate how DNA nanotechnology can be used to build active devices, thus taking a step closer to applications. By combining soft-surface integration with photonic functionalities, interesting DNA-based platforms for organization of various reaction centers can be envisaged. A lipid membrane provides dual separation possibilities, both membrane partitioned volumes and the phase separation between inside and outside the lipid bilayer. The creation of a structural scaffold for maintaining reaction centers in close vicinity to each other can also provide some directionality and circumvent certain problems associated with diffusion limited processes. Another advantage of developing soft-surface nanotechnology is that it paves the way for *in vivo* as well as biomimetic applications. Creation of surface-active functionalized nanodevices could open opportunities to mimic, and probe, processes *in vivo*. The fact that DNA is biocompatible may be both an advantage and a disadvantage in this context, and need to be carefully considered. Nature organizes many biochemical processes in the different membranes of cells, *e.g.* the photosynthesis of green plants, and this has been an inspiration for this work. Indeed, a completely artificial photosynthetic reaction center aiming at fuel production can easily be imagined building on the results presented in this thesis. Furthermore, facilitating high-precision localization at an interface could also provide junctions for different reaction centers in *e.g.* multi-step organic synthesis or catalytic cycles.

Our triplex recognition study shows that although promising, it needs further development to become a more versatile tool in the context of site-specific functionalization of DNA nanostructures. Incorporation of base analogues that recognizes all four bases is needed to expand the number of available target addresses beyond polypurines.²¹ In addition, functionalizations outside the context of light-induced energy transfer remain to be demonstrated. One potential application is “molecular imprinting”, where the high-resolution localization of an addressable DNA nanostructure is transferred to a solid support. Using triplex forming oligonucleotides, functionalized with surface anchoring moieties, it may prove possible to transfer these strands to a surface in a specific geometry defined by the nanostructural template, thus leaving a molecular imprint on the surface with the same high information density as in the template. Analogous to stamping, the DNA nanostructure then constitutes the “stamp” and the associated triplex strands represent the “ink”.

Finally, one of the corner stones in this ongoing endeavor of nanoscience, should be mentioned: *Integration*. This may be discussed from many perspectives. First of all, the “bottom-up” and “top-down” fabrication strategies should not be viewed as two competing strategies, but instead, as two complementary methods

with different strengths and weaknesses, which combined could provide solutions to scientific (and possibly technological) problems. Developing integration methods based on the different approaches is therefore of outmost importance, generating complex hybrid systems. Indeed, some work has already been performed aimed at bridging this gap between top-down and bottom-up, including a recent study interconnecting Au-discs on a lithographic pattern using DNA origami nanotubes with thiol functionalizations.²⁰³ This thesis also demonstrates another important perspective of integration; The incorporation with 2D surfaces. One may envisage either hybrid systems where the DNA nanostructure remain an integrated part of the device or that the structure permanently transfers a function with molecular resolution to a lithographic pattern, similar to the imprinting suggested above.

In conclusion, the work presented here has explored and provided insight into a few of the most fundamental aspects of self-assembled DNA nanotechnology. Some of the future challenges of this ever-growing research field have been identified, and suggestions on how to address them have been discussed. A couple of possible future applications utilizing the strategies outlined have been envisioned, but the only true limit for how much this may matter in the future is the imagination of the scientists continually developing this research field.

6. Acknowledgements - People that mattered

I would like to thank the following people:

My supervisor **Bengt** – thank you for inspiration and scientific guidance. Your never-ending enthusiasm for research is remarkable. I would not be the scholar I am today without your encouragement.

My co-supervisor **Marcus** – thank you for all your support, encouragement, advice and help with issues big & small. Your office door has always been open for me.

Tom Brown – thank you for all fruitful discussions. Without your chemistry knowledge, this thesis would have been impossible.

Per Lincoln – thank you for sharing your broad insights in science and for (often) making them comprehensible to me.

My co-authors on the papers of this thesis – thank you for your time and efforts.

My Master students **Calin, Lotta & Amir** – thank you for great work and making me learn a lot of new things as well.

All members of the **AMNA**-network at Chalmers & outside: **Jean-Marie Lehn's** group (Strasbourg), **Piero Baglioni's** group (Florence) & especially **Tom Brown's** group (Southampton) – thank you for enjoyable collaborations and interactions.

Paul Alivisatos – thank you for letting me visit your group. I really enjoyed my time at Berkeley.

Thank you **Elin, Nils, Moheb, Jens, Marcus & John** for proof-reading parts of or the entire thesis.

I would especially like to express an enormous gratitude to **Maria** for all your invaluable constructive comments and encouragement during the endeavor of writing this thesis. Also, thank you for reminding me that Victory Coffee at the department is not real coffee.

To all my colleges that have accompanied me on conferences – thank you for making these journeys more fun. Especially, **John, Jonas, Pär, Fredrik, Karl, Marcus & Joakim** for making the “Big in Japan”-tour an everlasting memory.

Everybody, past and present, at Physical Chemistry – thank you for an enjoyable atmosphere.

John, you were a good supervisor but, more importantly, you are a great friend.

Jonas, < Ch<3mist!?!|OOO|BiO³IO³g!?! > would not be the same without you.

My friends outside the academia – thank you for being there and reminding me of other important aspects of life. **Jens**, my best friend forever.

My Family – thank you for your support and for believing in me!

7. Bibliography

1. Moore, G. E., Cramping More Components onto Integrated Circuits. *Electronics* **1965**, *38*, 114-117.
2. Niemeyer, C. M., Nanoparticles, Proteins, and Nucleic Acids: Biotechnology Meets Materials Science. *Angew. Chem. Int. Ed.* **2001**, *40*, 4128-4158.
3. Watson, J. D.; Crick, F. H. C., Genetical Implications of the Structure of Deoxyribonucleic Acid. *Nature* **1953**, *171*, 964-967.
4. Watson, J. D.; Crick, F. H. C., Molecular Structure of Nucleic Acids: A Structure for Deoxyribose Nucleic Acid. *Nature* **1953**, *171*, 737-738.
5. Seeman, N. C., DNA in a Material World. *Nature* **2003**, *421*, 427-431.
6. Rothemund, P. W. K., Folding DNA to Create Nanoscale Shapes and Patterns. *Nature* **2006**, *440*, 297-302.
7. CORDIS, EU Nanotechnology Research: Exploring the Fundamentals, 2005.
8. Bloomfield, V. A.; Crothers, D. M.; Tinoco, I. J., *Nucleic Acids - Structures, Properties and Function*. University Science Books: Sausalito, CA, 2000.
9. Felsenfeld, G.; Davies, D. R.; Rich, A., Formation of a Three-Stranded Polynucleotide Molecule. *J. Am. Chem. Soc.* **1957**, *79*, 2023-2024.
10. Helene, C., The Anti-Gene Strategy: Control of Gene Expression by Triplex-Forming-Oligonucleotides. *Anticancer Drug Des.* **1991**, *6*, 569-584.
11. Hoogsteen, K., Crystal and Molecular Structure of a Hydrogen-Bonded Complex between 1-Methylthymine and 9-Methyladenine. *Acta Crystallogr.* **1963**, *16*, 907-916.
12. Duca, M.; Vekhoff, P.; Oussedik, K.; Halby, L.; Arimondo, P. B., The Triple Helix: 50 Years Later, the Outcome. *Nuc. Acids Res.* **2008**, *36*, 5123-5138.
13. Frank-Kamenetskii, M. D.; Mirkin, S. M., Triplex DNA Structures. *Annu. Rev. Biochem.* **1995**, *64*, 65-95.
14. Rusling, D. A.; Le Strat, L.; Powers, V. E. C.; Broughton-Head, V. J.; Booth, J.; Lack, O.; Brown, T.; Fox, K. R., Combining Nucleoside Analogues to Achieve Recognition of Oligopurine Tracts by Triplex-Forming Oligonucleotides at Physiological Ph. *FEBS Lett.* **2005**, *579*, 6616-6620.
15. Osborne, S. D.; Powers, V. E. C.; Rusling, D. A.; Lack, O.; Fox, K. R.; Brown, T., Selectivity and Affinity of Triplex-Forming Oligonucleotides Containing 2'-Aminoethoxy-5-(3-Aminoprop-1-Ynyl)Uridine for Recognizing at Base Pairs in Duplex DNA. *Nucleic Acids Res.* **2004**, *32*, 4439-4447.
16. Hildbrand, S.; Blaser, A.; Parel, S. P.; Leumann, C. J., 5-Substituted 2-Aminopyridine C-Nucleosides as Protonated Cytidine Equivalents: Increasing Efficiency and Selectivity in DNA Triple-Helix Formation. *J. Am. Chem. Soc.* **1997**, *119*, 5499-5511.

17. Cassidy, S. A.; Slickers, P.; Trent, J. O.; Capaldi, D. C.; Roselt, P. D.; Reese, C. B.; Neidle, S.; Fox, K. R., Recognition of Gc Base Pairs by Triplex Forming Oligonucleotides Containing Nucleosides Derived from 2-Aminopyridine. *Nuc. Acids Res.* **1997**, *25*, 4891-4898.
18. Xodo, L. E.; Manzini, G.; Quadrifoglio, F.; van der Marel, G. A.; van Boom, J. H., Effect of 5-Methylcytosine on the Stability of Triple-Stranded DNA - a Thermodynamic Study. *Nuc. Acids Res.* **1991**, *19*, 5625-5631.
19. Blommers, M. J. J.; Natt, F.; Jahnke, W.; Cuenoud, B., Dual Recognition of Double-Stranded DNA by 2'-Aminoethoxy-Modified Oligonucleotides: The Solution Structure of an Intramolecular Triplex Obtained by Nmr Spectroscopy. *Biochemistry* **1998**, *37*, 17714-17725.
20. Cuenoud, B.; Casset, F.; Huesken, D.; Natt, F.; Wolf, R. M.; Altmann, K.-H.; Martin, P.; Moser, H. E., Dual Recognition of Double-Stranded DNA by 2'-Aminoethoxy-Modified Oligonucleotides. *Angew. Chem. Int. Ed.* **1998**, *37*, 1288-1291.
21. Rusling, D. A.; Powers, V. E. C.; Ranasinghe, R. T.; Wang, Y.; Osborne, S. D.; Brown, T.; Fox, K. R., Four Base Recognition by Triplex-Forming Oligonucleotides at Physiological Ph. *Nuc. Acids Res.* **2005**, *33*, 3025-3032.
22. Seeman, N. C., Nucleic Acid Junctions and Lattices. *J. Theo. Bio.* **1982**, *99*, 237-247.
23. Kallenbach, N. R.; Ma, R. I.; Seeman, N. C., An Immobile Nucleic-Acid Junction Constructed from Oligonucleotides. *Nature* **1983**, *305*, 829-831.
24. Seeman, N. C.; Kallenbach, N. R., Design of Immobile Nucleic Acid Junctions. *Biophys. J.* **1983**, *44*, 201-209.
25. Seeman, N. C., Macromolecular Design, Nucleic Acid Junctions, and Crystal Formation. *J. Biomol. Struct. & Dyn.* **1985**, *3*, 11-34.
26. Seeman, N. C., Interactive Design and Manipulation of Macromolecular Architecture Utilizing Nucleic Acid Junctions. *J. Mol. Graph.* **1985**, *3*, 34-39.
27. Holliday, R., A Mechanism for Gene Conversion in Fungi. *Genet. Res.* **1964**, *5*, 282-304.
28. Fu, T. J.; Tsedinh, Y. C.; Seeman, N. C., Holliday Junction Crossover Topology. *Journal of Molecular Biology* **1994**, *236*, 91-105.
29. Fu, T. J.; Seeman, N. C., DNA Double-Crossover Molecules. *Biochemistry* **1993**, *32*, 3211-3220.
30. Li, X. J.; Yang, X. P.; Qi, J.; Seeman, N. C., Antiparallel DNA Double Crossover Molecules as Components for Nanoconstruction. *J. Am. Chem. Soc.* **1996**, *118*, 6131-6140.
31. LaBean, T. H.; Yan, H.; Kopatsch, J.; Liu, F. R.; Winfree, E.; Reif, J. H.; Seeman, N. C., Construction, Analysis, Ligation, and Self-Assembly of DNA Triple Crossover Complexes. *J. Am. Chem. Soc.* **2000**, *122*, 1848-1860.
32. Shen, Z. Y.; Yan, H.; Wang, T.; Seeman, N. C., Paranemic Crossover DNA: A Generalized Holliday Structure with Applications in Nanotechnology. *J. Am. Chem. Soc.* **2004**, *126*, 1666-1674.
33. Winfree, E.; Liu, F. R.; Wenzler, L. A.; Seeman, N. C., Design and Self-Assembly of Two-Dimensional DNA Crystals. *Nature* **1998**, *394*, 539-544.

34. Mao, C. D.; Sun, W. Q.; Seeman, N. C., Designed Two-Dimensional DNA Holliday Junction Arrays Visualized by Atomic Force Microscopy. *J. Am. Chem. Soc.* **1999**, *121*, 5437-5443.
35. Yan, H.; Park, S. H.; Finkelstein, G.; Reif, J. H.; LaBean, T. H., DNA-Templated Self-Assembly of Protein Arrays and Highly Conductive Nanowires. *Science* **2003**, *301*, 1882-1884.
36. Ding, B. Q.; Sha, R. J.; Seeman, N. C., Pseudo-hexagonal 2d DNA Crystals from Double Crossover Cohesion. *J. Am. Chem. Soc.* **2004**, *126*, 10230-10231.
37. Chelyapov, N.; Brun, Y.; Gopalkrishnan, M.; Reishus, D.; Shaw, B.; Adleman, L., DNA Triangles and Self-Assembled Hexagonal Tilings. *J. Am. Chem. Soc.* **2004**, *126*, 13924-13925.
38. He, Y.; Chen, Y.; Liu, H. P.; Ribbe, A. E.; Mao, C. D., Self-Assembly of Hexagonal DNA Two-Dimensional (2d) Arrays. *J. Am. Chem. Soc.* **2005**, *127*, 12202-12203.
39. Liu, H.; He, Y.; Ribbe, A. E.; Mao, C., Two-Dimensional (2d) DNA Crystals Assembled from Two DNA Strands. *Biomacromolecules* **2005**, *6*, 2943-2945.
40. He, Y.; Tian, Y.; Ribbe, A. E.; Mao, C., Highly Connected Two-Dimensional Crystals of DNA Six-Point-Stars. *J. Am. Chem. Soc.* **2006**, *128*, 15978-15979.
41. Sun, X.; Ko, S. H.; Zhang, C.; Ribbe, A. E.; Mao, C., Surface-Mediated DNA Self-Assembly. *J. Am. Chem. Soc.* **2009**, *131*, 13248-+.
42. Malo, J.; Mitchell, J. C.; Turberfield, A. J., A Two-Dimensional DNA Array: The Three-Layer Logpile. *J. Am. Chem. Soc.* **2009**, *131*, 13574-+.
43. Liu, D.; Wang, M. S.; Deng, Z. X.; Walulu, R.; Mao, C. D., Tensegrity: Construction of Rigid DNA Triangles with Flexible Four-Arm DNA Junctions. *J. Am. Chem. Soc.* **2004**, *126*, 2324-2325.
44. Zheng, J.; Birktoft, J. J.; Chen, Y.; Wang, T.; Sha, R.; Constantinou, P. E.; Ginell, S. L.; Mao, C.; Seeman, N. C., From Molecular to Macroscopic Via the Rational Design of a Self-Assembled 3d DNA Crystal. *Nature* **2009**, *461*, 74-77.
45. Zheng, J.; Constantinou, P. E.; Micheel, C.; Alivisatos, A. P.; Kiehl, R. A.; Seeman, N. C., Two-Dimensional Nanoparticle Arrays Show the Organizational Power of Robust DNA Motifs. *Nano Lett.* **2006**, *6*, 1502-1504.
46. Park, S. H.; Yin, P.; Liu, Y.; Reif, J. H.; LaBean, T. H.; Yan, H., Programmable DNA Self-Assemblies for Nanoscale Organization of Ligands and Proteins. *Nano Lett.* **2005**, *5*, 729-733.
47. Liu, Y.; Lin, C. X.; Li, H. Y.; Yan, H., Aptamer-Directed Self-Assembly of Protein Arrays on a DNA Nanostructure. *Angew. Chem. Int. Ed.* **2005**, *44*, 4333-4338.
48. Malo, J.; Mitchell, J. C.; Venien-Bryan, C.; Harris, J. R.; Wille, H.; Sherratt, D. J.; Turberfield, A. J., Engineering a 2d Protein-DNA Crystal. *Angew. Chem. Int. Ed.* **2005**, *44*, 3057-3061.
49. Selmi, D. N.; Adamson, R. J.; Attrill, H.; Goddard, A. D.; Gilbert, R. J. C.; Watts, A.; Turberfield, A. J., DNA-Templated Protein Arrays for Single-Molecule Imaging. *Nano Lett.* **2011**, *11*, 657-660.
50. Sharma, J.; Chhabra, R.; Liu, Y.; Ke, Y. G.; Yan, H., DNA-Templated Self-Assembly of Two-Dimensional and Periodical Gold Nanoparticle Arrays. *Angew. Chem. Int. Ed.* **2006**, *45*, 730-735.

51. Zhang, J. P.; Liu, Y.; Ke, Y. G.; Yan, H., Periodic Square-Like Gold Nanoparticle Arrays Templated by Self-Assembled 2d DNA Nanogrids on a Surface. *Nano Lett.* **2006**, *6*, 248-251.
52. Liu, Y.; Ke, Y.; Yan, H., Self-Assembly of Symmetric Finite-Size DNA Nanoarrays. *J. Am. Chem. Soc.* **2005**, *127*, 17140-17141.
53. Lund, K.; Liu, Y.; Lindsay, S.; Yan, H., Self-Assembling a Molecular Pegboard. *J. Am. Chem. Soc.* **2005**, *127*, 17606-17607.
54. Park, S. H.; Pistol, C.; Ahn, S. J.; Reif, J. H.; Lebeck, A. R.; Dwyer, C.; LaBean, T. H., Finite-Size, Fully Addressable DNA Tile Lattices Formed by Hierarchical Assembly Procedures. *Angew. Chem. Int. Ed.* **2006**, *45*, 735-739.
55. Liu, D.; Park, S. H.; Reif, J. H.; LaBean, T. H., DNA Nanotubes Self-Assembled from Triple-Crossover Tiles as Templates for Conductive Nanowires. *Proc. Natl. Acad. Sci. USA* **2004**, *101*, 717-722.
56. Rothmund, P. W. K.; Ekani-Nkodo, A.; Papadakis, N.; Kumar, A.; Fyngson, D. K.; Winfree, E., Design and Characterization of Programmable DNA Nanotubes. *J. Am. Chem. Soc.* **2004**, *126*, 16344-16352.
57. Mitchell, J. C.; Harris, J. R.; Malo, J.; Bath, J.; Turberfield, A. J., Self-Assembly of Chiral DNA Nanotubes. *J. Am. Chem. Soc.* **2004**, *126*, 16342-16343.
58. Mathieu, F.; Liao, S. P.; Kopatscht, J.; Wang, T.; Mao, C. D.; Seeman, N. C., Six-Helix Bundles Designed from DNA. *Nano Lett.* **2005**, *5*, 661-665.
59. Sherman, W. B.; Seeman, N. C., Design of Minimally Strained Nucleic Acid Nanotubes. *Biophys. J.* **2006**, *90*, 4546-4557.
60. Kuzuya, A.; Wang, R. S.; Sha, R. J.; Seeman, N. C., Six-Helix and Eight-Helix DNA Nanotubes Assembled from Half-Tubes. *Nano Lett.* **2007**, *7*, 1757-1763.
61. Wang, R.; Liu, W.; Seeman, N. C., Prototyping Nanorod Control: A DNA Double Helix Sheathed within a DNA Six-Helix Bundle. *Chem. Biol.* **2009**, *16*, 862-867.
62. Park, S. H.; Barish, R.; Li, H.; Reif, J. H.; Finkelstein, G.; Yan, H.; LaBean, T. H., Three-Helix Bundle DNA Tiles Self-Assemble into 2d Lattice or 1d Templates for Silver Nanowires. *Nano Lett.* **2005**, *5*, 693-696.
63. Yin, P.; Hariadi, R. F.; Sahu, S.; Choi, H. M. T.; Park, S. H.; LaBean, T. H.; Reif, J. H., Programming DNA Tube Circumferences. *Science* **2008**, *321*, 824-826.
64. Ke, Y. G.; Liu, Y.; Zhang, J. P.; Yan, H., A Study of DNA Tube Formation Mechanisms Using 4-, 8-, and 12-Helix DNA Nanostructures. *J. Am. Chem. Soc.* **2006**, *128*, 4414-4421.
65. Sharma, J.; Chhabra, R.; Cheng, A.; Brownell, J.; Liu, Y.; Yan, H., Control of Self-Assembly of DNA Tubules through Integration of Gold Nanoparticles. *Science* **2009**, *323*, 112-116.
66. Chen, J. H.; Seeman, N. C., Synthesis from DNA of a Molecule with the Connectivity of a Cube. *Nature* **1991**, *350*, 631-633.
67. Zhang, Y. W.; Seeman, N. C., Construction of a DNA-Truncated Octahedron. *J. Am. Chem. Soc.* **1994**, *116*, 1661-1669.
68. Goodman, R. P.; Schaap, I. A. T.; Tardin, C. F.; Erben, C. M.; Berry, R. M.; Schmidt, C. F.; Turberfield, A. J., Rapid Chiral Assembly of Rigid

- DNA Building Blocks for Molecular Nanofabrication. *Science* **2005**, *310*, 1661-1665.
69. He, Y.; Ye, T.; Su, M.; Zhang, C.; Ribbe, A. E.; Jiang, W.; Mao, C., Hierarchical Self-Assembly of DNA into Symmetric Supramolecular Polyhedra. *Nature* **2008**, *452*, 198-U41.
 70. Oliveira, C. L. P.; Juul, S.; Jorgensen, H. L.; Knudsen, B.; Tordrup, D.; Oteri, F.; Falconi, M.; Koch, J.; Desideri, A.; Pedersen, J. S.; Andersen, F. F.; Knudsen, B. R., Structure of Nanoscale Truncated Octahedral DNA Cages: Variation of Single-Stranded Linker Regions and Influence on Assembly Yields. *Acs Nano* **2010**, *4*, 1367-1376.
 71. Wong, N. Y.; Zhang, C.; Tan, L. H.; Lu, Y., Site-Specific Attachment of Proteins onto a 3d DNA Tetrahedron through Backbone-Modified Phosphorothioate DNA. *Small* **2011**, *7*, 1427-1430.
 72. Zhang, C.; Su, M.; He, Y.; Zhao, X.; Fang, P. A.; Ribbe, A. E.; Jiang, W.; Mao, C. D., Conformational Flexibility Facilitates Self-Assembly of Complex DNA Nanostructures. *Proc. Natl. Acad. Sci. USA* **2008**, *105*, 10665-10669.
 73. He, Y.; Su, M.; Fang, P.-a.; Zhang, C.; Ribbe, A. E.; Jiang, W.; Mao, C., On the Chirality of Self-Assembled DNA Octahedra. *Angew. Chem. Int. Ed.* **2010**, *49*, 748-751.
 74. Zhang, C.; Su, M.; He, Y.; Leng, Y.; Ribbe, A. E.; Wang, G.; Jiang, W.; Mao, C., Exterior Modification of a DNA Tetrahedron. *Chem. Commun.* **2010**, *46*, 6792-6794.
 75. Andersen, F. F.; Knudsen, B.; Oliveira, C. L. P.; Frohlich, R. F.; Kruger, D.; Bungert, J.; Agbandje-McKenna, M.; McKenna, R.; Juul, S.; Veigaard, C.; Koch, J.; Rubinstein, J. L.; Guldbrandtsen, B.; Hede, M. S.; Karlsson, G.; Andersen, A. H.; Pedersen, J. S.; Knudsen, B. R., Assembly and Structural Analysis of a Covalently Closed Nano-Scale DNA Cage. *Nuc. Acids Res.* **2008**, *36*, 1113-1119.
 76. Falconi, M.; Oteri, F.; Chillemi, G.; Andersen, F. F.; Tordrup, D.; Oliveira, C. L. P.; Pedersen, J. S.; Knudsen, B. R.; Desideri, A., Deciphering the Structural Properties That Confer Stability to a DNA Nanocage. *Acs Nano* **2009**, *3*, 1813-1822.
 77. Oteri, F.; Falconi, M.; Chillemi, G.; Andersen, F. F.; Oliveira, C. L. P.; Pedersen, J. S.; Knudsen, B. R.; Desideri, A., Simulative Analysis of a Truncated Octahedral DNA Nanocage Family Indicates the Single-Stranded Thymidine Linkers as the Major Player for the Conformational Variability. *J. Phys. Chem. C* **2011**, *115*, 16819-16827.
 78. Goodman, R. P.; Berry, R. M.; Turberfield, A. J., The Single-Step Synthesis of a DNA Tetrahedron. *Chem. Commun.* **2004**, 1372-1373.
 79. Mastroianni, A. J.; Claridge, S. A.; Alivisatos, A. P., Pyramidal and Chiral Groupings of Gold Nanocrystals Assembled Using DNA Scaffolds. *J. Am. Chem. Soc.* **2009**, *131*, 8455-8459.
 80. Ozhalici-Unal, H.; Armitage, B. A., Fluorescent DNA Nanotags Based on a Self-Assembled DNA Tetrahedron. *Acs Nano* **2009**, *3*, 425-433.
 81. Li, Z.; Wei, B.; Nangreave, J.; Lin, C.; Liu, Y.; Mi, Y.; Yan, H., A Replicable Tetrahedral Nanostructure Self-Assembled from a Single DNA Strand. *J. Am. Chem. Soc.* **2009**, *131*, 13093-13098.
 82. Han, D.; Huang, J.; Zhu, Z.; Yuan, Q.; You, M.; Chen, Y.; Tan, W., Molecular Engineering of Photoresponsive Three-Dimensional DNA Nanostructures. *Chem. Commun.* **2011**, *47*, 4670-4672.

83. Goodman, R. P.; Heilemann, M.; Doose, S.; Erben, C. M.; Kapanidis, A. N.; Turberfield, A. J., Reconfigurable, Braced, Three-Dimensional DNA Nanostructures. *Nat. Nanotechnol.* **2008**, *3*, 93-96.
84. Erben, C. M.; Goodman, R. P.; Turberfield, A. J., Single-Molecule Protein Encapsulation in a Rigid DNA Cage. *Angew. Chem. Int. Ed.* **2006**, *45*, 7414-7417.
85. Bhatia, D.; Mehtab, S.; Krishnan, R.; Indi, S. S.; Basu, A.; Krishnan, Y., Icosahedral DNA Nanocapsules by Modular Assembly. *Angew. Chem. Int. Ed.* **2009**, *48*, 4134-4137.
86. Walsh, A. S.; Yin, H.; Erben, C. M.; Wood, M. J. A.; Turberfield, A. J., DNA Cage Delivery to Mammalian Cells. *Acs Nano* **2011**, *5*, 5427-5432.
87. McLaughlin, C. K.; Hamblin, G. D.; Sleiman, H. F., Supramolecular DNA Assembly. *Chem. Soc. Rev.* **2011**, *40*, 5647-5656.
88. Aldaye, F. A.; Sleiman, H. F., Sequential Self-Assembly of a DNA Hexagon as a Template for the Organization of Gold Nanoparticles. *Angew. Chem. Int. Ed.* **2006**, *45*, 2204-2209.
89. Aldaye, F. A.; Sleiman, H. F., Modular Access to Structurally Switchable 3d Discrete DNA Assemblies. *J. Am. Chem. Soc.* **2007**, *129*, 13376-+.
90. Lo, P. K.; Altvater, F.; Sleiman, H. F., Templated Synthesis of DNA Nanotubes with Controlled, Predetermined Lengths. *J. Am. Chem. Soc.* **2010**, *132*, 10212-10214.
91. Lo, P. K.; Karam, P.; Aldaye, F. A.; McLaughlin, C. K.; Hamblin, G. D.; Cosa, G.; Sleiman, H. F., Loading and Selective Release of Cargo in DNA Nanotubes with Longitudinal Variation. *Nat. Chem.* **2010**, *2*, 319-328.
92. Scheffler, M.; Dorenbeck, A.; Jordan, S.; Wustefeld, M.; von Kiedrowski, G., Self-Assembly of Trisilgonucleotidyls: The Case for Nano-Acetylene and Nano-Cyclobutadiene. *Angew. Chem. Int. Ed.* **1999**, *38*, 3312-3315.
93. Zimmermann, J.; Cebulla, M. R. J.; Monninghoff, S.; von Kiedrowski, G., Self-Assembly of a DNA Dodecahedron from 20 Trisilgonucleotides with C-3h Linkers. *Angew. Chem. Int. Ed.* **2008**, *47*, 3626-3630.
94. Williamson, J. R., Rna Origami. *Nat. Struct. Biol.* **1994**, *1*, 270-272.
95. Yan, H.; LaBean, T. H.; Feng, L. P.; Reif, J. H., Directed Nucleation Assembly of DNA Tile Complexes for Barcode-Patterned Lattices. *Proc. Natl. Acad. Sci. USA* **2003**, *100*, 8103-8108.
96. Shih, W. M.; Quispe, J. D.; Joyce, G. F., A 1.7-Kilobase Single-Stranded DNA That Folds into a Nanoscale Octahedron. *Nature* **2004**, *427*, 618-621.
97. Andersen, E. S.; Dong, M. D.; Nielsen, M. M.; Jahn, K.; Lind-Thomsen, A.; Mamdouh, W.; Gothelf, K. V.; Besenbacher, F.; Kjems, J., DNA Origami Design of Dolphin-Shaped Structures with Flexible Tails. *Acs Nano* **2008**, *2*, 1213-1218.
98. Zhao, Z.; Yan, H.; Liu, Y., A Route to Scale up DNA Origami Using DNA Tiles as Folding Staples. *Angew. Chem. Int. Ed.* **2010**, *49*, 1414-1417.
99. Li, Z.; Liu, M.; Wang, L.; Nangreave, J.; Yan, H.; Liu, Y., Molecular Behavior of DNA Origami in Higher-Order Self-Assembly. *J. Am. Chem. Soc.* **2010**, *132*, 13545-13552.

100. Hogberg, B.; Liedl, T.; Shih, W. M., Folding DNA Origami from a Double-Stranded Source of Scaffold. *J. Am. Chem. Soc.* **2009**, *131*, 9154-9155.
101. Dietz, H.; Douglas, S. M.; Shih, W. M., Folding DNA into Twisted and Curved Nanoscale Shapes. *Science* **2009**, *325*, 725-730.
102. Douglas, S. M.; Dietz, H.; Liedl, T.; Hogberg, B.; Graf, F.; Shih, W. M., Self-Assembly of DNA into Nanoscale Three-Dimensional Shapes. *Nature* **2009**, *459*, 414-418.
103. Ke, Y. G.; Douglas, S. M.; Liu, M. H.; Sharma, J.; Cheng, A. C.; Leung, A.; Liu, Y.; Shih, W. M.; Yan, H., Multilayer DNA Origami Packed on a Square Lattice. *J. Am. Chem. Soc.* **2009**, *131*, 15903-15908.
104. Ke, Y. G.; Sharma, J.; Liu, M. H.; Jahn, K.; Liu, Y.; Yan, H., Scaffolded DNA Origami of a DNA Tetrahedron Molecular Container. *Nano Lett.* **2009**, *9*, 2445-2447.
105. Kuzuya, A.; Komiyama, M., Design and Construction of a Box-Shaped 3d-DNA Origami. *Chem. Commun.* **2009**, 4182-4184.
106. Andersen, E. S.; Dong, M.; Nielsen, M. M.; Jahn, K.; Subramani, R.; Mamdouh, W.; Golas, M. M.; Sander, B.; Stark, H.; Oliveira, C. L. P.; Pedersen, J. S.; Birkedal, V.; Besenbacher, F.; Gothelf, K. V.; Kjems, J., Self-Assembly of a Nanoscale DNA Box with a Controllable Lid. *Nature* **2009**, *459*, 73-76.
107. Han, D. R.; Pal, S.; Liu, Y.; Yan, H., Folding and Cutting DNA into Reconfigurable Topological Nanostructures. *Nat. Nanotechnol.* **2010**, *5*, 712-717.
108. Steinhauer, C.; Jungmann, R.; Sobey, T. L.; Simmel, F. C.; Tinnefeld, P., DNA Origami as a Nanoscopic Ruler for Super-Resolution Microscopy. *Angew. Chem. Int. Ed.* **2009**, *48*, 8870-8873.
109. Stein, I. H.; Schueller, V.; Boehm, P.; Tinnefeld, P.; Liedl, T., Single-Molecule FRET Ruler Based on Rigid DNA Origami Blocks. *ChemPhysChem* **2011**, *12*, 689-695.
110. Stein, I. H.; Steinhauer, C.; Tinnefeld, P., Single-Molecule Four-Color FRET Visualizes Energy-Transfer Paths on DNA Origami. *J. Am. Chem. Soc.* **2011**, *133*, 4193-4195.
111. Rinker, S.; Ke, Y.; Liu, Y.; Chhabra, R.; Yan, H., Self-Assembled DNA Nanostructures for Distance-Dependent Multivalent Ligand-Protein Binding. *Nat. Nanotechnol.* **2008**, *3*, 418-422.
112. Ding, B.; Deng, Z.; Yan, H.; Cabrini, S.; Zuckermann, R. N.; Bokor, J., Gold Nanoparticle Self-Similar Chain Structure Organized by DNA Origami. *J. Am. Chem. Soc.* **2010**, *132*, 3248-3249.
113. Shen, X.; Song, C.; Wang, J.; Shi, D.; Wang, Z.; Liu, N.; Ding, B., Rolling up Gold Nanoparticle-Dressed DNA Origami into Three-Dimensional Plasmonic Chiral Nanostructures. *J. Am. Chem. Soc.* **2012**, *134*, 146-149.
114. Kuzyk, A.; Schreiber, R.; Fan, Z.; Pardatscher, G.; Roller, E.-M.; Högele, A.; Simmel, F. C.; Govorov, A. O.; Liedl, T. DNA-Based Self-Assembly of Chiral Plasmonic Nanostructures with Tailored Optical Response *Condensed Matter - Mesoscale and Nanoscale Physics* [Online], 2011.
115. Voigt, N. V.; Topping, T.; Rotaru, A.; Jacobsen, M. F.; Ravnsbaek, J. B.; Subramani, R.; Mamdouh, W.; Kjems, J.; Mokhir, A.; Besenbacher, F.; Gothelf, K. V., Single-Molecule Chemical Reactions on DNA Origami. *Nat. Nanotechnol.* **2010**, *5*, 200-203.

116. Gu, H. Z.; Chao, J.; Xiao, S. J.; Seeman, N. C., A Proximity-Based Programmable DNA Nanoscale Assembly Line. *Nature* **2010**, *465*, 202-206.
117. Mao, C. D.; Sun, W. Q.; Shen, Z. Y.; Seeman, N. C., A Nanomechanical Device Based on the B-Z Transition of DNA. *Nature* **1999**, *397*, 144-146.
118. Yurke, B.; Turberfield, A. J.; Mills, A. P.; Simmel, F. C.; Neumann, J. L., A DNA-Fuelled Molecular Machine Made of DNA. *Nature* **2000**, *406*, 605-608.
119. Yan, H.; Zhang, X. P.; Shen, Z. Y.; Seeman, N. C., A Robust DNA Mechanical Device Controlled by Hybridization Topology. *Nature* **2002**, *415*, 62-65.
120. Ding, B.; Seeman, N. C., Operation of a DNA Robot Arm Inserted into a 2d DNA Crystalline Substrate. *Science* **2006**, *314*, 1583-1585.
121. Turberfield, A. J.; Mitchell, J. C.; Yurke, B.; Mills, A. P.; Blakey, M. I.; Simmel, F. C., DNA Fuel for Free-Running Nanomachines. *Phys. Rev. Lett.* **2003**, *90*, 1-4.
122. Green, S. J.; Lubrich, D.; Turberfield, A. J., DNA Hairpins: Fuel for Autonomous DNA Devices. *Biophys. J.* **2006**, *91*, 2966-2975.
123. Tyagi, S.; Kramer, F. R., Molecular Beacons: Probes That Fluoresce Upon Hybridization. *Nat. Biotechnol.* **1996**, *14*, 303-308.
124. Liang, X. G.; Nishioka, H.; Takenaka, N.; Asanuma, H., A DNA Nanomachine Powered by Light Irradiation. *ChemBioChem* **2008**, *9*, 702-705.
125. Burge, S.; Parkinson, G. N.; Hazel, P.; Todd, A. K.; Neidle, S., Quadruplex DNA: Sequence, Topology and Structure. *Nuc. Acids Res.* **2006**, *34*, 5402-5415.
126. Fahlman, R. P.; Hsing, M.; Sporer-Tuhten, C. S.; Sen, D., Duplex Pinching: A Structural Switch Suitable for Contractile DNA Nanoconstructions. *Nano Lett.* **2003**, *3*, 1073-1078.
127. Niemeyer, C. M.; Adler, M.; Lenhart, S.; Gao, S.; Fuchs, H.; Chi, L. F., Nucleic Acid Supercoiling as a Means for Ionic Switching of DNA-Nanoparticle Networks. *ChemBioChem* **2001**, *2*, 260-264.
128. Gehring, K.; Leroy, J. L.; Gueron, M., A Tetrameric DNA-Structure with Protonated Cytosine Cytosine Base-Pairs. *Nature* **1993**, *363*, 561-565.
129. Gueron, M.; Leroy, J. L., The I-Motif in Nucleic Acids. *Curr. Opin. Struct. Biol.* **2000**, *10*, 326-331.
130. Liu, D. S.; Balasubramanian, S., A Proton-Fuelled DNA Nanomachine. *Angew. Chem. Int. Ed.* **2003**, *42*, 5734-5736.
131. Liedl, T.; Simmel, F. C., Switching the Conformation of a DNA Molecule with a Chemical Oscillator. *Nano Lett.* **2005**, *5*, 1894-1898.
132. Liedl, T.; Olapinski, M.; Simmel, F. C., A Surface-Bound DNA Switch Driven by a Chemical Oscillator. *Angew. Chem. Int. Ed.* **2006**, *45*, 5007-5010.
133. Modi, S.; Swetha, M. G.; Goswami, D.; Gupta, G. D.; Mayor, S.; Krishnan, Y., A DNA Nanomachine That Maps Spatial and Temporal Ph Changes inside Living Cells. *Nat. Nanotechnol.* **2009**, *4*, 325-330.
134. Chen, Y.; Lee, S. H.; Mao, C., A DNA Nanomachine Based on a Duplex-Triplex Transition. *Angew. Chem. Int. Ed.* **2004**, *43*, 5335-5338.

135. Sherman, W. B.; Seeman, N. C., A Precisely Controlled DNA Biped Walking Device. *Nano Lett.* **2004**, *4*, 1203-1207.
136. Shin, J. S.; Pierce, N. A., A Synthetic DNA Walker for Molecular Transport. *J. Am. Chem. Soc.* **2004**, *126*, 10834-10835.
137. Yin, P.; Yan, H.; Daniell, X. G.; Turberfield, A. J.; Reif, J. H., A Unidirectional DNA Walker That Moves Autonomously Along a Track. *Angew. Chem. Int. Ed.* **2004**, *43*, 4906-4911.
138. Bath, J.; Green, S. J.; Turberfield, A. J., A Free-Running DNA Motor Powered by a Nicking Enzyme. *Angew. Chem. Int. Ed.* **2005**, *44*, 4358-4361.
139. Bath, J.; Green, S. J.; Allen, K. E.; Turberfield, A. J., Mechanism for a Directional, Processive, and Reversible DNA Motor. *Small* **2009**, *5*, 1513-1516.
140. Omabegho, T.; Sha, R.; Seeman, N. C., A Bipedal DNA Brownian Motor with Coordinated Legs. *Science* **2009**, *324*, 67-71.
141. Green, S. J.; Bath, J.; Turberfield, A. J., Coordinated Chemomechanical Cycles: A Mechanism for Autonomous Molecular Motion. *Phys. Rev. Lett.* **2008**, *101*.
142. Yin, P.; Choi, H. M. T.; Calvert, C. R.; Pierce, N. A., Programming Biomolecular Self-Assembly Pathways. *Nature* **2008**, *451*, 318-U4.
143. Tian, Y.; He, Y.; Chen, Y.; Yin, P.; Mao, C. D., A Dnazyme That Walks Processively and Autonomously Along a One-Dimensional Track. *Angew. Chem. Int. Ed.* **2005**, *44*, 4355-4358.
144. Pei, R.; Taylor, S. K.; Stefanovic, D.; Rudchenko, S.; Mitchell, T. E.; Stojanovic, M. N., Behavior of Polycatalytic Assemblies in a Substrate-Displaying Matrix. *J. Am. Chem. Soc.* **2006**, *128*, 12693-12699.
145. Lund, K.; Manzo, A. J.; Dabby, N.; Michelotti, N.; Johnson-Buck, A.; Nangreave, J.; Taylor, S.; Pei, R.; Stojanovic, M. N.; Walter, N. G.; Winfree, E.; Yan, H., Molecular Robots Guided by Prescriptive Landscapes. *Nature* **2010**, *465*, 206-210.
146. He, Y.; Liu, D. R., Autonomous Multistep Organic Synthesis in a Single Isothermal Solution Mediated by a DNA Walker. *Nat. Nanotechnol.* **2010**, *5*, 778-782.
147. Kolb, H. C.; Finn, M. G.; Sharpless, K. B., Click Chemistry: Diverse Chemical Function from a Few Good Reactions. *Angew. Chem. Int. Ed.* **2001**, *40*, 2004-2021.
148. Rostovtsev, V. V.; Green, L. G.; Fokin, V. V.; Sharpless, K. B., A Stepwise Huisgen Cycloaddition Process: Copper(I)-Catalyzed Regioselective "Ligation" Of Azides and Terminal Alkynes. *Angew. Chem. Int. Ed.* **2002**, *41*, 2596-2599.
149. Tornøe, C. W.; Christensen, C.; Meldal, M., Peptidotriazoles on Solid Phase: [1,2,3]-Triazoles by Regiospecific Copper(I)-Catalyzed 1,3-Dipolar Cycloadditions of Terminal Alkynes to Azides. *J. Org. Chem.* **2002**, *67*, 3057-3064.
150. Meldal, M.; Tornøe, C. W., Cu-Catalyzed Azide-Alkyne Cycloaddition. *Chem. Rev.* **2008**, *108*, 2952-3015.
151. Bock, V. D.; Hiemstra, H.; van Maarseveen, J. H., Cu-I-Catalyzed Alkyne-Azide "Click" Cycloadditions from a Mechanistic and Synthetic Perspective. *Eur. J. Org. Chem.* **2006**, 51-68.
152. Chan, T. R.; Hilgraf, R.; Sharpless, K. B.; Fokin, V. V., Polytriazoles as Copper(I)-Stabilizing Ligands in Catalysis. *Org. Lett.* **2004**, *6*, 2853-2855.

153. Kolb, H. C.; Sharpless, K. B., The Growing Impact of Click Chemistry on Drug Discovery. *Drug Discovery Today* **2003**, *8*, 1128-1137.
154. Ornelas, C.; Aranzaes, J. R.; Cloutet, E.; Alves, S.; Astruc, D., Click Assembly of 1,2,3-Triazole-Linked Dendrimers, Including Ferrocenyl Dendrimers, Which Sense Both Oxo Anions and Metal Cations. *Angew. Chem. Int. Ed.* **2007**, *46*, 872-877.
155. Wu, P.; Feldman, A. K.; Nugent, A. K.; Hawker, C. J.; Scheel, A.; Voit, B.; Pyun, J.; Frechet, J. M. J.; Sharpless, K. B.; Fokin, V. V., Efficiency and Fidelity in a Click-Chemistry Route to Triazole Dendrimers by the Copper(I)-Catalyzed Ligation of Azides and Alkynes. *Angew. Chem. Int. Ed.* **2004**, *43*, 3928-3932.
156. Angell, Y. L.; Burgess, K., Peptidomimetics Via Copper-Catalyzed Azide-Alkyne Cycloadditions. *Chem. Soc. Rev.* **2007**, *36*, 1674-1689.
157. Speers, A. E.; Adam, G. C.; Cravatt, B. F., Activity-Based Protein Profiling in Vivo Using a Copper(I)-Catalyzed Azide-Alkyne [3+2] Cycloaddition. *J. Am. Chem. Soc.* **2003**, *125*, 4686-4687.
158. Devaraj, N. K.; Collman, J. P., Copper Catalyzed Azide-Alkyne Cycloadditions on Solid Surfaces: Applications and Future Directions. *Qsar & Comb. Science* **2007**, *26*, 1253-1260.
159. Rozkiewicz, D. I.; Gierlich, J.; Burley, G. A.; Gutmiedl, K.; Carell, T.; Ravoo, B. J.; Reinhoudt, D. N., Transfer Printing of DNA By "Click" Chemistry. *ChemBioChem* **2007**, *8*, 1997-2002.
160. Seo, T. S.; Bai, X. P.; Kim, D. H.; Meng, Q. L.; Shi, S. D.; Ruparel, H.; Li, Z. M.; Turro, N. J.; Ju, J. Y., Four-Color DNA Sequencing by Synthesis on a Chip Using Photocleavable Fluorescent Nucleotides. *Proc. Natl. Acad. Sci. USA* **2005**, *102*, 5926-5931.
161. Gierlich, J.; Burley, G. A.; Gramlich, P. M. E.; Hammond, D. M.; Carell, T., Click Chemistry as a Reliable Method for the High-Density Postsynthetic Functionalization of Alkyne-Modified DNA. *Org. Lett.* **2006**, *8*, 3639-3642.
162. Seo, T. S.; Li, Z. M.; Ruparel, H.; Ju, J. Y., Click Chemistry to Construct Fluorescent Oligonucleotides for DNA Sequencing. *J. Org. Chem.* **2003**, *68*, 609-612.
163. Kumar, R.; El-Sagheer, A.; Tumpene, J.; Lincoln, P.; Wilhelmsson, L. M.; Brown, T., Template-Directed Oligonucleotide Strand Ligation, Covalent Intramolecular DNA Circularization and Catenation Using Click Chemistry. *J. Am. Chem. Soc.* **2007**, *129*, 6859-6864.
164. El-Sagheer, A. H.; Kumar, R.; Findlow, S.; Werner, J. M.; Lane, A. N.; Brown, T., A Very Stable Cyclic DNA Miniduplex with Just Two Base Pairs. *ChemBioChem* **2008**, *9*, 50-52.
165. Kocalka, P.; El-Sagheer, A. H.; Brown, T., Rapid and Efficient DNA Strand Cross-Linking by Click Chemistry. *ChemBioChem* **2008**, *9*, 1280-1285.
166. Wiener, M. C.; White, S. H., Structure of a Fluid Dioleoylphosphatidylcholine Bilayer Determined by Joint Refinement of X-Ray and Neutron Diffraction Data. Iii. Complete Structure. *Biophys. J.* **1992**, *61*, 434-447.
167. Whitesides, G. M.; Boncheva, M., Beyond Molecules: Self-Assembly of Mesoscopic and Macroscopic Components. *Proc. Natl. Acad. Sci. USA* **2002**, *99*, 4769-4774.

168. Lehn, J. M., Supramolecular Chemistry - Scope and Perspectives Molecules, Supermolecules, and Molecular Devices. *Angew. Chem. Int. Ed.* **1988**, *27*, 89-112.
169. Lehn, J. M., Perspectives in Supramolecular Chemistry - from Molecular Recognition Towards Molecular Information Processing and Self-Organization. *Angew. Chem. Int. Ed.* **1990**, *29*, 1304-1319.
170. Nordén, B.; Rodger, A.; Dafforn, T., *Linear Dichroism and Circular Dichroism: A Textbook on Polarized-Light Spectroscopy*. Royal Society of Chemistry Publishing: Cambridge, UK, 2010.
171. Ardhammar, M.; Lincoln, P.; Norden, B., Invisible Liposomes: Refractive Index Matching with Sucrose Enables Flow Dichroism Assessment of Peptide Orientation in Lipid Vesicle Membrane. *Proc. Natl. Acad. Sci. USA* **2002**, *99*, 15313-15317.
172. Garding, L.; Norden, B., Simple Formulas for Rotation Averages of Spectroscopic Intensities. *Chem. Phys.* **1979**, *41*, 431-437.
173. Svensson, F. R.; Lincoln, P.; Norden, B.; Esbjorner, E. K., Retinoid Chromophores as Probes of Membrane Lipid Order. *J. Phys. Chem. B* **2007**, *111*, 10839-10848.
174. Matsuoka, Y.; Norden, B., Linear Dichroism Studies of Nucleic Acids. Ii. Calculation of Reduced Dichroism Curves of a-and B-Form DNA. *Biopolymers* **1982**, *21*, 2433-2452.
175. Matsuoka, Y.; Norden, B., Linear Dichroism Studies of Nucleic Acids. Iii. Reduced Dichroism Curves of DNA in Ethanol–Water and in Poly(Vinyl Alcohol) Films. *Biopolymers* **1983**, *22*, 1731-1746.
176. Couette, M., Étude Sur Le Frottement Des Liquides ('Study on the Frictions of Liquids'). *Annales de Chimie et de Physique* **1890**, *21*, 433-510.
177. Ogston, A. G., The Spaces in a Uniform Random Suspension of Fibres. *Trans. Faraday Soc.* **1958**, *54*, 1754-1757.
178. Slater, G. W.; Rousseau, J.; Noolandi, J.; Turmel, C.; Lalande, M., Quantitative Analysis of the Three Regimes of DNA Electrophoresis in Agarose Gels. *Biopolymers* **1988**, *27*, 509-524.
179. CORDIS, EU Nanotechnology Research: Exploring the Fundamentals, 2005.
180. SantaLucia, J.; Allawi, H. T.; Seneviratne, A., Improved Nearest-Neighbor Parameters for Predicting DNA Duplex Stability. *Biochemistry* **1996**, *35*, 3555-3562.
181. Sandin, P.; Lincoln, P.; Albinsson, B., Conformational Flexibility in DNA Nanoconstructs: A Time-Resolved Fluorescence Resonance Energy Transfer Study. *J. Phys. Chem. C* **2008**, *112*, 13089-13094.
182. Sandin, P.; Tumpene, J.; Borjesson, K.; Wilhelmsson, L. M.; Brown, T.; Norden, B.; Albinsson, B.; Lincoln, P., Thermodynamic Aspects of DNA Nanoconstruct Stability and Design. *J. Phys. Chem. C* **2009**, *113*, 5941-5946.
183. Pal, S.; Deng, Z. T.; Ding, B. Q.; Yan, H.; Liu, Y., DNA-Origami-Directed Self-Assembly of Discrete Silver-Nanoparticle Architectures. *Angew. Chem. Int. Ed.* **2010**, *49*, 2700-2704.
184. Zhao, Z.; Liu, Y.; Yan, H., Organizing DNA Origami Tiles into Larger Structures Using Preformed Scaffold Frames. *Nano Lett.* **2011**, *11*, 2997-3002.
185. Aldaye, F. A.; Sleiman, H. F., Dynamic DNA Templates for Discrete Gold Nanoparticle Assemblies: Control of Geometry, Modularity,

- Write/Erase and Structural Switching. *J. Am. Chem. Soc.* **2007**, *129*, 4130-4131.
186. Kato, T.; Goodman, R. P.; Erben, C. M.; Turberfield, A. J.; Namba, K., High-Resolution Structural Analysis of a DNA Nanostructure by Cryoem. *Nano Lett.* **2009**, *9*, 2747-2750.
187. Erben, C. M.; Goodman, R. P.; Turberfield, A. J., A Self-Assembled DNA Bipyramid. *J. Am. Chem. Soc.* **2007**, *129*, 6992-6993.
188. Yoshimura, Y.; Fujimoto, K., Ultrafast Reversible Photo-Cross-Linking Reaction: Toward in Situ DNA Manipulation. *Org. Lett.* **2008**, *10*, 3227-3230.
189. Borjesson, K.; Tumpane, J.; Ljungdahl, T.; Wilhelmsson, L. M.; Nordén, B.; Brown, T.; Martensson, J.; Albinsson, B., Membrane-Anchored DNA Assembly for Energy and Electron Transfer. *J. Am. Chem. Soc.* **2009**, *131*, 2831-2839.
190. Borjesson, K.; Wiberg, J.; El-Sagheer, A. H.; Ljungdahl, T.; Martensson, J.; Brown, T.; Norden, B.; Albinsson, B., Functionalized Nanostructures: Redox-Active Porphyrin Anchors for Supramolecular DNA Assemblies. *Acc Nano* **2010**, *4*, 5037-5046.
191. Borjesson, K.; Woller, J. G.; Parsa, E.; Martensson, J.; Albinsson, B., A Bioinspired Self Assembled Dimeric Porphyrin Pocket That Binds Electron Accepting Ligands. *Chem. Commun.* **2012**, *48*, 1793-1795.
192. Jakobsen, U.; Simonsen, A. C.; Vogel, S., DNA-Controlled Assembly of Soft Nanoparticles. *J. Am. Chem. Soc.* **2008**, *130*, 10462-10463.
193. Stengel, G.; Zahn, R.; Hook, F., DNA-Induced Programmable Fusion of Phospholipid Vesicles. *J. Am. Chem. Soc.* **2007**, *129*, 9584-9585.
194. Chan, Y.-H. M.; van Lengerich, B.; Boxer, S. G., Effects of Linker Sequences on Vesicle Fusion Mediated by Lipid-Anchored DNA Oligonucleotides. *Proc. Natl. Acad. Sci. USA* **2009**, *106*, 979-984.
195. Li, H. Y.; Park, S. H.; Reif, J. H.; LaBean, T. H.; Yan, H., DNA-Templated Self-Assembly of Protein and Nanoparticle Linear Arrays. *J. Am. Chem. Soc.* **2004**, *126*, 418-419.
196. Wilner, O. I.; Weizmann, Y.; Gill, R.; Lioubashevski, O.; Freeman, R.; Willner, I., Enzyme Cascades Activated on Topologically Programmed DNA Scaffolds. *Nat. Nanotechnol.* **2009**, *4*, 249-254.
197. Lilley, D. M. J.; Wilson, T. J., Fluorescence Resonance Energy Transfer as a Structural Tool for Nucleic Acids. *Curr. Opin. Chem. Biol.* **2000**, *4*, 507-517.
198. Iqbal, A.; Arslan, S.; Okumus, B.; Wilson, T. J.; Giraud, G.; Norman, D. G.; Ha, T.; Lilley, D. M. J., Orientation Dependence in Fluorescent Energy Transfer between Cy3 and Cy5 Terminally Attached to Double-Stranded Nucleic Acids. *Proc. Natl. Acad. Sci. USA* **2008**, *105*, 11176-11181.
199. Krishnan, Y.; Simmel, F. C., Nucleic Acid Based Molecular Devices. *Angew. Chem. Int. Ed.* **2011**, *50*, 3124-3156.
200. Lubrich, D.; Green, S. J.; Turberfield, A. J., Kinetically Controlled Self-Assembly of DNA Oligomers. *J. Am. Chem. Soc.* **2009**, *131*, 2422-+.
201. Hannestad, J. K.; Sandin, P.; Albinsson, B., Self-Assembled DNA Photonic Wire for Long-Range Energy Transfer. *J. Am. Chem. Soc.* **2008**, *130*, 15889-15895.

202. Hannestad, J. K.; Gerrard, S. R.; Brown, T.; Albinsson, B., Self-Assembled DNA-Based Fluorescence Waveguide with Selectable Output. *Small* **2011**, *7*, 3178-3185.
203. Ding, B.; Wu, H.; Xu, W.; Zhao, Z.; Liu, Y.; Yu, H.; Yan, H., Interconnecting Gold Islands with DNA Origami Nanotubes. *Nano Lett.* **2010**, *10*, 5065-5069.